

# Adsorption analysis of polymer and small molecules onto carbon materials based on adsorption isotherm measurements

イスラム エー ビー エム ナズムル

<https://hdl.handle.net/2324/7329463>

---

出版情報 : Kyushu University, 2024, 博士 (工学), 課程博士  
バージョン :  
権利関係 :

**Adsorption analysis of polymer and small molecules onto  
carbon materials based on adsorption isotherm  
measurements**

Doctoral Thesis



**A. B. M. Nazmul Islam**

Kyushu University

Faculty of Engineering

Department of Applied Chemistry

July 2024

# Contents

Contents	-----	2
<b>Chapter 1 General Introduction</b>		
1.1	Carbon materials-----	5
1.2	Polymer-carbon composite-----	6
1.3	Carbon dispersibility and surface modification by polymer-----	8
1.4	Polymer adsorption-----	9
1.5	Indole (small) molecule and chronic kidney disease (CKD)-----	11
1.6	Progression, treatment of CKD and indole molecule -----	13
1.7	Mesoporous carbon (MC)-----	14
1.8	Small molecule adsorption using porous carbon materials-----	15
1.9	Research approach for indole adsorption-----	17
1.10	Adsorption isotherm for polymer/ small molecule adsorption on carbon--	17
1.11	Selectivity of indole adsorption-----	18
1.12	Overview of the thesis-----	19
1.12	References-----	21
<b>Chapter 2 Analysis of polybenzimidazole adsorption onto carbon materials</b>		
2.1	Introduction-----	27
2.2	Materials and Methods-----	28
2.2.1	Materials used-----	28
2.2.2	Equipment's used-----	28
2.2.3	Time course of adsorption-----	29
2.2.4	Adsorption experiments-----	29
2.2.5	Adsorption thermodynamics-----	31
2.3	Results and Discussion-----	31
2.3.1	Characterization of the carbon materials-----	31
2.3.2	Adsorption time course-----	34
2.3.3	Adsorption isotherm of PBI-----	36
2.3.4	PBI coating of pores-----	39

2.3.5	Effect of temperature on the adsorption-----	40
2.4	Summary of the chapter 2-----	43
2.5	References-----	44

### **Chapter 3 Selective adsorption of indole onto mesoporous carbon**

3.1	Introduction-----	48
3.2	Materials and method-----	49
3.2.1	Materials used-----	49
3.2.2	Equipment's used-----	50
3.2.3	Synthesis of mesoporous carbon (MC) -----	50
3.2.4	Process of adsorption isotherm of indole-----	51
3.2.5	Competitive adsorption of indole in presence of amino acids-----	52
3.2.6	MD simulation-----	54
3.3	Results and Discussion-----	54
3.3.1	Structural characterization-----	54
3.3.2	Indole adsorption isotherms-----	58
3.3.3	Selective adsorption of indole-----	62
3.4	Summary of the chapter 3-----	64
3.5	References-----	65

### **Chapter 4 Kinetics of polybenzimidazole and indole adsorption on carbon materials**

4.1	Introduction-----	68
4.2	Materials and method-----	69
4.2.1	Materials used-----	69
4.2.2	Equipment's used-----	70
4.2.3	Kinetic experiments and models-----	70
4.3	Results and Discussion-----	71
4.3.1	PBI adsorption kinetics-----	71
4.3.2	Indole adsorption kinetics and activation energy-----	75
4.4	Summary of the chapter 4-----	81

4.5	References-----	82
-----	-----------------	----

**Chapter 5 Conclusions and perspectives**

5.1	Conclusions-----	84
-----	------------------	----

5.2	Future perspectives-----	85
-----	--------------------------	----

	Acknowledgements-----	88
--	-----------------------	----

# Chapter 1

## General Introduction

### 1.1 Carbon materials

Carbon black (CB) is indeed a fascinating material with a complex structure that contributes to its unique properties. CB's structure consists of spherical particles composed of interconnected graphite-like layers, with functional groups decorating its surface. This structure not only defines its physical properties but also enhances its versatility in industrial applications<sup>1-3</sup>. CB particles typically have a diameter ranging from several 10 to 100 nanometres which are generally spherical in shape. CB primarily consists of carbon atoms arranged in a manner that forms numerous graphite-like layers and each layer is composed of benzene rings fused together (Fig. 1.1).

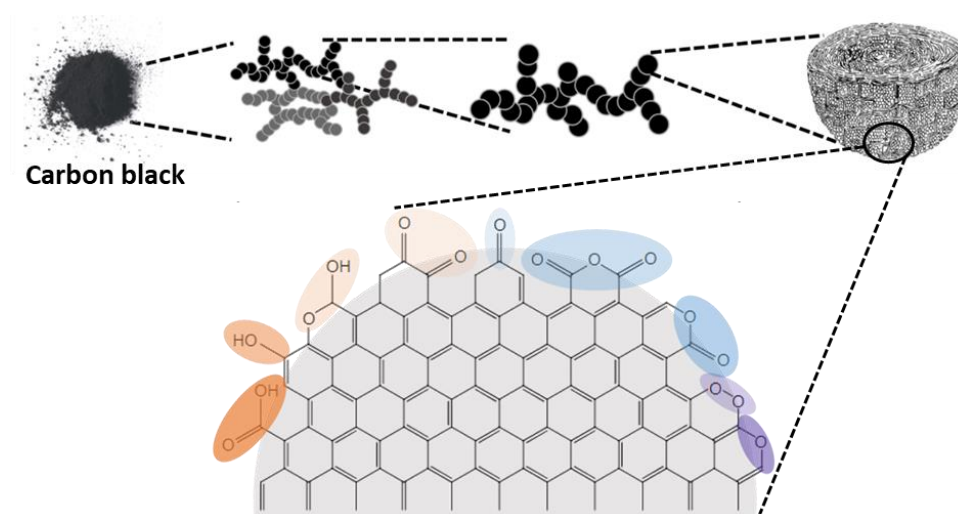


**Fig. 1.1** Granules carbon black and its surface structure, taken from ref<sup>4</sup>

The surface of CB particles is not simply carbon atoms in a graphite-like structure, it also features various functional groups attached to the surface such as hydroxyl (-OH), carboxyl (-COOH), and others, depending on the method of production and treatment. Internally, CBs are composed of crystallites that are interconnected in a way that resembles a sponge-like structure.

This interconnected network of crystallites gives CB its characteristic high surface area and porosity due to the differences in manufacturing method and raw materials, and the size of the pores varies depending on the type of CB. According to the definition of IUPAC (International Union of Pure and Applied Chemistry), pores are roughly classified into micropores (2 nm or less), mesopores (2-50 nm), and macropores (50 nm or more) based on the diameter of the pores <sup>5</sup>. Most of the CB is furnace black obtained by the different incomplete combustion of oil and gas in high-temperature gas, such as Vulcan, Ketjen Black (KB), acetylene black (AB) which have different micropore, mesopore, surface area, surface functional group etc (Fig. 1.2). Due to their unique structure, CB has properties such as high mechanical strength, high thermal and electrical conductivity, and is used as an additive in a wide range of products, such as reinforcing materials for tires, coloring materials for black paints, and conductive materials for dry batteries <sup>6,7</sup>.



**Fig. 1.2** Different types of carbon black

## 1.2 Polymer-carbon composite

Composite materials refer to materials that are made by combining two or more constituent materials with significantly different physical or chemical properties. Generally, carbon composite consist a matrix surrounded by reinforcement material where polymer such as epoxy, polyester used as a matrix and carbon materials used as a reinforcement material <sup>8</sup>. The resulting carbon composite material often exhibits characteristics that are superior to those of its individual components alone. CB is used a reinforcing material and composite materials play a crucial role in modern engineering and technology, offering a diverse range of properties that make them suitable for various demanding applications across different industries <sup>3</sup>.

Carbon-based polymer composite has achieved great attention globally for its applications like automobile tires, ink and mechanical rubber goods (Fig.1.3). Mixing of a soft polymer matrix

with nanoscopic carbon material filler like CB is used to enhance the properties especially when high strength is essential <sup>2</sup>. In the industry, the enhancement of mechanical properties is considered importantly for many years and researchers are working on it. For the reinforcement of rubber, nano-scale CB as filler is a prominent candidate to enhance the mechanical, thermal and electrical properties. Due to cost, ease availability and high surface area of traditional CB, with some surface modification of CB filler it is widely used to enhance the properties of nanocomposite <sup>9,10</sup>.

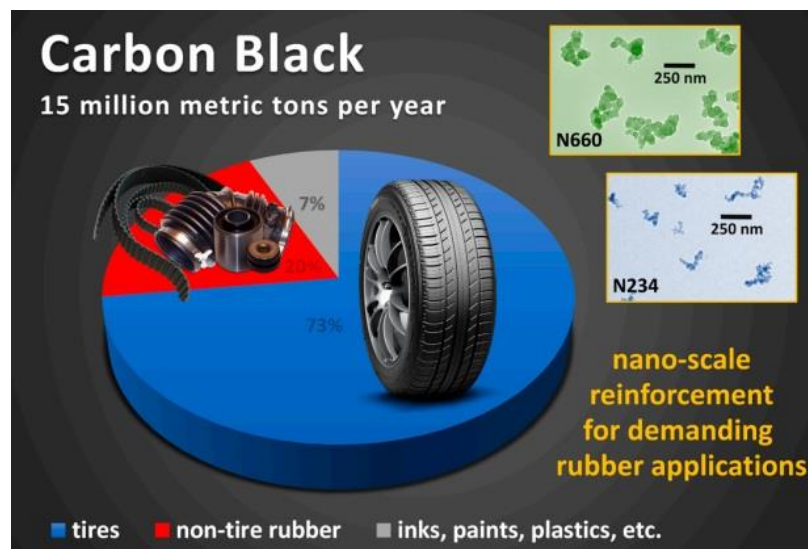


**Fig. 1.3** Global annual production of carbon black and its distribution in the indicated end-use industrial application areas, taken from ref <sup>11</sup>.

However, the development of carbon material/polymer composites with properties that exceed those of conventional materials has not been achieved. One of the reasons for this current situation is the low dispersibility of carbon materials in polymer matrices <sup>12</sup>. In addition, carbon materials have very poor dispersibility in polymer matrices as well as poor solubility in solvents. It is known that this dispersibility greatly affects the performance of the composite. It has been revealed that the formation of large aggregates results in low wear resistance <sup>13</sup>. Therefore, there is a demand for improving the dispersibility of carbon materials in the matrix.

### 1.3 Carbon dispersibility and surface modification by polymer

Surface modification of carbon materials has been performed efficiently and uniformly to disperse carbon materials in the matrix<sup>14-16</sup>. Chemical modification has been used as the main surface modification method, and there have been reports of introducing functional groups such as -OH, -COOH, and -C=O onto the carbon nanotube surface through surface treatments such as strong acid treatment and plasma oxidation treatment to improve electrostatic stability in polar solvents, reports of introducing fluorine and thiol groups to improve solubility in organic solvents, and furthermore, polymerizing the surface to improve dispersibility in the matrix.

Chemical approach based on covalent-bond formation and physical approach based on noncovalent way are used for the functionalization. Particularly, chemical modifications have been frequently used owing to their stability of the functionalization<sup>17-19</sup>. One of the issues of the chemical modifications of the carbons is the difficulty of the intactness, which often decrease the characteristic properties of carbon particles such as high surface area, electrical conductivity and mechanical toughness<sup>20, 21</sup>. Physical modification is a method in which dispersant molecules are physically adsorbed onto the carbon material surface through van der Waals forces,  $\pi$ - $\pi$  stacking interactions or fitted into the pore to disperse the material uniformly, allowing the carbon material to be dispersed while maintaining its properties. Instead of chemical modification, to improve dispersibility by physically modifying the carbon surface with a polymer such as polybenzimidazole (poly(2,2'-m-(phenylene-5,5'-bibenzimidazole)) (PBI) have developed in our laboratory<sup>20, 22, 23</sup>. PBI is classified as a super engineering plastic<sup>24</sup>, and has the highest level of heat resistance among currently existing engineering plastics (it does not melt even at 770 °C or higher in a N<sub>2</sub> atmosphere).

To improve the properties like mechanical, surface morphology, conductivity and others the filler materials like CB, carbon nanotube, graphene, clay are applied in nanosized for reinforcement of polymer-carbon composite. Polymer-wrapped on carbon materials technique is excellent one to consider research interest due to solution disposition and stable under environmental conditions. Moreover, our laboratory already developed polymer-coating method (Fig. 1.4) to disperse carbon into polymers and explored a novel approach, called PBI-wrapping onto carbon support<sup>20, 23</sup>.

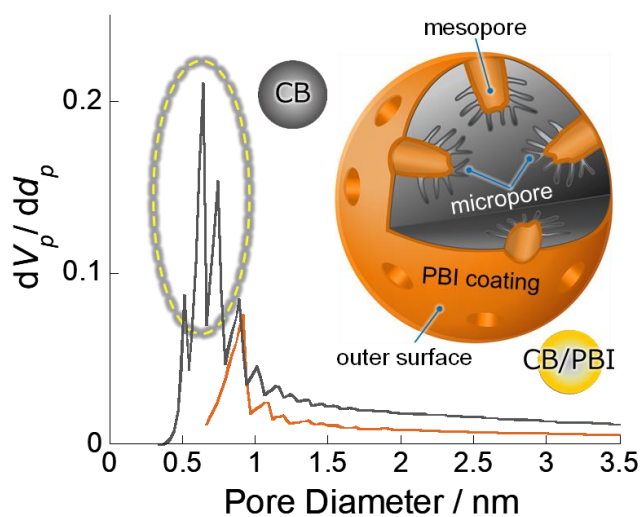
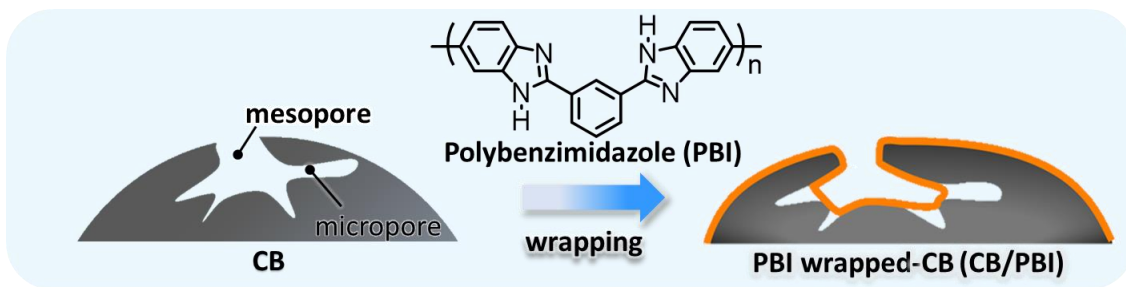


**Fig. 1.4** PBI wrapping approach onto CB, taken from ref <sup>20</sup>

#### 1.4 Polymer adsorption

The adsorption behaviour of polymers onto a solid surface in the solution phase has been extensively studied, mainly that onto a flat substrate such as a silicon wafer <sup>25</sup> as well as glass and silica substrates <sup>26</sup>, owing to the availability of the measurement techniques for these flat substrates (e.g. AFM and ellipsometry) <sup>27-29</sup>; however, measurement techniques for rough <sup>30-32</sup> and particle <sup>33-35</sup> are limited. For carbon materials, effects of the polymer composition <sup>36</sup>, molecular weight of the polymer <sup>37</sup>, and thickness of the adsorbed polymer layer <sup>38, 39</sup> have been studied for polymer adsorption.

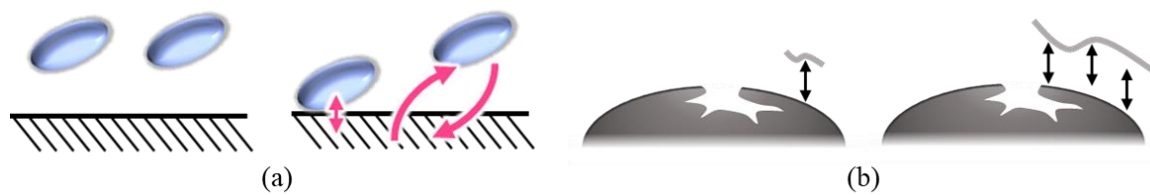


**Fig. 1.5** Flat surface adsorption (a) and porous surface adsorption (b)

Adsorption on flat surface many researchers studied but the polymer adsorption on rough or porous surface will be the innovative one (Fig. 1.5). However, polymer adsorption involves the polymer chains attaching to the surface of particles through various interactions such as electrostatic forces, hydrogen bonding, and van der Waals forces. It is reported that during polymer adsorption there are many factors need to consider like re-conformation of polymer chain, adsorption time or surface coverage (Fig. 1.6) <sup>40, 41</sup>. Physical modification, typically based on the adsorption of small molecules in a solution, can preserve the surface structure, offering a significant advantage <sup>42, 43</sup>. However, physical modifications using small molecules can cause instability owing to the dynamic adsorption/desorption of molecules from the surface <sup>44, 45</sup>.

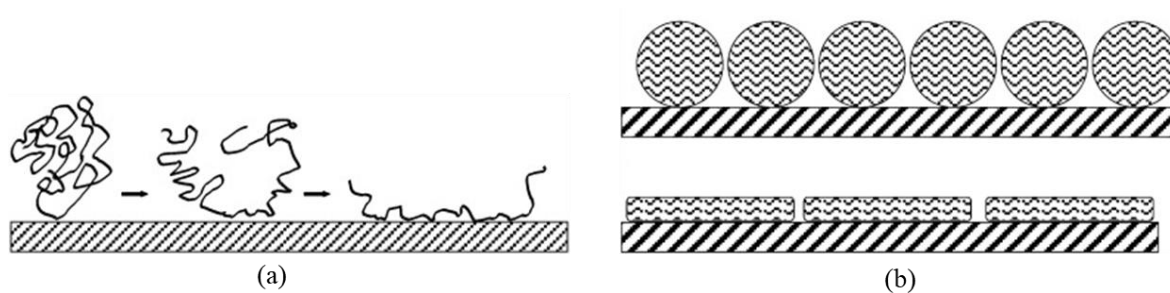


**Fig. 1.6** Schematic picture of (a) polymer reconfirmation of an adsorbed polymer (b) effect of adsorption time on surface coverage, where globular structure for high surface coverage and flatter structure for slower adsorption, take from ref <sup>40</sup>

Modi S. *et.al.* investigated the effect of molecular weight on the deposition behaviour of polystyrene and CB composite (Fig.1.7) and reported that the preferential adsorption of the longer polystyrene chains on the carbon black <sup>37</sup>.

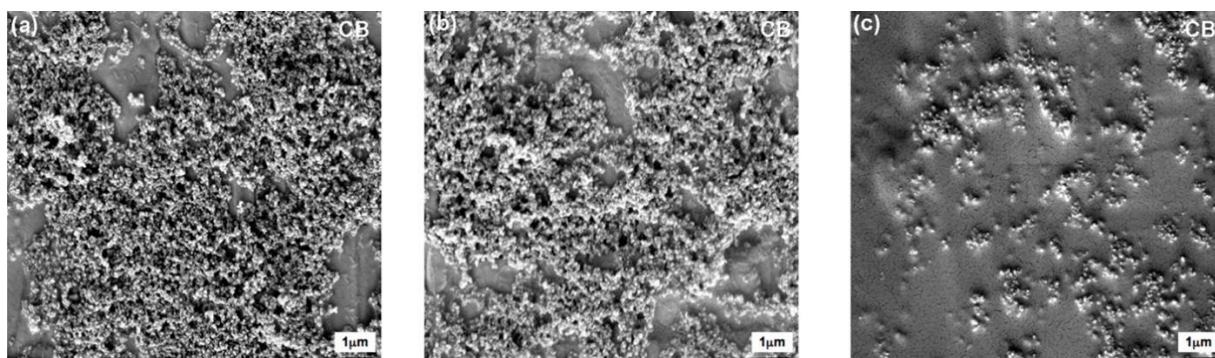


**Fig. 1.7** SEM micrographs for (a) molecular weight of 13.2 kgmol<sup>-1</sup>, (b) molecular weight of 18.1 kgmol<sup>-1</sup>, (c) molecular weight of 151.5 kgmol<sup>-1</sup>, carbon black/polystyrene suspension, take from ref <sup>37</sup>

The kinetic and equilibrium of triblock copolymers of the poly(ethylene oxide)-poly-(propylene oxide)-poly(ethylene oxide) (PPO) adsorption on CB was studied by Tiberg F. *et.al.* to assess the relation to the phase behavior of the bulk solution using adsorption isotherm <sup>46</sup>. Very high adsorbed amounts detected near the phase boundary are thought to be a significance, presumably resulting in the formation of multilayers at the surface. They suggested the understanding of the segment density profiles in the adsorbed layers as well as of the favoured adsorption of PPO segments to the surface. Also, the kinetics and equilibrium properties of polymer adsorption was closely linked and play significant roles in determining the performance and efficiency.

Therefore, polymer adsorption as well as the small molecule adsorption on carbon surface by considering adsorption behavior is a fabulous technique, which is familiar, and researchers considered for the different molecular size polymer adsorption as well as for the smaller molecules.

### **1.5 Indole (small) molecule and chronic kidney disease (CKD)**

Indole is a small heterocyclic molecule consisting of a bicyclic structure containing a six-membered benzene ring fused to a five-membered nitrogen-containing pyrrole ring <sup>47</sup>. Indole is notable for its presence in many natural compounds, including certain amino acids, hormones,

and neurotransmitters. Indoxyl sulfate (IS), a uremic toxin that accumulates in the body, is directly related to the decline of renal function<sup>48,49</sup>. IS is an aromatic low molecular weight compound that is produced when indole, synthesized from tryptophan, is metabolized by intestinal bacteria such as *Escherichia coli*. It is produced when indole absorbed from the intestine is transported to the liver.

On the other hand, CKD is a disease in which kidney function declines chronically<sup>50</sup>. CKD is defined by reduced renal function and evidence of kidney damage for at least 3 months and it is a serious problem worldwide<sup>51-53</sup>. The renal system consists of the kidney, ureters, and the urethra. The overall function of the system filters approximately 200 liters of fluid a day from renal blood flow which allows for toxins, metabolic waste products, and excess ion to be excreted while keeping essential substances in the blood. When CKD progresses further to end-stage renal failure with an eGFR of less than 15 mL/min, patients are forced to undergo renal replacement therapy such as dialysis or kidney transplantation which is difficult. As a result, most patients are forced to undergo haemodialysis treatment three days a week for four hours each time, and the number of dialysis patients will exceed 340,000 by the end of 2021. The number of dialysis patients is increasing year by year, and it has become a major social problem due to many reasons (Fig. 1.8), so preventing the worsening of CKD is an important issue.

CKD is lifestyle-related diseases. When kidney function declines, waste products cannot be excreted, and uremic toxins accumulate in the body. Once function declines, it is almost impossible to recover, so CKD progresses and ultimately leads to end-stage renal failure.

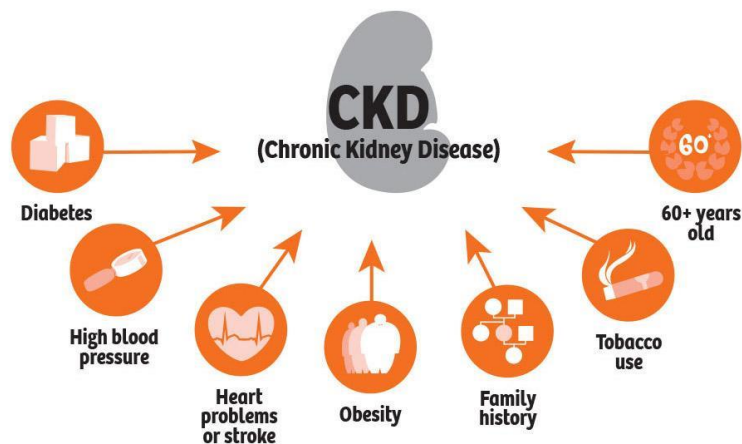


**Fig. 1.8** Reasons of CKD, taken from ref<sup>54</sup>

## 1.6 Progression, treatment of CKD and indole molecule

The indole molecule or their derivatives like IS is responsible for CKD, therefore, reducing the amount of IS accumulated suppresses the progression of CKD<sup>55</sup>. Saito *et. al.* reported on sulfotransferase inhibitors as a method to inhibit the accumulation of IS in the kidney<sup>52</sup>. Oral carbon adsorbent is currently widely used, which adsorbs and removes indole, a precursor of IS, in the intestinal tract and inhibits the intestinal absorption of indole, thereby inhibiting the accumulation of IS since indole can initiate the CKD progression (Fig. 1.9).

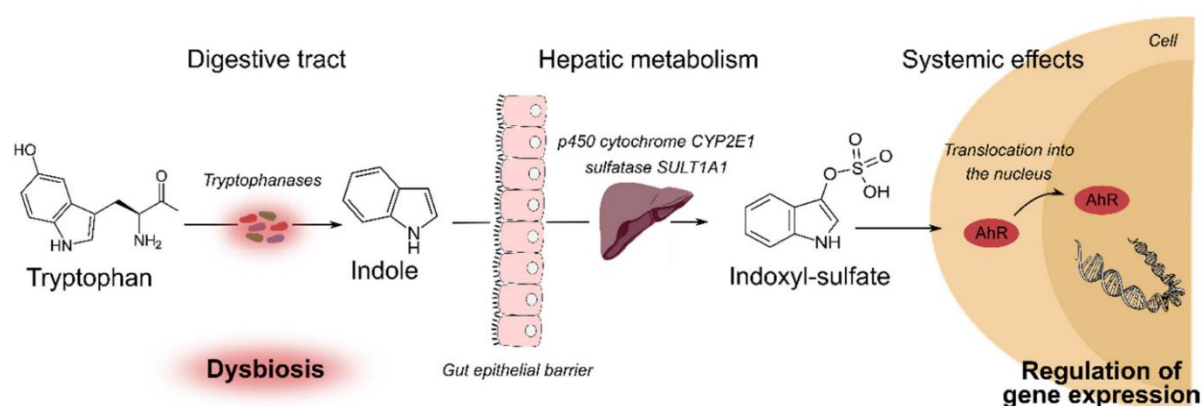


**Fig. 1.9** Mechanism of CKD generation (AhR: aryl hydrocarbon receptor), taken from ref<sup>56</sup>

Currently, AST-120 (Fig. 1.10) is widely used as an orally adsorbed carbon agent. AST-120 is mainly composed of porous spherical activated carbon. AST-120 has high adsorption capacity for uremic toxins<sup>57,58</sup>. It has been on the market since 1991 (Japan) S. Korea (2004), and has been shown to treat the symptoms of CKD patients. However, there are side effects such as secretions and loss of appetite, and the daily dose is as high as 6 g. This may cause negative effects on patients due to reasons such as poor adsorption (low adsorption amount). In addition, there is also the problem of non-specific capture of essential amino acids in addition to uremic toxins. Therefore, the current challenge is to improve both the adsorption amount and selectivity.



**Figure 1.10** Kremezin drug (AST-120), taken from ref <sup>59</sup>

### 1.7 Mesoporous carbon (MC)

Mesoporous carbon (MC) is a type of carbon material that contains a network of pores with diameters typically ranging from 2 to 50 nm whereas microporous (< 2nm) and macropores (>50 nm) (Fig. 1.10). These MC have a high surface area and are characterized by their unique pore structure, which allows for high adsorption capacities and efficient diffusion of molecules within the pores. The pore size and surface chemistry of MC can be tailored during synthesis to meet specific application requirements <sup>60</sup>. This tunability is advantageous for optimizing performance in different applications. MC finds applications in various fields such as energy storage (e.g., supercapacitors, batteries), environmental remediation (e.g., water treatment, air purification), and catalysis (e.g., as catalyst supports) <sup>61, 62</sup>.

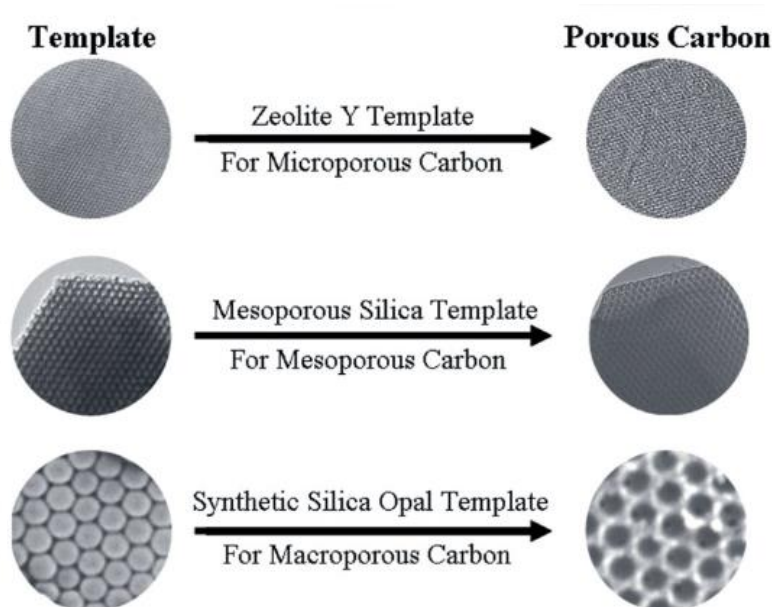


**Fig. 1.10** Schematic representation of microporous, mesoporous and macropores carbon, taken from ref <sup>63</sup>.

MC can be synthesized by either the hard template method or the soft template method (solvent evaporation-induced self-assembly method) <sup>64, 65</sup>. Whereas, the soft template method is advantageous, easy to remove the template and allowing direct control of structure and morphology. In the soft template method, first, an amphiphilic block copolymer serving as a template is mixed with a molecule serving as a carbon source to form an ordered nanostructure, and this nanostructure is carbonized to obtain ordered mesoporous carbon.

### 1.8 Small molecule adsorption using porous carbon materials

Porous carbon materials have been proposed as a novel high performance adsorbent material since they have high surface area, large pore volume, chemical inertness and functional groups on their surface. Adsorption of small molecule like methylene blue or phenol on activated carbon have been reported (Fig. 1.11) and they revealed how the molecules interact or diffuse into the carbon surface <sup>72</sup>. It is reported from the adsorption kinetics that the general adsorption mechanism of small molecule on activated carbon and pore blocking phenomenon, mono or multi-layer, desorption etc.

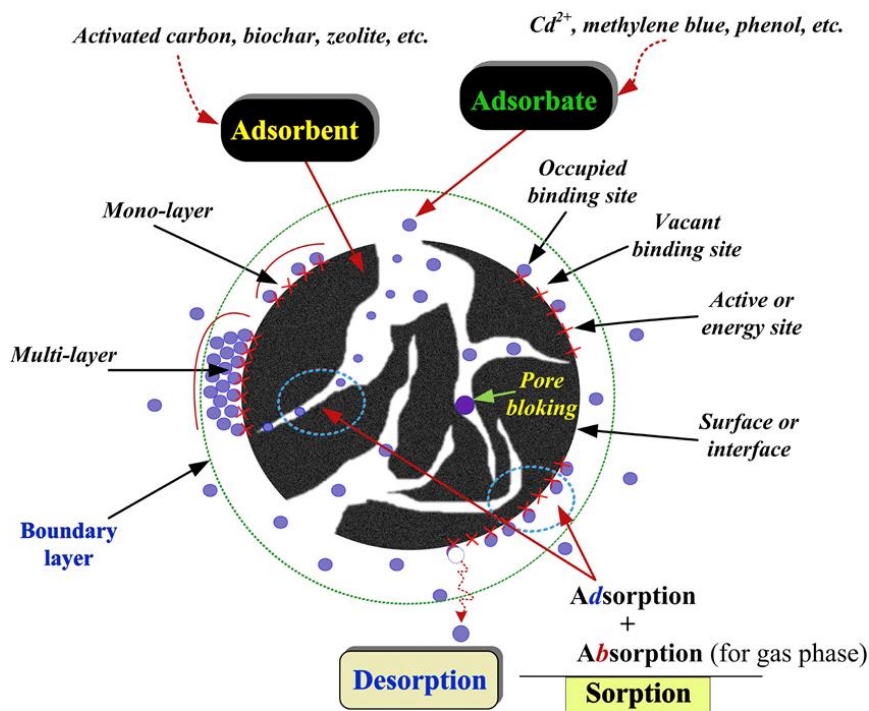


**Figure 1.11** Basic terms of in adsorption science and technology, taken from ref <sup>72</sup>

Especially, ordered mesoporous carbons have been studied for adsorbents because they have both micropore and mesopore with narrow pore size distributions. The modification of porous carbon materials has been investigated to improve the indole (small molecule) adsorption capacity. However, the adsorption selectivity for certain amino acids was unclear due to its size being similar to that of indole. Therefore, the selectivity for amino acids remains unknown. Due to the  $\pi$ - $\pi$  interaction and quadrupole interaction of the fluorophenyl group, indole can be selectively adsorbed regardless of the presence or absence of other indole derivatives. In addition, Mitome *et. al.* reported that activated mesoporous carbon and with a highly controlled pore structure suppresses the adsorption of indole due to large molecules such as phospholipids in artificial intestinal juice (Fig. 1.12) <sup>66</sup>. This research suggested that the indole adsorption amount and selectivity can be developed by designing an accurate mesopore size and increasing the micropore surface area.

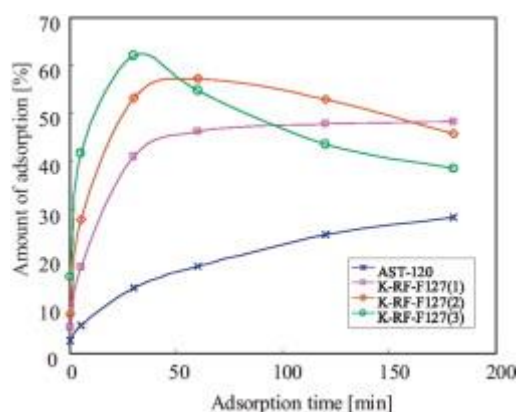


**Figure 1.12** Time course of the amount of indole adsorbed of the various mesoporous carbon from the artificial intestinal juice solution, taken from ref <sup>66</sup>.

However, due to the large pore size and the absence of small molecules such as amino acids in the artificial intestinal fluid used in this experiment, there is a problem that the selectivity for small molecules such as amino acids remain unknown. In other words, no research has yet been reported that has achieved both an improvement in the amount of indole adsorption and indole adsorption selectivity over amino acids, and the optimal pore size and surface composition characteristics have yet to be elucidated.

## 1.9 Research approach for indole adsorption

MC have the advantage that the pore size can be easily tailored by changing the solvent composition used in the preparation, the carbonization temperature, and the type of surfactant used as the template, and the template can be easily removed during the carbonization process<sup>62,67</sup>. In addition, the pore size can be controlled to a size of about a few nm, which is considered to be suitable for indole adsorption, so we determined that it is suitable for this purpose.

By synthesizing carbon materials such as MC with appropriate pore sizes and develop new drugs that can selectively and efficiently capture indole from amino acids. Indole adsorption experiments in the presence of hydrophobic amino acids using soft-templated mesoporous carbons will be my objective. Therefore, by finely adjusting the pore size, it is thought that it is possible to suppress the adsorption of amino acids and achieve selective adsorption of indole. Furthermore, commonly used drug AST-120 and Ketjen Black (KB), which is known to have a wide pore size distribution of 0.5 to 50 nm, is also used for comparison to more deeply inspect the effect of mesoporous carbon with a narrow pore size distribution on indole adsorption.

## 1.10 Adsorption isotherm for polymer/ small molecule adsorption on carbon

The interpretation of polymer as well as small molecule adsorption by measuring adsorption isotherms is a fantastic way, and it is well-known, many researchers studied for the larger molecule's adsorption as well as for the smaller molecules by using this<sup>19, 68, 69</sup>. In the adsorption isotherm measurement, not only the adsorption behavior and the adsorption state can be elucidated but also the coating conditions can be optimized by analyzing the thermodynamic parameters. Adsorption isotherms are used to create an adsorption isotherm that shows the relationship between the equilibrium adsorption amount  $\Gamma$  (mg/mg) per unit mass of adsorbent and the equilibrium solute concentration  $C_e$  (mg/mL) at a constant temperature. This is the most common method for showing the adsorption stoichiometry. The equilibrium adsorption amount  $\Gamma$  (mg/mg) is calculated using the adsorbent mass  $M$  (mg), total amount  $V$  (mL), solute concentration  $C_o$  (mg/mL), and equilibrium solute concentration  $C_e$  (mg/mL) using the following formula:

$$\Gamma = (C_o - C_e) V / M \dots \dots \dots \text{(Eq. 1.1)}$$

Generally, from the adsorption isotherm, it is possible to observe the adsorption phenomenon such as amount of adsorption, monolayer adsorption, interaction between the adsorbates etc.

However, unlike gas-phase adsorption, liquid-phase adsorption requires adsorbent-adsorbate interaction, the adsorbate-solvent and adsorbent-solvent interactions must also be taken into account, making the handling of the system more complicated.

In general, it is possible to calculate thermodynamic parameters from the adsorption isotherm using the Langmuir equation and van't Hoff equation. If the measured value is fitted to the Langmuir equation,  $C_e$  and  $C_e/\Gamma$  are plotted, and a linear relationship is established, it can be said that the Langmuir equation fits, and the maximum adsorption amount  $\Gamma_{max}$  can be estimated. Therefore, in order to make easier, research has been conducted to consider the adsorption behaviour by calculating thermodynamic parameters (Gibbs free energy change:  $\Delta G$ , entropy change:  $\Delta S$ , enthalpy change:  $\Delta H$ )<sup>70</sup>.

$$\text{Langmuir: } C_e/\Gamma = C_e/\Gamma_{max} + 1/\Gamma_{max} K_L \dots\dots\dots \text{(Eq. 1.2)}$$

$$\Delta G = -RT \ln K_L \dots\dots\dots \text{(Eq. 1.3)}$$

$$\Delta G = \Delta H - T\Delta S \dots\dots\dots \text{(Eq. 1.4)}$$

$$\ln K_L = \Delta S/R - \Delta H/RT \dots\dots\dots \text{(Eq. 1.5)}$$

The value of the  $\Delta S$  and  $\Delta H$  can be determined based on the plot of  $\ln K_L$  versus  $1/T$ .  $T$  is the absolute temperature (K) and  $R$  is the universal gas constant. Langmuir adsorption constant,  $K_L$  and  $\Gamma_{max}$  is the Langmuir adsorption constant and maximum adsorption amount, respectively. If the system is spontaneous, the Gibbs free energy of adsorption becomes negative, and the stronger the adsorption, the negative value becomes larger. The adsorption enthalpy allows us to consider the magnitude of the direct interaction between polymer/small molecule and the carbon material, while the adsorption entropy allows us to consider the contribution of the interaction with the solvent.

Moreover, polymer adsorption kinetics on carbon surfaces is a complex phenomenon influenced by polymer characteristics, carbon surface properties, and environmental conditions. Polymer adsorption kinetics involves understanding how polymers interact with surfaces, specifically focusing on the rate and mechanisms by which polymers adhere to solid substrates such as carbon surfaces. Larger surface area and appropriate pore size distribution facilitate high adsorption capacities and efficient mass transfer kinetics. Adsorption kinetics of small molecule like indole on MC, investigating how indole molecules interact with the porous carbon material over time.

### 1.11 Selectivity of indole adsorption

Bile acids are essential for digestion, absorption, and metabolic regulation in the body, playing a crucial role in maintaining overall health and metabolic balance. Dahlgren *et al.* reported that intestinal fluid before and after eating a meal from humans contains many components like phospholipids, bile acids as impurities with proteins<sup>71</sup>. However, if the adsorption of small protein amino acids can be suppressed by finely crafting the pore size, the adsorption of large lipids and bile acids can also be suppressed.

In particular, since it is presumed that hydrophobic amino acids inhibit the adsorption of indole to the carbon material due to the hydrophobic interaction of the carbon material. The indole adsorption ability of the carbon material is confirmed in the coexistence of hydrophobic amino acids (glycine, alanine, leucine, isoleucine, valine, phenylalanine, proline, tryptophan). The adsorption ratio is calculated by the following formula using the solute concentration  $C_0$  (mg/mL) and the equilibrium solute concentration  $C_e$  (mg/mL).

$$\text{Adsorption ratio (\%)} = (C_0 - C_e) / C_0 \times 100 \dots \dots \dots (\text{Eq. 1.6})$$

Towards practical application, the goal is to achieve an indole adsorption capacity in an aqueous solution containing a mixture of indole and hydrophobic amino acids.

### 1.12 Overview of the thesis

This thesis focusing on both a polymeric material like PBI and a small molecule like indole, primarily aims to provide insights into different aspects of adsorption onto carbon surfaces, contributing to the broader understanding and application of carbon-based materials in various fields. The surface modification of carbon materials is an effective method for enhancing the properties of carbon-based functional materials, especially via a polymer coating, which is advantageous owing to its intactness and simplicity. On the other hand, the removal of uremic toxins such as indole using carbon-based adsorbents is essential for preventing the progression of chronic kidney disease. This research involves studying the adsorption kinetics, thermodynamics, and mechanisms involved in the interaction between these molecules and the carbon surface.

In chapter 2, PBI has been used to modify carbon surfaces, yet its adsorption behavior has not been thoroughly studied. The adsorption thermodynamics of PBI adsorption on various types

of carbon black with different surface morphologies and chemical compositions were analyzed via isotherm measurements. The adsorption behavior was compared to that of the PBI monomer, 1,3-bis(1H-benzo[d]imidazol-2-yl)benzene, to clarify the effects of the polymer. The surface adsorption of PBI was slower than that of the PBI unit, but PBI exhibited a larger adsorption capacity. PBI adsorption was driven by entropy, whereas the PBI unit adsorption was driven by enthalpy. The adsorption of PBI was more thermodynamically favourable on carbon surfaces with a higher crystallinity (lower oxygenation) owing to the easier detachment of solvent molecules from the carbon surface, leading to a higher adsorption constant.

In chapter 3, MC with a uniform diameter of 3.1 nm was used as an adsorbent for indole in aqueous media, and its thermodynamics were studied using the conventional adsorbent AST-120 as a control. Compared to AST-120, MC shows highly efficient indole adsorption as well as remarkable adsorption selectivity for indole in the presence of various amino acids. The excellent selectivity of MC can lower the dose of the adsorbent, which may improve the treatment strategy for CKD patients.

In chapter 4, my focus is on the adsorption kinetics of PBI and Indole over carbon materials. The adsorption kinetics explored that the adsorption of PBI onto carbon materials is suitable for the efficient adsorption where the trend of adsorption capacity and the adsorption rate constant was  $KB > Vulcan > AB$ . Also, the trend of surface area including micropores and mesopores was  $KB > Vulcan > AB$  which allow us above explanation where the intraparticle diffusion into the porous carbons have a significant role as well. The adsorption of indole on MC is faster than that on AST-120, suggesting the particle size and pore structure of MC may play a vital role in determining the adsorption rate, and the larger portion of physisorption play active role which is relatively quicker. The intraparticle diffusion is a rate-controlling step on both PBI and Indole adsorption together with the adsorption reaction.

In chapter 5, provide a concise summary of results alongside a thoughtful exploration of future perspectives which can effectively communicate the significance of the research outcomes and inspire further scientific inquiry in the field of adsorption and carbon material applications.

### 1.13 References

- (1) Pantea, D.; Darmstadt, H.; Kaliaguine, S.; Roy, C. Electrical conductivity of conductive carbon blacks: influence of surface chemistry and topology. *Appl. Surf. Sci.* **2003**, *217* (1), 181-193.
- (2) Srivastava, S. K.; Mishra, Y. K. Nanocarbon Reinforced Rubber Nanocomposites: Detailed Insights about Mechanical, Dynamical Mechanical Properties, Payne, and Mullin Effects. *Nanomaterials*, **2018**, *8*, 945.
- (3) Long, C. M.; Nascarella, M. A.; Valberg, P. A. Carbon black vs. black carbon and other airborne materials containing elemental carbon: Physical and chemical distinctions. *Environ. Pollut.*, **2013**, *181*, 271-286.
- (4) Asia, C. C. Carbon Black. *Continental Carbon Asia*, **2024**.  
<https://www.continentalcarbonasia.com/en/productCarbonBlack.html> (accessed).
- (5) Thommes, M.; Kaneko, K.; Neimark, A. V.; Olivier, J. P.; Rodriguez-Reinoso, F.; Rouquerol, J.; Sing, K. S. W. Physisorption of gases, with special reference to the evaluation of surface area and pore size distribution, *IUPAC Technical Report*, **2015**, *87* (9-10), 1051-1069.
- (6) Lungulescu, E. M.; Stancu, C.; Setnescu, R.; Notingher, P. V.; Badea, T. A. Electrical and Electro-Thermal Characteristics of (Carbon Black-Graphite)/LLDPE Composites with PTC Effect. *Materials*, **2024**, *17* (5).
- (7) Costa, S. M. R.; Fowler, D.; Carreira, G. A.; Portugal, I.; Silva, C. M. Production and Upgrading of Recovered Carbon Black from the Pyrolysis of End-of-Life Tires. *Materials*, **2022**, *15*, 2030.
- (8) Park, S.-J.; Seo, M.-K. Chapter 7 - Types of Composites. In *Interface Science and Technology*, Park, S.-J., Seo, M.-K. Eds.; Vol. 18; Elsevier, 2011; p 501-629.
- (9) Hoshikawa, Y.; An, B.; Kashihara, S.; Ishii, T.; Ando, M.; Fujisawa, S.; Hayakawa, K.; Hamatani, S.; Yamada, H.; Kyotani, T. Analysis of the interaction between rubber polymer and carbon black surfaces by efficient removal of physisorbed polymer from carbon-rubber composites. *Carbon*, **2016**, *99*, 148-156.
- (10) Atif, M.; Bongiovanni, R.; Giorelli, M.; Celasco, E.; Tagliaferro, A. Modification and characterization of carbon black with mercaptopropyltrimethoxysilane. *Appl. Surf. Sci.* **2013**, *286*, 142-148.
- (11) Robertson, C. G.; Hardman, N. J. Nature of Carbon Black Reinforcement of Rubber: Perspective on the Original Polymer Nanocomposite. *Polymers*, 2021, *13*, 538.

- (12) Andrews, R.; Weisenberger, M. C. Carbon nanotube polymer composites. *Curr. Opin. Solid State Mater. Sci.* **2004**, *8* (1), 31-37.
- (13) Velasco-Santos, C.; Martinez-Hernandez, A. L.; Castano, V. M. Carbon nanotube-polymer nanocomposites: The role of interfaces. *Compos. Interfaces*, **2005**, *11* (8-9), 567-586.
- (14) Prithi, J. A.; Vedarajan, R.; Ranga Rao, G.; Rajalakshmi, N. Functionalization of carbons for Pt electrocatalyst in PEMFC. *Int. J. Hydrogen Energy*, **2021**, *46* (34), 17871-17885.
- (15) Worsley, K. A.; Kalinina, I.; Bekyarova, E.; Haddon, R. C. Functionalization and Dissolution of Nitric Acid Treated Single-Walled Carbon Nanotubes. *J. Am. Chem. Soc.*, **2009**, *131* (50), 18153-18158.
- (16) Khodabakhshi, S.; Fulvio, P. F.; Andreoli, E. Carbon black reborn: Structure and chemistry for renewable energy harnessing. *Carbon*, **2020**, *162*, 604-649.
- (17) Kang, S.; Jones, A. R.; Moore, J. S.; White, S. R.; Sottos, N. R. Microencapsulated Carbon Black Suspensions for Restoration of Electrical Conductivity. *Adv. Funct. Mater.*, **2014**, *24* (20), 2947-2956.
- (18) Amornwachirabodee, K.; Tantimekin, N.; Pan-In, P.; Palaga, T.; Pienpinijtham, P.; Pipattanaboon, C.; Sukmanee, T.; Ritprajak, P.; Charoenpat, P.; Pitaksajjakul, P.; et al. Oxidized Carbon Black: Preparation, Characterization and Application in Antibody Delivery across Cell Membrane. *Sci. Rep.*, **2018**, *8* (1), 2489.
- (19) Oe, N.; Hosono, N.; Uemura, T. Revisiting molecular adsorption: unconventional uptake of polymer chains from solution into sub-nanoporous media. *Chem. Sci.*, **2021**, *12* (38), 12576-12586.
- (20) Fujigaya, T.; Hirata, S.; Berber, M. R.; Nakashima, N. Improved Durability of Electrocatalyst Based on Coating of Carbon Black with Polybenzimidazole and their Application in Polymer Electrolyte Fuel Cells. *ACS Appl. Mater. Interfaces*, **2016**, *8* (23), 14494-14502.
- (21) Le, V. T.; Ngo, C. L.; Le, Q. T.; Ngo, T. T.; Nguyen, D. N.; Vu, M. T. Surface modification and functionalization of carbon nanotube with some organic compounds. *Adv. Nat. Sci: Nanosci. Nanotechnol.*, **2013**, *4* (3), 35017.
- (22) Fujigaya, T.; Nakashima, N. Non-covalent polymer wrapping of carbon nanotubes and the role of wrapped polymers as functional dispersants. *Sci. Technol. Adv. Mater.*, **2015**, *16* (2), 024802.
- (23) Jayawickrama, S. M.; Fujigaya, T. Effect of polymer-coating on carbon blacks for Pt utilization efficiency of polymer electrolyte membrane fuel cells. *J. Power Sources*, **2021**, *482*, 228932.

- (24) Samms, S. R.; Wasmus, S.; Savinell, R. F. Thermal Stability of Proton Conducting Acid Doped Polybenzimidazole in Simulated Fuel Cell Environments. *J. Electrochem. Soc.*, **1996**, *143* (4), 1225.
- (25) Awan, M. A.; Dimonie, V. L.; Filippov, L. K.; El-Aasser, M. S. Adsorption Kinetics of Amphipathic Polystyrene-block-polybutadiene onto Silicon Wafer and Polystyrene Planar Surfaces. *Langmuir*, **1997**, *13* (2), 130-139.
- (26) Balastre, M.; Berquier, J.-M. Effect of Water Traces upon Adsorption of PMMA on Flat Substrates of Glass and Silica. *Langmuir*, **1999**, *15* (25), 8691-8694.
- (27) Linse, P.; Källrot, N. Polymer Adsorption from Bulk Solution onto Planar Surfaces: Effect of Polymer Flexibility and Surface Attraction in Good Solvent. *Macromolecules*, **2010**, *43* (4), 2054-2068.
- (28) Simavilla, D. N.; Huang, W.; Vandestruck, P.; Ryckaert, J.-P.; Sferrazza, M.; Napolitano, S. Mechanisms of Polymer Adsorption onto Solid Substrates. *ACS Macro Letters*, **2017**, *6* (9), 975-979.
- (29) Takahashi, A.; Kawaguchi, M.; Hirota, H.; Kato, T. Adsorption of Polystyrene at the  $\theta$  Temperature. *Macromolecules*, **1980**, *13* (4), 884-889.
- (30) Venkatakrisnan, A.; Kuppa, V. K. Polymer adsorption on rough surfaces. *Curr. Opin. Chem. Eng.*, **2018**, *19*, 170-177.
- (31) Kurata, N.; Anada, S.; Kawaguchi, M. Competitive Adsorption of Polymer Chains at Fractal Surfaces. In *Studies in Surface Science and Catalysis*, Suzuki, M. Ed.; Vol. 80; Elsevier, **1993**; p 341-348.
- (32) Kawaguchi, M.; Mikura, M.; Takahashi, A. Hydrodynamic studies on adsorption of poly(ethylene oxide) in porous media. 2. Molecular weight dependence of hydrodynamic thickness. *Macromolecules*, **1984**, *17* (10), 2063-2065.
- (33) Kawaguchi, M.; Maeda, K.; Kato, T.; Takahashi, A. Preferential adsorption of monodisperse polystyrene on silica surface. *Macromolecules*, **1984**, *17* (9), 1666-1671.
- (34) Wang, W.; Zheng, B.; Deng, Z.; Feng, Z.; Fu, L. Kinetics and equilibriums for adsorption of poly(vinyl alcohol) from aqueous solution onto natural bentonite. *Chem. Eng. J.*, **2013**, *214*, 343-354.
- (35) Kawaguchi, M.; Kawaguchi, H.; Takahashi, A. Competitive and displacement adsorption of polyelectrolyte and water-soluble nonionic polymer at the silica surface. *J. Colloid Interface Sci.*, **1988**, *124* (1), 57-62.

- (36) Shar, J. A.; Cosgrove, T.; Obey, T. M.; Warne, M. R.; Wedlock, D. J. Adsorption Studies of Diblock Copolymers at the Cyclohexane/Carbon Black Interface. *Langmuir*, **1999**, *15* (22), 7688-7694.
- (37) Modi, S.; Panwar, A.; Mead, J. L.; Barry, C. M. F. Effect of Molecular Weight on the Electrophoretic Deposition of Carbon Black Nanoparticles in Moderately Viscous Systems. *Langmuir*, **2013**, *29* (31), 9702-9711.
- (38) Lin, Y.; Smith, T. W.; Alexandridis, P. Adsorption of a Rake-Type Siloxane Surfactant onto Carbon Black Nanoparticles Dispersed in Aqueous Media. *Langmuir*, **2002**, *18* (16), 6147-6158.
- (39) Shibayama, M.; Matsunaga, T.; Kusano, T.; Amemiya, K.; Kobayashi, N.; Yoshida, T. SANS studies on catalyst ink of fuel cell. *J. Appl. Polym. Sci.*, **2014**, *131* (3).
- (40) Gregory, J.; Barany, S. Adsorption and flocculation by polymers and polymer mixtures. *Adv. Colloid Interface Sci.*, **2011**, *169* (1), 1-12.
- (41) Brotherson, B.; Deng, Y. Site blocking effect on the conformation of adsorbed cationic polyacrylamide on a solid surface. *J. Colloid Interface Sci.*, **2008**, *326* (2), 324-328.
- (42) Ju, S.-Y.; Utz, M.; Papadimitrakopoulos, F. Enrichment Mechanism of Semiconducting Single-Walled Carbon Nanotubes by Surfactant Amines. *J. Am. Chem. Soc.*, **2009**, *131* (19), 6775-6784.
- (43) Chen, R. J.; Zhang, Y.; Wang, D.; Dai, H. Noncovalent Sidewall Functionalization of Single-Walled Carbon Nanotubes for Protein Immobilization. *J. Am. Chem. Soc.*, **2001**, *123* (16), 3838-3839.
- (44) Petrie, K.; Docoslis, A.; Vasic, S.; Kontopoulou, M.; Morgan, S.; Ye, Z. Non-covalent/non-specific functionalization of multi-walled carbon nanotubes with a hyperbranched polyethylene and characterization of their dispersion in a polyolefin matrix. *Carbon*, **2011**, *49* (10), 3378-3382.
- (45) Wu, G.; Asai, S.; Sumita, M. Carbon Black as a Self-Diagnosing Probe To Trace Polymer Dynamics in Highly Filled Compositions. *Macromolecules*, **2002**, *35* (5), 1708-1713.
- (46) Tiberg, F.; Malmsten, M.; Linse, P.; Lindman, B. Kinetic and equilibrium aspects of block copolymer adsorption. *Langmuir*, **1991**, *7* (11), 2723-2730.
- (47) Chadha, N.; Silakari, O. Indoles as therapeutics of interest in medicinal chemistry: Bird's eye view. *E. J. Med. Chem.*, **2017**, *134*, 159-184.
- (48) Vanholder, R.; Schepers, E.; Pletinck, A.; Nagler, E. V.; Glorieux, G. The uremic toxicity of indoxyl sulfate and p-cresyl sulfate: a systematic review. *J. Am. Soc. Nephrol*, **2014**, *25* (9), 1897-1907.

- (49) Vanholder, R.; De Smet, R.; Glorieux, G.; Argilés, A.; Baurmeister, U.; Brunet, P.; Clark, W.; Cohen, G.; De Deyn, P. P.; Deppisch, R.; et al. Review on uremic toxins: Classification, concentration, and interindividual variability. *Kidney International*, **2003**, *63* (5), 1934-1943.
- (50) Association, J. K. *Chronic Kidney Diseases (CKD)*, **2023**. <https://j-ka.or.jp/ckd/>.
- (51) Duranton, F.; Cohen, G.; De Smet, R.; Rodriguez, M.; Jankowski, J.; Vanholder, R.; Argiles, A. Normal and pathologic concentrations of uremic toxins. *J. Am. Soc. Nephrol*, **2012**, *23* (7), 1258-1270.
- (52) Sato, E.; Hosomi, K.; Sekimoto, A.; Mishima, E.; Oe, Y.; Saigusa, D.; Ito, S.; Abe, T.; Sato, H.; Kunisawa, J.; et al. Effects of the oral adsorbent AST-120 on fecal p-cresol and indole levels and on the gut microbiota composition. *Biochem. Biophys. Res. Commun.*, **2020**, *525* (3), 773-779.
- (53) Asai, M.; Kumakura, S.; Kikuchi, M. Review of the efficacy of AST-120 (KREMEZIN®) on renal function in chronic kidney disease patients. *Renal Failure*, **2019**, *41* (1), 47-56.
- (54) Smith, D. *Chronic Kidney Disease: A Global Crisis*. 2018. <https://www.siemens-healthineers.com/en-uk/news/chronic-kidney-disease.html>.
- (55) Niwa, T. Indoxyl sulfate is a nephro-vascular toxin. *J. Ren. Nutr.*, **2010**, *20*, 6.
- (56) Espi, M.; Koppe, L.; Fouque, D.; Thaunat, O. Chronic Kidney Disease-Associated Immune Dysfunctions: Impact of Protein-Bound Uremic Retention Solutes on Immune Cells. *Toxins*, **2020**, *12* (5), 300.
- (57) Yamamoto, S.; Kazama, J. J.; Omori, K.; Matsuo, K.; Takahashi, Y.; Kawamura, K.; Matsuto, T.; Watanabe, H.; Maruyama, T.; Narita, I. Continuous Reduction of Protein-Bound Uraemic Toxins with Improved Oxidative Stress by Using the Oral Charcoal Adsorbent AST-120 in Haemodialysis Patients. *Sci. Rep.*, **2015**, *5* (1), 14381.
- (58) Lee, C.-T.; Hsu, C.-Y.; Tain, Y.-L.; Ng, H.-Y.; Cheng, B.-C.; Yang, C.-C.; Wu, C.-H.; Chiou, T. T.-Y.; Lee, Y.-T.; Liao, S.-C. Effects of AST-120 on Blood Concentrations of Protein-Bound Uremic Toxins and Biomarkers of Cardiovascular Risk in Chronic Dialysis Patients. *Blood Purification*, **2014**, *37* (1), 76-83.
- (59) Kremezin. Kureha Chemical Industry Co. Ltd., <https://www.kureha.co.jp/en/business/chemical/medicine.html>.
- (60) Inagaki, M.; Orikasa, H.; Morishita, T. Morphology and pore control in carbon materials via templating. *RSC Advances*, **2011**, *1* (9), 1620-1640.
- (61) Sakintuna, B.; Yürüm, Y. Templated Porous Carbons: A Review Article. *Ind. Eng. Chem. Res.*, **2005**, *44* (9), 2893-2902.

- (62) Inagaki, M. Pores in carbon materials-importance of their control. *New Carbon Materials* **2009**, *24* (3), 193-232.
- (63) Lee, J.; Kim, J.; Hyeon, T. Recent Progress in the Synthesis of Porous Carbon Materials. *Adv. Mater.*, **2006**, *18* (16), 2073-2094.
- (64) Inagaki, M.; Toyoda, M.; Soneda, Y.; Tsujimura, S.; Morishita, T. Templated mesoporous carbons: Synthesis and applications. *Carbon*, **2016**, *107*, 448-473.
- (65) Liang, C.; Li, Z.; Dai, S. Mesoporous Carbon Materials: Synthesis and Modification. *Angew. Chem. Int. Ed.*, **2008**, *47* (20), 3696-3717.
- (66) Mitome, T.; Uchida, Y.; Egashira, Y.; Hayashi, K.; Nishiura, A.; Nishiyama, N. Adsorption of indole on KOH-activated mesoporous carbon. *Colloids Surf. A*, **2013**, *424*, 89-95.
- (67) Meng, Y.; Gu, D.; Zhang, F.; Shi, Y.; Cheng, L.; Feng, D.; Wu, Z.; Chen, Z.; Wan, Y.; Stein, A.; Zhao, D. A Family of Highly Ordered Mesoporous Polymer Resin and Carbon Structures from Organic–Organic Self-Assembly. *Chem. Mater.*, **2006**, *18* (18), 4447-4464.
- (68) Stuart, M. A. C.; Scheutjens, J. M. H. M.; Fleer, G. J. Polydispersity effects and the interpretation of polymer adsorption isotherms. *J. Polym. Sci.: Poly. Phys. Ed.*, **1980**, *18* (3), 559-573.
- (69) Ferreira, V. H. S.; Moreno, R. B. Z. L. Polyacrylamide Adsorption and Readsorption in Sandstone Porous Media. *SPE Journal*, **2020**, *25* (01), 497-514.
- (70) Moradi, O.; Fakhri, A.; Adami, S.; Adami, S. Isotherm, thermodynamic, kinetics, and adsorption mechanism studies of Ethidium bromide by single-walled carbon nanotube and carboxylate group functionalized single-walled carbon nanotube. *J. Colloid Interface Sci.*, **2013**, *395*, 224-229.
- (71) Dahlgren, D.; Venczel, M.; Ridoux, J. P.; Skjöld, C.; Müllertz, A.; Holm, R.; Augustijns, P.; Hellström, P. M.; Lennernäs, H. Fasted and fed state human duodenal fluids: Characterization, drug solubility, and comparison to simulated fluids and with human bioavailability. *E. J. Pharm. Biopharm.*, **2021**, *163*, 240-251.
- (72) Tran, H. N.; You, S.-J.; Hosseini-Bandegharai, A.; Chao, H.-P. Mistakes and inconsistencies regarding adsorption of contaminants from aqueous solutions: A critical review. *Water Res.*, **2017**, *120*, 88-116.

## Chapter 2

### Analysis of polybenzimidazole adsorption onto carbon materials

#### 2.1 Introduction

Surface modification of carbon materials plays a crucial role in tailoring their properties to suit specific applications or to alter the surface properties such as wettability and reactivity. This modification can improve the functionality of these materials, including the dispersibility in solvents, miscibility with host matrices, and biocompatibility in biological materials<sup>1-5</sup>. Both chemical and physical approaches based on covalent and non-covalent bonding, respectively, have been employed for functionalization. Chemical modifications are frequently utilized owing to their stability<sup>6-9</sup>; however, they can occasionally deteriorate the main characteristics of the surfaces, such as the high surface area, electrical conductivity, and mechanical toughness<sup>10,11</sup>. This is particularly problematic for nanocarbons such as carbon nanotubes and graphene, where chemical modifications can dramatically alter the properties owing to the limited number of carbon layers, often only a single layer<sup>12</sup>. Conversely, a physical modification, typically based on the adsorption of small molecules in a solution, can preserve the surface structure<sup>13-16</sup>, offering a significant advantage. However, physical modifications using small molecules can cause instability owing to the dynamic adsorption/desorption of molecules from the surface<sup>17,18</sup>.

To address this issue, the physical modification method using polymers (polymer coating) has been developed<sup>19</sup>. Polymer adsorption onto solid surfaces is generally an irreversible process, making desorption difficult<sup>20</sup>. Thus, polymer coating provides a more stable functionalization compared to small molecules. Various polymers, including polybenzimidazole (PBI)<sup>21</sup>, polyimide<sup>22,23</sup> and polyvinylpyrrolidone<sup>24</sup>, and polyallylamine<sup>25</sup> have been reported as coating agents. PBI, known as a super engineering plastic, is frequently used, and PBI-coated carbons are utilized as supporting materials for electrocatalysts<sup>26-29</sup>. In this application, PBI acts as an effective anchoring site for the metal nanoparticle loading, addressing the challenge of loading on carbon materials with few anchoring sites, such as highly graphitized carbon (e.g., carbon nanotubes)<sup>30,31</sup>. Despite the various applications of polymer-coated carbon materials, systematic studies regarding adsorption behaviors including the adsorption kinetics, thermodynamics, coverage ratio, and coating thickness remain limited.

In this chapter, we investigated the PBI adsorption behaviour onto various types of carbon black via adsorption isotherm measurements. Three types of carbon black, including Vulcan, Ketjen Black (KB), and Acetylene Black (AB), which have different surface morphologies and chemical compositions, were selected to assess the effect of the surface morphology as well as the chemical composition of the carbon materials for PBI adsorption. The adsorption experiments in the solution were conducted with and without sonication treatment to consider the effect of sonication on adsorption. These findings will significantly contribute to the analysis of polymer adsorption onto carbon materials, for which existing literature is limited to our knowledge.

## 2.2 Materials and Methods

### 2.2.1 Materials used

- ✓ *N, N*-dimethylacetamide (DMAc), Kishida Chemical Co. (Osaka, Japan)
- ✓ *N*-methyl-2-pyrrolidone (NMP), Millipore Sigma (St. Louis, USA)
- ✓ Dimethyl sulfoxide (DMSO), FUJIFILM Wako Pure Chemicals Corp (Tokyo, Japan)
- ✓ Vulcan XC-72R (Vulcan), Cabot Chemicals Co. (Boston, USA)
- ✓ Ketjen black 600JD (KB), Lion Specialty Chemicals Co. (Tokyo, Japan)
- ✓ Acetylene black (AB), Denka Co. (Tokyo, Japan)
- ✓ Poly[2,2'-m-(phenylene)-5,5'-bibenzimidazole] (polybenzimidazole: PBI), Sato Light Industrial Co., Ltd. (Mie, Japan).
- ✓ 1,3-bis(1H-benzo[d]imidazol-2-yl)benzene (PBI-unit) was synthesized via condensation of isophthalic acid and 1,2-phenylenediamine using polyphosphoric acid as a condensation reagent ( from S. Hirata, MS thesis, 2015).

### 2.2.2 Equipment's used

The specific surface area and micropore distribution were determined using the Brunauer–Emmett–Teller (BET) and Horvath–Kawazoe (HK) (applying the carbon–N<sub>2</sub> interaction parameter at 77 K) methods, respectively, based on the N<sub>2</sub> adsorption isotherm measurements (77 K,  $1 \times 10^{-8} < P/P_0 < 1$ ) using a BELSORP-mini (Microtrac BEL, Japan). The dispersion of carbon materials was determined via dynamic light scattering (DLS), which was measured using an ELSZ-2 particle size analysis system (Otsuka Electronics, Osaka Japan).

Raman spectra were obtained by RAMANtouch (Nano photon, Osaka, Japan) at an excitation wavelength of 532 nm using an objective-lens magnification of 20x, diffraction grating of 600 gr/mm, exposure time of 2 s, and 30 integrations. X-ray photoelectron spectroscopy (XPS) was performed using AXIS ULTRA<sup>DLD</sup> (Shimadzu, Kyoto, Japan). AFM (Aligent 5500, Toyo Co., Japan) performed for the images. The UV-vis absorption was detected using V670 (JASCO, Tokyo, Japan), Oven (Eyela, Tokyo, Japan) and Mechanical shaker (AS-ONE, Osaka, Japan) were also used for drying and shaking, respectively.

### 2.2.3 Time course of adsorption

Vulcan (1.0 mg) and 0.01 mg/mL PBI solution (10 mL) in DMAc were shaken at intervals of 10, 30, 60, 120, 180, 240, and 300 min at 200 rpm at 298 K. After removal of the solid using a filter membrane with a pore diameter of 0.2  $\mu\text{m}$  (ADVANTEC), the PBI concentration was measured via UV-vis spectroscopy. The same procedure was applied for the PBI-unit. The overall experimental scheme is summarized in Fig. 2.1.

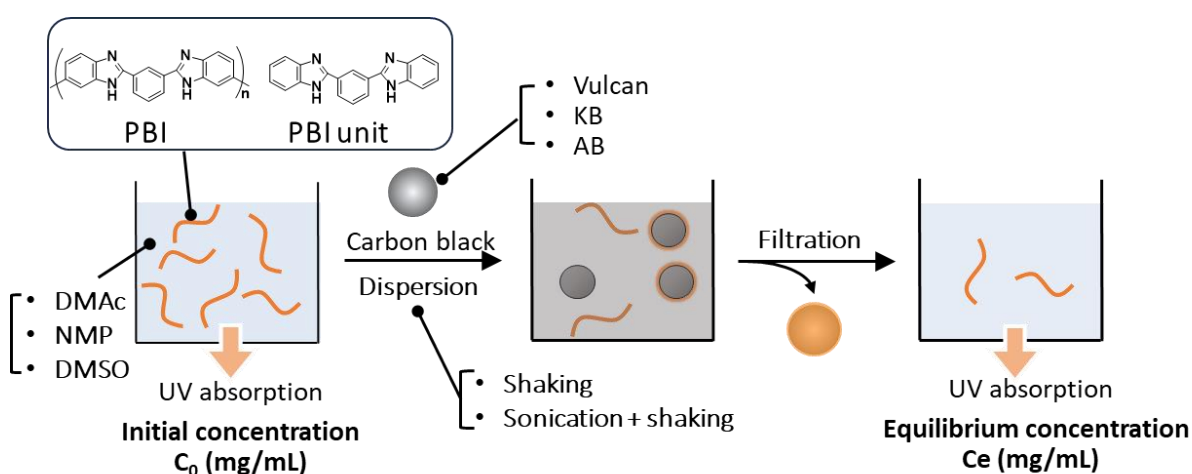


**Fig. 2.1** Experimental scheme of PBI adsorption onto carbon materials.

### 2.2.4 Adsorption experiments

Carbon adsorbents (1 mg) were dispersed in PBI solutions in DMAc (10 mL) with various concentrations (0.003, 0.005, 0.007, 0.01, and 0.015  $\text{mg mL}^{-1}$ ) by sonication for 1 min in a

bath-type sonicator (Branson 5510, Branson), and shaking for 180 min in a mechanical shaker (Neo Shaker, AS ONE) at 200 rpm. After removing the solid using a filter membrane with a pore diameter of 0.2  $\mu\text{m}$  (ADVANTEC), the UV-vis absorption spectra of the obtained filtrate were recorded. The concentration of the PBI in the filtrate solution was calculated based on the PBI absorption (Fig. 2.1 & Fig. 2.2) at a wavelength of 347 nm; the adsorption capacity of PBI ( $\Gamma$  [ $\text{mg mg}^{-1}$ ]) on the adsorbates was calculated according to the following equation:

$$\Gamma = V(C_0 - C_e) / M \dots \dots \dots (\text{Eq. 2.1})$$

Here,  $C_0$  is the initial concentration of PBI ( $\text{mg mL}^{-1}$ ),  $C$  is the concentration of PBI after the filtration ( $\text{mg mL}^{-1}$ ),  $V$  is the volume of the solution (mL), and  $M$  is the amount of the Vulcan (mg). The same procedure was applied for the other adsorbents (KB and AB). The adsorption capacities without sonication were also measured.

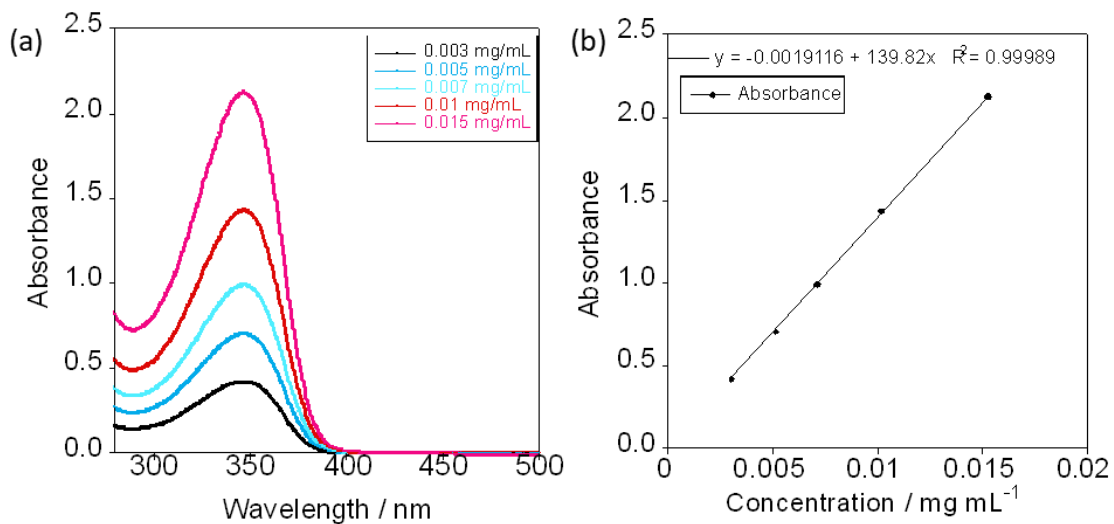


**Fig. 2.2** (a) UV absorption spectra at 347nm of PBI/ DMac (b) Calibration curve of PBI/DMAc.

The Langmuir (Eq. 2.2), Freundlich (Eq. 2.3), and Dubinin-Radushkevich (Eq. 2.4) isotherm models were applied for PBI adsorption.

Langmuir:  $C_e / \Gamma = C_e / \Gamma_{max} + 1 / \Gamma_{max} K_L \dots \dots \dots (\text{Eq. 2.2})$

Freundlich:  $\ln \Gamma = \ln K_f + 1/n (\ln C_e) \dots \dots \dots (\text{Eq. 2.3})$

Dubinin-Radushkevich:  $\ln \Gamma = \ln q_m + \beta \varepsilon^2$  .....(Eq. 2.4)

Where,  $\Gamma$  (mg mg<sup>-1</sup>) is equilibrium adsorption amount,  $C_e$  (mg mL<sup>-1</sup>) is equilibrium concentration,  $K_L$  is Langmuir adsorption constant,  $K_f$  and  $n$  are Freundlich constant which indicates the adsorption capacity and adsorption intensity,  $q_m$  (mg mg<sup>-1</sup>) is the adsorption capacity,  $\beta$  is the activity constant, and  $\varepsilon$  is the Polanyi potential which is expressed by Eq. 2.5.

$$\varepsilon = RT \ln(1 + 1/C_e).....(Eq. 2.5)$$

**2.2.5 Adsorption thermodynamics**

To establish the adsorption standard Gibbs free energy ( $\Delta G$ ), adsorption standard entropy ( $\Delta S$ ), and adsorption standard enthalpy ( $\Delta H$ ) in the adsorption process, the following equations were adopted.

$\Delta G$  (kJ mol<sup>-1</sup>) can be calculated using the Eq. 2.6.

$$\Delta G = -RT \ln K_L.....(Eq. 2.6)$$

Additionally,  $\Delta S$  and  $\Delta H$  were calculated using the van't Hoff equation.

$$\Delta G = \Delta H - T \Delta S.....(Eq. 2.7)$$

$$\ln K_L = \Delta S/R - \Delta H/RT.....(Eq. 2.8)$$

The value of the  $\Delta S$  and  $\Delta H$  were determined based on the plot of  $\ln K_L$  versus  $1/T$ . Here, the values of  $\Delta S$  (J mol<sup>-1</sup> K<sup>-1</sup>) and  $\Delta H$  (kJ mol<sup>-1</sup>) were determined based on those of the slope and intercept, respectively.  $T$  was the absolute temperature (K) and R was the universal gas constant. Langmuir adsorption constant,  $K_L$  was calculated using Eq. 2.2.

**2.3 Results and Discussion**

**2.3.1 Characterization of the carbon materials**

Prior to the adsorption experiments, the surface properties of the carbons were evaluated to determine the differences in Vulcan, KB, and AB). Fig. 2.3 (a-c) presents the N<sub>2</sub> adsorption isotherm (Figs. 2.3a-2.3c), Brunauer–Joyner–Halenda (BJH) plots (Figs. 2.3d-2.3f) of the carbons. According to the IUPAC classification, Vulcan demonstrates a type-II adsorption profile without any hysteresis, indicating that the micropores and mesopores are the main

component (Fig. 2.3a), whereas KB demonstrates a type-IV adsorption profile with hysteresis in the relative pressure range of 0.4 to 0.8, suggesting the presence of a mesopore structure (Fig. 2.3b). Regarding AB, the increase of the N<sub>2</sub> adsorption at a high relative pressure range ( $P/P_0 > 0.8$ ) suggests the enrichment of a large mesopore or micropore (Fig. 2.3c). Based on the adsorption profiles, the surface areas of the Vulcan, KB, and AB were calculated to be 206, 1338, and 59 m<sup>2</sup>g<sup>-1</sup> using the BET method, respectively. The BJH plots demonstrate that both Vulcan (Fig. 2.3d) and KB (Fig. 2.3e) consist of micropores (< 2 nm) and mesopores (2 nm ~ 50 nm), whereas AB only possesses a large mesopore surface (~ 20 nm) (Fig. 2.3f). Their compositions were determined by t-plot method, the values of which are listed in Table 2.1. To investigate the chemical composition of the carbon materials, X-ray photoelectron spectroscopy (XPS) C1s narrow scans and the Raman spectra of the carbons were also analysed. Considering the XPS C1s deconvolution (Fig. 2.3g), the C=C, C-C, C=O, C-O compositions of Vulcan, KB, and AB are shown in Table 2.1. The total contents of the oxygenated functional groups (-C=O and C-O) for KB, Vulcan, and AB were approximately 20%, 10%, 7%, respectively; thus, the degree of surface functional groups was in the order of KB > Vulcan > AB. The atomic composition C/O ratio follows the similar trend. Fig. 2.3h shows the Raman spectra of Vulcan (red line), KB (blue line), and AB (black line). The peaks assigned to the D- and G-bands originating from the defect structure of the carbon materials and the in-plane expansion and contraction of the six-membered ring structure in the graphite structure were observed at approximately 1310 cm<sup>-1</sup> and 1560 cm<sup>-1</sup>, respectively. The G/D ratio, which is often used to evaluate the degree of graphitization, was 0.95, 0.94, and 0.70 for Vulcan, AB, and KB, respectively, indicating that KB possesses a larger amount of sp<sup>3</sup> defects.

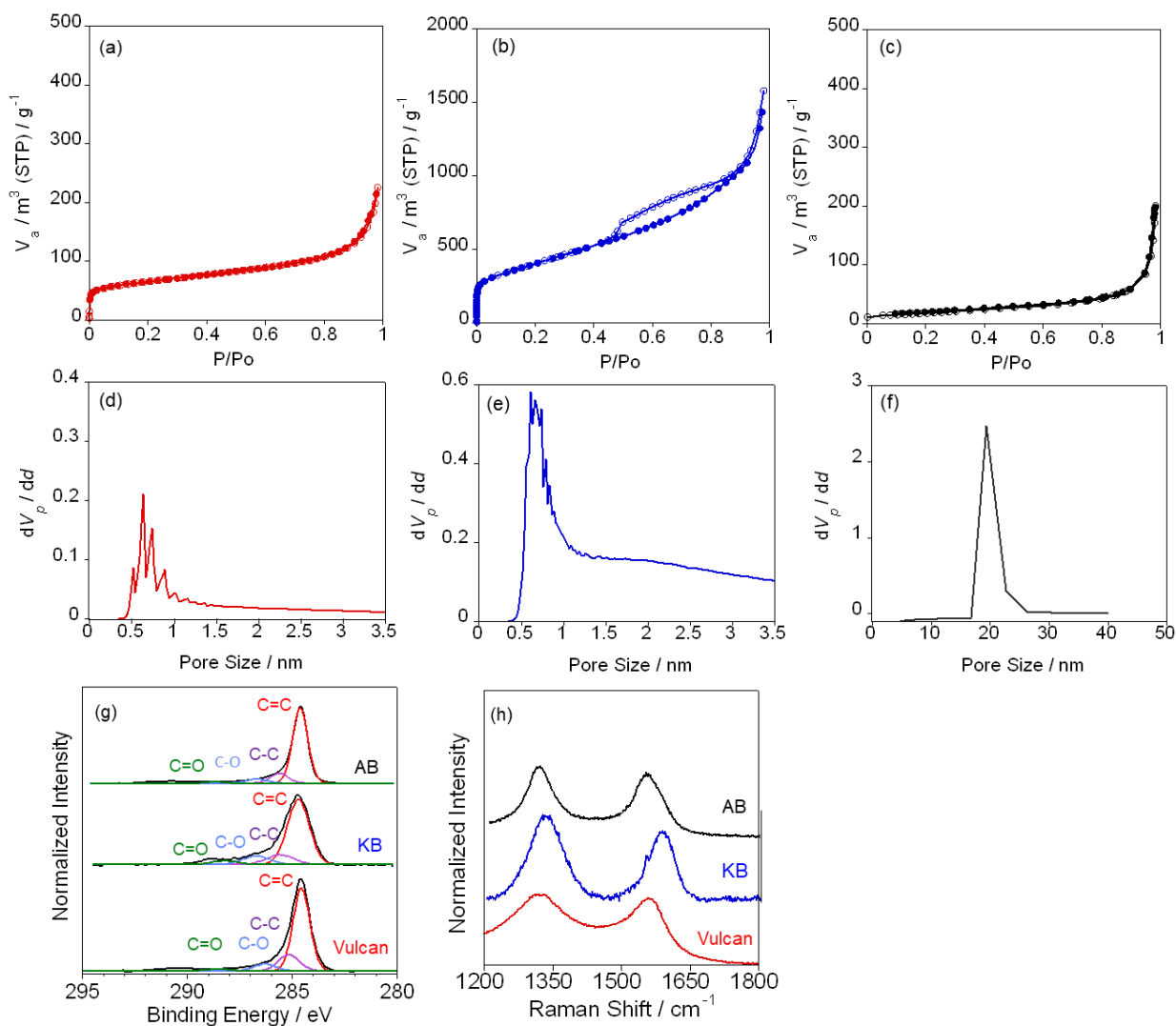


**Fig. 2.3** (a-c)  $N_2$  adsorption/desorption isotherms and (d-f) BJH pore size distribution for (a, d) Vulcan (b, e) KB, and (c, f) AB. (g) XPS C1s deconvolution and (h) Raman spectra of Vulcan, KB, and AB

**Table 2.1** Characterization of carbon materials (Vulcan, KB, and AB).

	BET surface ( $m^2 / g$ )	Micro pores ( $m^2/g$ )	Macro + meso pores ( $m^2/g$ )	XPS C/O ratio			XPS C1s (%)				Raman (G/D)
				C%	O%	C/O	C=C	C-C	C=O	C-O	
Vulcan	206	92	114	98.8	1.2	0.012	68.9	14.3	6.8	3.2	0.95
KB	1338	639	699	97.1	2.9	0.029	66.0	13.3	9.3	11.4	0.70
AB	59	8	51	99.2	0.8	0.008	71.1	15.8	1.9	5.6	0.94

### 2.3.2 Adsorption time course

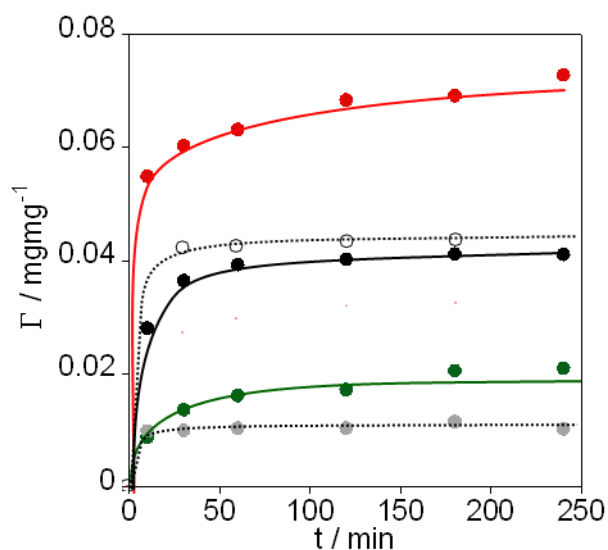


**Fig. 2.4** Time course of PBI adsorption onto Vulcan (black solid), KB (red solid), and AB (green solid) at 298 K; the adsorption time course of PBI with sonication (black open) and that of the PBI-unit (without sonication) onto Vulcan were also plotted (gray solid).

Adsorption time course experiments were conducted to study the time required to reach equilibrium. Fig. 2.4 demonstrates the adsorption time course of the adsorption onto Vulcan (black), KB (red), and AB (green) in DMAc measured at 298 K. The amount of PBI adsorbed on the carbon surface was calculated based on the change of the concentration of PBI solutions before and after the adsorption experiments (see Experimental section), in which the PBI with a molecular weight of  $M_n \sim 15000$  was used. The unit structure of PBI (referred as PBI-unit), that is, 1,3-bis(1H-benzo[d]imidazol-2-yl) benzene, was used as the control and tested to clarify the effect of the polymeric structure. Compared to the PBI-unit that spontaneously reached equilibrium ( $< 1$  h), PBI required more than 60 min to reach the plateau region. A slower adsorption kinetics of the polymer compared to that of the small molecules is characteristic to polymer adsorption<sup>20, 32</sup>. Displacement of the PBI from a lower to higher molecular weight, and/or the slow diffusion process of PBI into the porous surface, may have resulted in the slow adsorption. The three carbons (Vulcan, KB, and AB) showed similar profiles at the early stage ( $< 100$  min); thus, the slow adsorption may have not originated from the slow diffusion into the pore, rather owing to the displacement of the lower molecular weight.

PBI adsorption onto Vulcan was also performed with sonication to consider its effect (open circles in Fig. 2.4), demonstrating that PBI adsorption on Vulcan was greater with sonication. Dynamic light scattering (DLS) observations revealed that the particle size distribution of the Vulcan after sonication was smaller than that without sonication (Fig. 2.5), and for the photos of the dispersions, see Fig. 2.6. Therefore, the higher amount of adsorption observed under sonication was apparently owing to the increase of the accessible surface area by the disassembly of the Vulcan aggregations. The higher adsorption may also be considered to have occurred owing to the higher penetration of the PBI into the Vulcan pores; however, the pore size distribution of the Vulcan with and without sonication was almost comparable (Fig. 2.7), suggesting that the adsorption inside the pore did not change regardless of the sonication treatment.

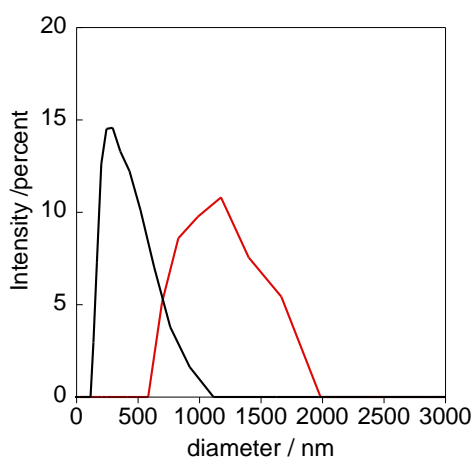


**Fig. 2.5** Diameter distribution of Vulcan in DMAc ( $0.01 \text{ mg mL}^{-1}$ ) treated with (black) and without (red) sonication at 298 K

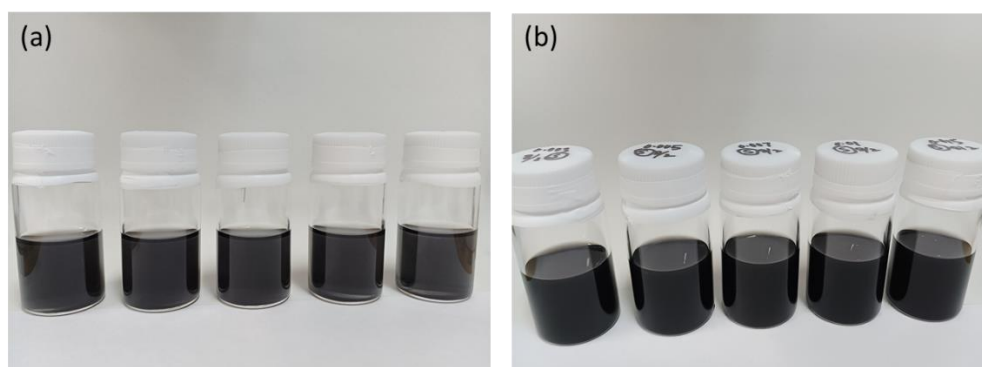


**Fig. 2.6** Dispersion photos of Vulcan in DMAc (a) Shaking (b) Sonication

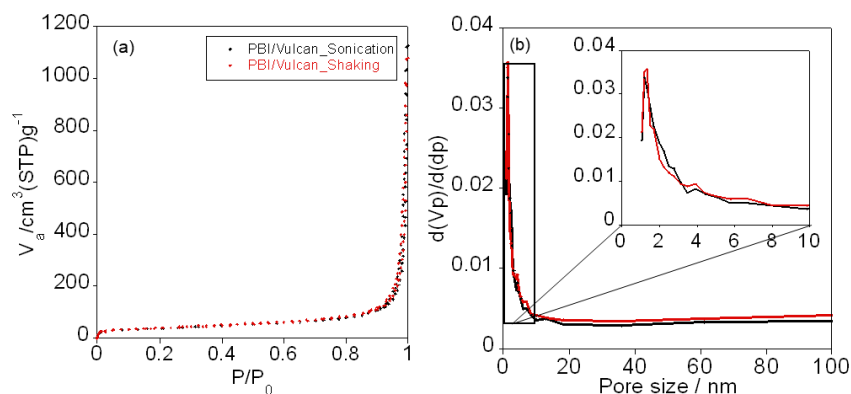


**Fig. 2.7** (a) Adsorption-desorption isotherms of N<sub>2</sub> for Vulcan/PBI with sonication and without sonication treatment (b) Pore distribution of PBI/Vulcan treated with (black) and without (red) sonication at 298 K.

### 2.3.3 Adsorption isotherm of PBI

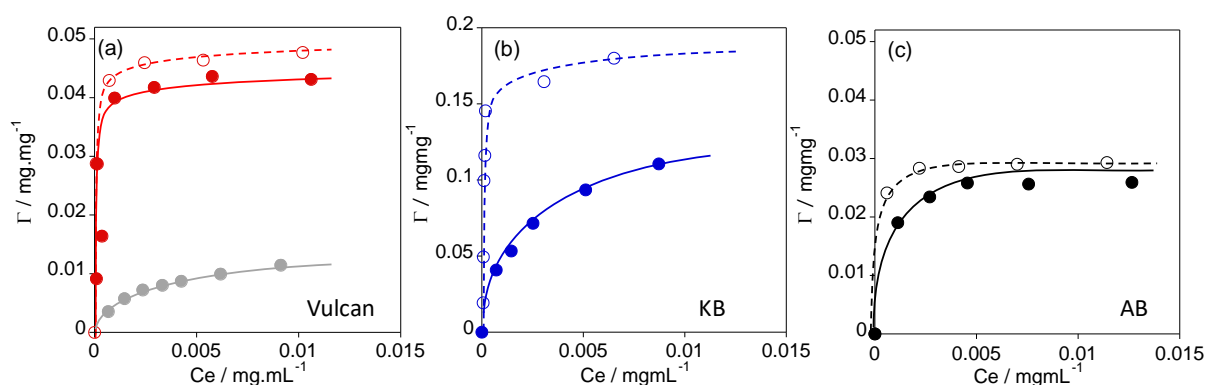


**Fig. 2.8** Adsorption isotherm of PBI onto (a) Vulcan, (b) KB, and (c) AB with (○ open circle) and without (● solid circle) sonication in DMAc at 298 K. The adsorption isotherm of the PBI-unit on Vulcan is also plotted in Fig. (a) (● grey solid circle).

Fig. 2.8 presents the adsorption isotherms of PBI onto Vulcan (Fig. 2.8a), KB (Fig. 2.8b), and AB (Fig. 2.8c) in DMAc treated with (dotted lines) and without (solid lines) sonication at 298 K. The amount of adsorption increases as the concentration of PBI increases. The adsorption isotherm clearly suggests that adsorption reached the plateau at extremely low concentration <

0.01 mg mL<sup>-1</sup>, which is characteristics of the polymer adsorption<sup>32</sup>. For example, for 1.0 mg of Vulcan, only 0.04 mg of PBI was necessary for coating to obtain the maximum adsorption, whereas the PBI monomer did not reach the maximum adsorption range at this concentration (Fig. 2.8a). Therefore, polymer coating can be considered as a highly efficient method as a surface modification technique that does not require an excess amount of coating molecules.

Based on the adsorption isotherms obtained from the adsorption without sonication, the Langmuir (Eq. 2.2), Freundlich (Eq. 2.3), and Dubinin-Radushkevich (Eq. 2.4) isotherm models were applied<sup>33, 34</sup>. The adsorption of PBI onto carbons was the best fitted to the Langmuir isotherm model ( $R^2 > 0.99$ ) (Fig. 2.9 and Table 2.2), similar to the other polymer adsorption systems<sup>32</sup>. The maximum adsorption ( $\Gamma_{max}$ ) and Langmuir constant ( $K_L$ ) were calculated based on the Langmuir model (Table 2.3).

**Table 2.2** Adsorption constants for the adsorption of PBI onto Vulcan, KB and AB at 298K.

Carbon materials	Langmuir		Freundlich			Dubinin-Radushkevich		
	$K_L$	$R^2$	$K_f$	$n$	$R^2$	$\beta$	$qm$	$R^2$
Vulcan	1642.35	0.99	0.24	2.68	0.91	$4.57 \times 10^{-9}$	0.07	0.95
KB	497.94	0.99	0.78	2.46	0.99	$5.54 \times 10^{-9}$	0.24	0.99
AB	2866.05	0.99	0.05	7.85	0.81	$1.19 \times 10^{-9}$	0.03	0.86

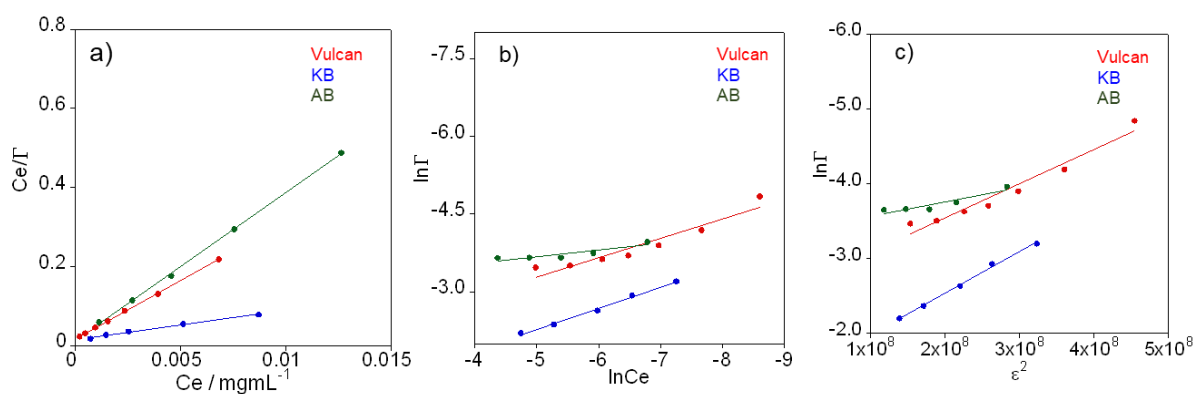


**Fig. 2.9** Adsorption isotherm model plot of PBI onto carbon materials (a) Langmuir (b) Freundlich (c) Dubinin-Radushkevich (D-R) at 298 K

A comparison of the values with and without sonication indicated that both  $\Gamma_{max}$  and  $K_L$  were higher with sonication. The higher  $\Gamma_{max}$  values obtained with sonication indicate the dissociation of the aggregation, as discussed in the aforementioned. Meanwhile, the higher  $K_L$  values obtained when sonication was applied indicate that sonication promotes the adsorption reaction and that adsorption is an irreversible process. For  $K_L$ , the values obtained for both with and without the sonication conditions provided a similar trend of AB > Vulcan > KB. The difference in the surface structure may result in varying adsorption thermodynamics; namely, AB demonstrated to be a superior surface for PBI adsorption. On the other hand, regarding  $\Gamma_{max}$ , the values were in the order of KB > Vulcan > AB for both with and without sonication. The  $\Gamma_{max}$  values demonstrated a similar trend to that of the BET surface area of the carbons measured via nitrogen adsorption: KB ( $1338 \text{ m}^2\text{g}^{-1}$ ) > Vulcan ( $206 \text{ m}^2\text{g}^{-1}$ ) > AB ( $59 \text{ m}^2\text{g}^{-1}$ ). However, the values did not linearly increase as the surface area increased, indicating that the coverage ratio differs based on the carbon type. To evaluate the efficiency of the surface adsorption, a specific adsorption ( $\Gamma_{sp} = \Gamma_{max}/(\text{BET surface area})$ ) was defined. As shown in Table 2.3, for both conditions with and without sonication, AB demonstrated the highest values (0.51 and 0.44), whereas KB demonstrated the lowest (0.13 and 0.09), indicating that the coverage ratio differs based on the carbon type. The results indicate that a surface with small pores does not adsorb PBI most likely owing to the size of the molecules and the difference in the pore size distribution resulting in varying  $\Gamma_{sp}$  values.

Compared to the PBI adsorption, both the  $K_L$  and  $\Gamma_{max}$  values were significantly lower for the PBI-unit adsorption. For small molecules, the dynamic adsorption/desorption lower both the  $K_L$  and  $\Gamma_{max}$  values, whereas high  $K_L$  and  $\Gamma_{max}$  values are possible for polymer adsorption owing to the multipoint interaction between the polymer and adsorbent. The result confirms the superiority of the coating using polymers rather than small molecules.

**Table 2.3** Maximum adsorption ( $\Gamma_{max}$ ), adsorption constant ( $K_L$ ), and specific adsorption ( $\Gamma_{sp}$ ) of PBI adsorption onto carbons with and without (w/o) sonication at 298 K

adsorbate	adsorbent	$\Gamma_{max}$ (mg mg <sup>-1</sup> )		$K_L$		$\Gamma_{sp}$	
		with	w/o	with	w/o	with	w/o
PBI	Vulcan	$4.8 \times 10^{-2}$	$4.0 \times 10^{-2}$	$6.3 \times 10^3$	$1.64 \times 10^3$	0.23	0.19
	KB	$18.0 \times 10^{-2}$	$13.4 \times 10^{-2}$	$4.9 \times 10^3$	$0.50 \times 10^3$	0.13	0.09
	AB	$3.0 \times 10^{-2}$	$2.68 \times 10^{-2}$	$7.9 \times 10^3$	$2.87 \times 10^3$	0.51	0.44
PBI-unit	Vulcan	-	$1.37 \times 10^{-2}$	-	$4.58 \times 10^2$	-	0.06

### 2.3.4 PBI coating of pores

As indicated above, the coverage ratio ( $\Theta$ ) may be different based on the carbon type. To assess the value of  $\Theta$ , we estimated the theoretical amount of PBI adsorption ( $\Gamma_{\text{the}}$ ) based on the thickness of the PBI coating, density of PBI ( $1.33 \text{ mg cm}^{-3}$ )<sup>11</sup>, and BET surface area. To measure the PBI thickness, PBI solution ( $0.01 \text{ mg mL}^{-1}$ ) was incubated on highly oriented pyrolytic graphite (HOPG) as a model substrate of the carbon surface, and atomic force microscope (AFM) measurements were obtained. The AFM image of PBI on HOPG (Fig. 2.10a) clearly demonstrates that the HOPG surface was partially covered by PBI, and the height analysis of the PBI layer revealed that the average thickness was  $0.52 \text{ nm}$  (Fig. 2.10b).

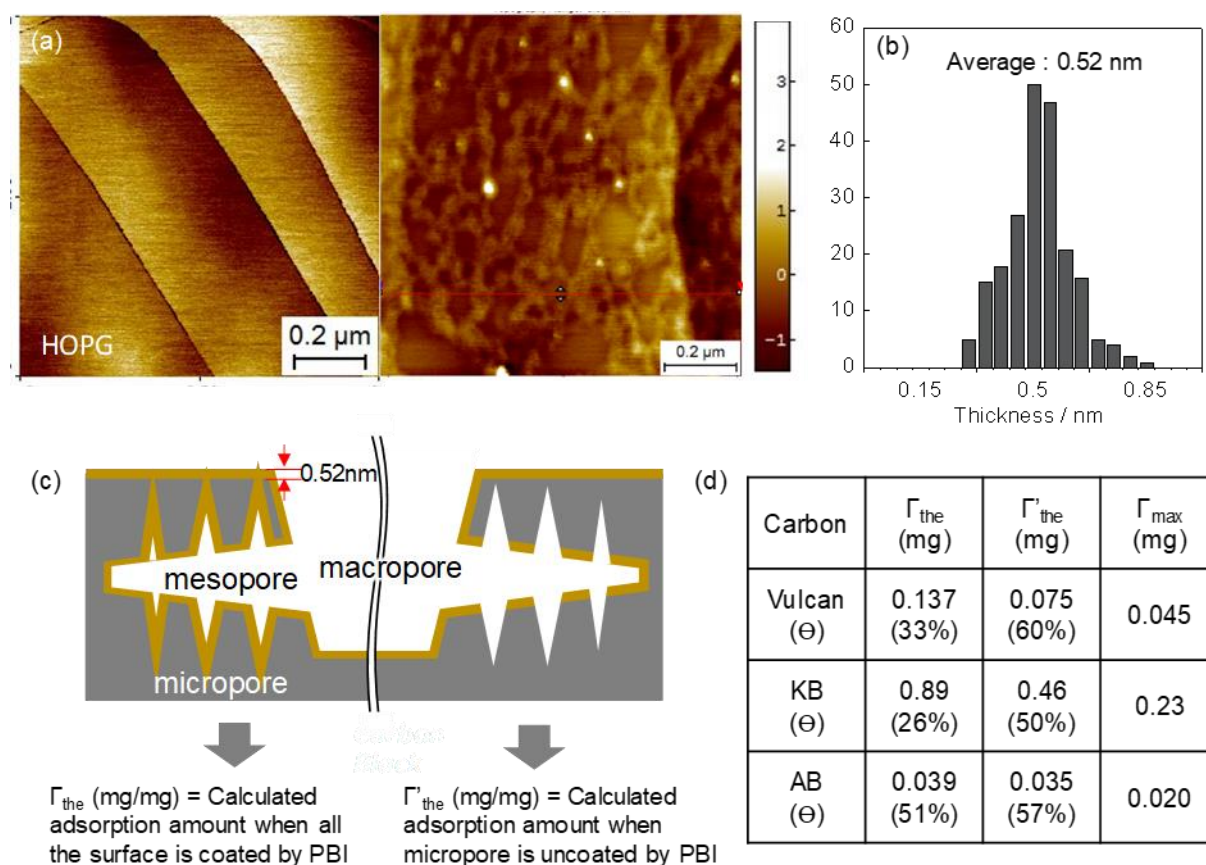


**Fig. 2.10** (a) AFM image of HOPG (left panel) and PBI on HOPG (right panel). (b) Height histogram of the PBI thickness. (c) Illustration of PBI coating situation for the calculations of  $\Gamma_{\text{the}}$  (left side) and  $\Gamma'_{\text{the}}$  (right side). (d) List of  $\Gamma_{\text{the}}$ ,  $\Gamma'_{\text{the}}$ ,  $\Gamma_{\text{max}}$ , and  $\theta$  for PBI adsorption under sonication for Vulcan, KB, and AB, where  $\theta = \Gamma_{\text{max}}/\Gamma_{\text{the}}$  or  $\Gamma_{\text{max}}/\Gamma'_{\text{the}}$ .

The  $\Gamma_{\text{the}}$  values were estimated by assuming that all the surfaces were homogeneously coated by PBI with a thickness of 0.52 nm. In addition,  $\Gamma'_{\text{the}}$  values excluding the micropore surface adsorption ( $\Gamma'_{\text{the}}$ ) were also estimated to consider the difficulty of polymer penetration into the micropores (Fig. 2.10c). We found that the values of  $\Gamma_{\text{max}}$  were even lower than the  $\Gamma'_{\text{the}}$  and  $\Theta$  to  $\Gamma_{\text{the}}$  values for Vulcan, KB, and AB by 33%, 26%, and 51%, respectively, and the values of  $\Theta$  to  $\Gamma'_{\text{the}}$  were 60%, 50%, and 57%, respectively (Fig. 2.10d). PBI diffusion into the micropores and small mesopores is apparently difficult owing to the size of PBI, and a certain amount of the macropore surface remains uncovered. This model sufficiently agreed with our previous results, which demonstrated the large decrease in the micropore surface area after PBI coating based on the  $\text{N}_2$  adsorption isotherm, and capping of the micropore entrance by PBI was proposed<sup>11</sup>. Furthermore, the trend of  $\Theta$  ( $\text{AB} > \text{Vulcan} > \text{KB}$ ) sufficiently agreed with the order of  $K_L$  ( $\text{AB} > \text{Vulcan} > \text{KB}$ ).

### 2.3.5 Effect of temperature on the adsorption

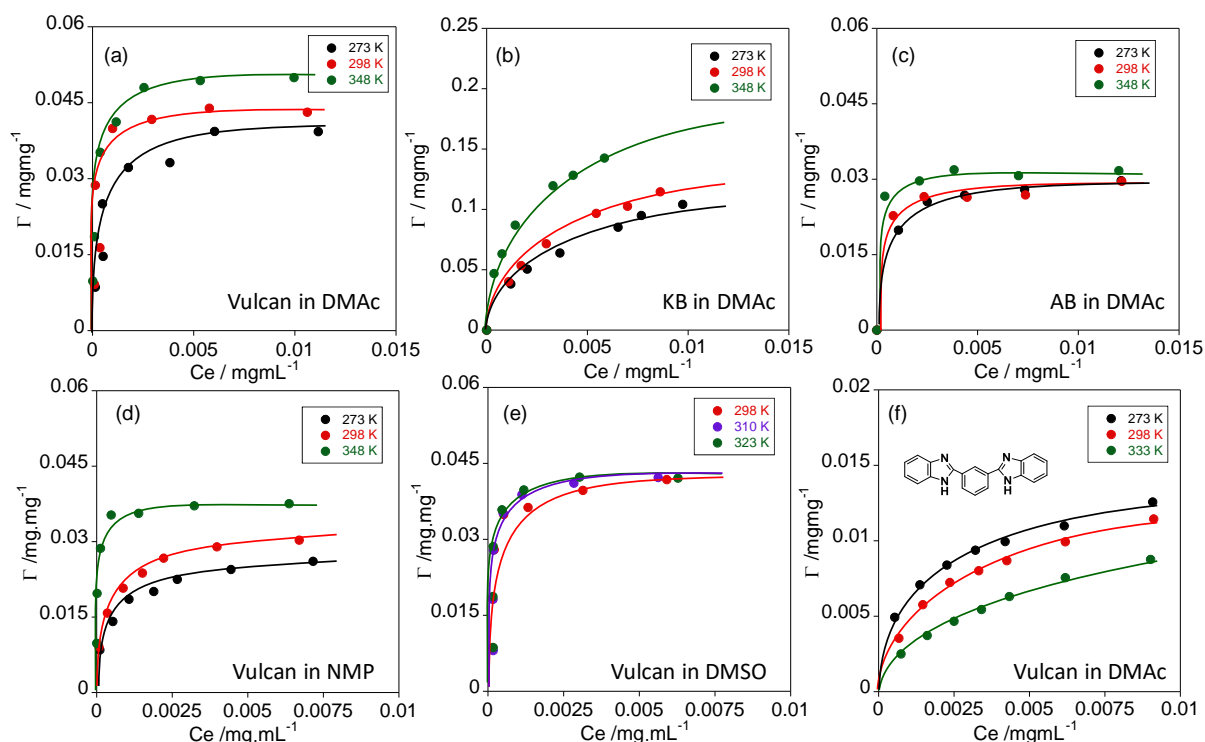


**Fig. 2.11** (Temperature dependent) Adsorption isotherm of PBI for (a) Vulcan, (b) KB, and (c) AB in DMAc. Adsorption isotherm of PBI onto Vulcan in (d) NMP and (e) DMSO (f) Adsorption isotherm of the PBI-unit onto Vulcan

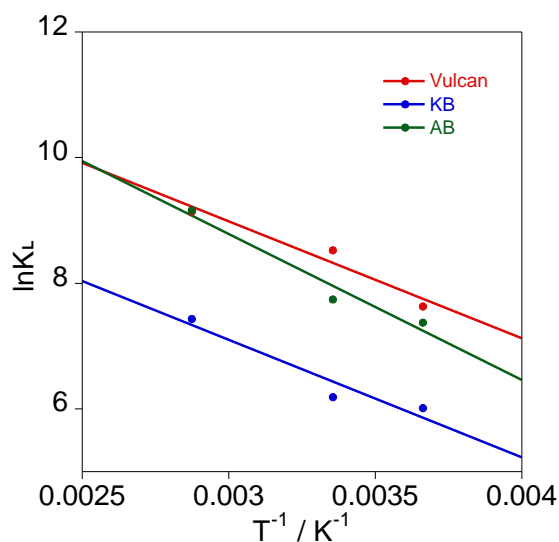
**Fig. 2.11** presents the temperature and solvent dependence isotherms of PBI adsorption onto carbons. For PBI adsorption,  $\Gamma_{\max}$  increased as the temperature increased, indicating that the adsorption is an endothermic process, whereas  $\Gamma_{\max}$  decreased as the temperature increased for the PBI-unit. This entropy-driven adsorption is characteristic to the adsorption of the polymers on the solid surface <sup>35</sup>. For Vulcan, at 348 K,  $\Gamma_{\max}$  ( $4.6 \times 10^{-2}$  mg mg<sup>-1</sup>) reached the value obtained upon sonication treatment at 298 K ( $4.8 \times 10^{-2}$  mg mg<sup>-1</sup>; **Table 2.3**), indicating that the effect of sonication treatment is equivalent to that of a high temperature treatment.

The  $K_L$  value of KB was significantly lower than those of the other two types of carbon black in the order of Vulcan > AB >> KB. Based on the temperature dependency profiles, the  $\Delta G$  values of each adsorption were calculated using the van't Hoff equations ( $\Delta G = -RT \ln K_L$ ) and were confirmed to be  $\Delta G$  negative, verifying that adsorption is a spontaneous reaction <sup>36</sup>.  $\Delta S$  and  $\Delta H$  were calculated based on the plot of  $\ln K_L$  versus  $1/T$  (Fig. 2.12) and the thermodynamic parameter results were shown in Table 2.4. The positive values of  $\Delta H$  for PBI adsorption suggest that the adsorption process is endothermic. The larger values of  $|-T\Delta S|$  compared to  $|\Delta H|$  confirm that the adsorption process is dominated by entropic effects rather than enthalpic effects. The driving force of the PBI adsorption can be explained by the entropy gain from the detachment of the solvated molecules on the carbon surface and PBI, which compensate for the entropy loss originating from the PBI adsorption (loss of freedom of the polymer chain). The trend in  $K_L$  (Vulcan > AB >> KB) can be explained by the difference in the interaction between the carbon surface and solvent molecules. Regarding the higher oxygenated groups for KB, the interaction between the solvent (DMAc) and oxygenated groups on the carbon surface may be superior compared to that of Vulcan/DMAc and AB/DMAc, resulting in the lower  $K_L$  values. Therefore, carbon materials with a lower sp<sup>3</sup> defect (higher crystalline) are superior for PBI adsorption, which was also supported by the result of  $\Theta$  (Fig. 2.10d).

On the other hand, we found that the PBI-unit adsorption is an exothermic (negative  $\Delta H$  value) process, indicating that the interaction between the carbon surface and PBI-unit act as the driving force of the adsorption. The  $\Delta H$  value ( $-11.7$  kJ mol<sup>-1</sup>) was in the range of physical adsorption ( $-20$  to  $40$  kJ mol<sup>-1</sup>) <sup>34</sup>. The significantly lower  $K_L$  value compared to the polymer adsorption indicates the dynamic adsorption/desorption of the PBI-unit onto the carbon surface.

**Table 2.4** Thermodynamic parameters of PBI adsorption onto different carbon materials

Adsorbate	Adsorbent	Solvent	$K_L$			$\Delta G$ (kJ/mol)			$\Delta H$ (kJ/mol)	$\Delta S$ (kJ/mol)	$R^2$
			Temperature (K)			Temperature (K)					
			273	298	348	273	298	348			
PBI	Vulcan	DMAc	2063	5027	9358	-17.3	-21.1	-26.5	15.4	0.12	0.95
		NMP	2040	2650	2990	-17.6	-19.5	-28.5	38.2	0.19	0.96
		DMSO	3560 (298 K)	3450 (310 K)	4530 (333 K)	-20.3 (298 K)	-21.0 (310 K)	-23.3 (333 K)	6.35	0.08	0.98
	KB	DMAc	407	486	1687	-13.6	-15.3	-21.5	15.5	0.10	0.92
	AB	DMAc	1592	2300	9515	-16.7	-19.2	-26.5	19.3	0.13	0.96
PBI-unit	Vulcan	DMAc	711	458	284	-14.9	-15.2	-15.6	-11.7	0.01	0.99

**Fig. 2.12** Plot of  $1/T$  vs  $\ln K_L$  for Vulcan (red), KB (blue) and AB (green).

The adsorption in a solution is complex owing to balancing between the solute-solvent, solute-surface, and surface-solvent interactions. To study the effect of solvents for the adsorption thermodynamics, the adsorption isotherms were also obtained in NMP and DMSO without sonication, the results of which are displayed in Fig. 2.11d and Fig. 2.11e, respectively. In both cases,  $\Gamma_{\max}$  increased as the temperature increased, demonstrating that the adsorption reaction is entropy driven. We found that the  $K_L$  value of NMP is lower than that of DMAc, but that of

DMSO is significantly higher than DMAc ( $K_L$ : DMSO  $\gg$  DMAc  $>$  NMP). This trend can be explained by the difference of the PBI-solvent interaction. To estimate the affinity between the solvents and PBI, the solubility parameter ( $R_a$ ) values were calculated based on the Hansen parameters of the PBI and solvents<sup>37</sup>, where a smaller  $R_a$  value suggests a stronger interaction<sup>38</sup>. The  $R_a$  values between PBI and NMP, DMAc, and DMSO were 8.97, 10.7, and 11.6, respectively. This trend sufficiently agreed with that of  $K_L$  (DMSO  $>$  DMAc  $>$  NMP). Because the interaction between DMSO and PBI is weak, the solvated molecules can easily detach between DMSO and PBI, indicating that the entropy driven PBI adsorption on the carbon surface is superior. The various  $R_a$  values may also explain the difference in  $\Gamma_{max}$ . In a solvent with a low affinity such as DMSO, PBI may form a globular structure and adsorb on the carbon surface with a more packed structure, leading to a higher  $\Gamma_{max}$  for DMSO.

## 2.4 Summary of the chapter 2

The adsorption phenomenon of polybenzimidazole (PBI) in an organic solvent onto different carbon materials (Vulcan, KB, and AB) with varying surface morphologies and chemical compositions was studied to assess the effects of the pore structure and degree of graphitization. The interactions among the polymer-solvent-carbon interface, surface crystallinity, and porous morphology played vital roles in the PBI adsorption mechanism and kinetics. Our study clearly demonstrated the superiority of the polymer coating compared to the small-molecule coating in terms of the coating efficiency and stability. The PBI adsorption on the carbon materials followed the Langmuir isotherm model, where carbon black with a higher graphitization demonstrated higher  $K_L$  values and coverage ratios. The temperature-dependent analysis revealed that PBI adsorption is an entropy-driven process. Therefore, the higher  $K_L$  and coverage ratio for AB (with its  $sp^2$ -rich surface) can be explained by the weaker interaction between the solvent molecules and graphitized surface, leading to a higher entropy gain upon PBI adsorption. A similar scenario applies when different solvents are used. Solvents with weaker interactions with PBI (e.g., PBI/DMSO) provide greater  $K_L$  values, leading to a higher entropy gain upon PBI adsorption. The Hansen parameters provided a good indication of the adsorption behavior between the polymer and carbon surface. Overall, these findings significantly contribute to the understanding of polymer adsorption on carbon materials, which is rarely addressed in current literature.

## 2.5 References

- (1) Prithi, J. A.; Vedarajan, R.; Ranga Rao, G.; Rajalakshmi, N. Functionalization of carbons for Pt electrocatalyst in PEMFC. *Int. J. Hydrogen Energy*, **2021**, *46* (34), 17871-17885.
- (2) Worsley, K. A.; Kalinina, I.; Bekyarova, E.; Haddon, R. C. Functionalization and Dissolution of Nitric Acid Treated Single-Walled Carbon Nanotubes. *J. Am. Chem. Soc.*, **2009**, *131* (50), 18153-18158.
- (3) Khodabakhshi, S.; Fulvio, P. F.; Andreoli, E. Carbon black reborn: Structure and chemistry for renewable energy harnessing. *Carbon*, **2020**, *162*, 604-649.
- (4) Jariwala, D. H.; Patel, D.; Wairkar, S. Surface functionalization of nanodiamonds for biomedical applications. *Mat. Sci. Eng. C*, **2020**, *113*, 110996.
- (5) Chapter 8 Chemical modification of silica: applications and procedures. Vansant, E. F., Van Der Voort, P., Vrancken, K. C. Eds.; Vol. 93; Elsevier, **1995**, 149-192.
- (6) Xue, P.; Bao, Y.; Li, Q.; Wu, C. Impact of modification of carbon black on morphology and performance of polyimide/carbon black hybrid composites. *Phy. Chem. Chem. Phy.*, **2010**, *12* (37), 11342-11350.
- (7) Amornwachirabodee, K.; Tantimekin, N.; Pan-In, P.; Palaga, T.; Pienpinijtham, P.; Pipattanaboon, C.; Sukmanee, T.; Ritprajak, P.; Charoenpat, P.; Pitaksajjakul, P.; et al. Oxidized Carbon Black: Preparation, Characterization and Application in Antibody Delivery across Cell Membrane. *Sci. Rep.*, **2018**, *8* (1), 2489.
- (8) Kang, S.; Jones, A. R.; Moore, J. S.; White, S. R.; Sottos, N. R. Microencapsulated Carbon Black Suspensions for Restoration of Electrical Conductivity. *Adv. Funct. Mater.*, **2014**, *24* (20), 2947-2956.
- (9) Oe, N.; Hosono, N.; Uemura, T. Revisiting molecular adsorption: unconventional uptake of polymer chains from solution into sub-nanoporous media. *Chem.Sci.*, **2021**, *12* (38), 12576-12586.
- (10) Le, V. T.; Ngo, C. L.; Le, Q. T.; Ngo, T. T.; Nguyen, D. N.; Vu, M. T. Surface modification and functionalization of carbon nanotube with some organic compounds. *Adv. Nat. Sci: Nanosci. Nanotechnol.*, **2013**, *4* (3), 035017.
- (11) Fujigaya, T.; Hirata, S.; Berber, M. R.; Nakashima, N. Improved Durability of Electrocatalyst Based on Coating of Carbon Black with Polybenzimidazole and their Application in Polymer Electrolyte Fuel Cells. *ACS Appl. Mater. Interfaces*, **2016**, *8* (23), 14494-14502.

- (12) Tasis, D.; Tagmatarchis, N.; Bianco, A.; Prato, M. Chemistry of Carbon Nanotubes. *Chem. Rev.*, **2006**, *106* (3), 1105-1136.
- (13) Ju, S.-Y.; Utz, M.; Papadimitrakopoulos, F. Enrichment Mechanism of Semiconducting Single-Walled Carbon Nanotubes by Surfactant Amines. *J. Am. Chem. Soc.*, **2009**, *131* (19), 6775-6784.
- (14) Chen, R. J.; Zhang, Y.; Wang, D.; Dai, H. Noncovalent Sidewall Functionalization of Single-Walled Carbon Nanotubes for Protein Immobilization. *J. Am. Chem. Soc.*, **2001**, *123* (16), 3838-3839.
- (15) Chen, J.; Liu, H.; Weimer, W. A.; Halls, M. D.; Waldeck, D. H.; Walker, G. C. Noncovalent Engineering of Carbon Nanotube Surfaces by Rigid, Functional Conjugated Polymers. *J. Am. Chem. Soc.*, **2002**, *124* (31), 9034-9035.
- (16) Fujigaya, T.; Nakashima, N. Methodology for Homogeneous Dispersion of Single-walled Carbon Nanotubes by Physical Modification. *Polym. J.*, **2008**, *40* (7), 577-589.
- (17) Petrie, K.; Docoslis, A.; Vasic, S.; Kontopoulou, M.; Morgan, S.; Ye, Z. Non-covalent/non-specific functionalization of multi-walled carbon nanotubes with a hyperbranched polyethylene and characterization of their dispersion in a polyolefin matrix. *Carbon*, **2011**, *49* (10), 3378-3382.
- (18) Wu, G.; Asai, S.; Sumita, M.; Yui, H. Entropy Penalty-Induced Self-Assembly in Carbon Black or Carbon Fiber Filled Polymer Blends. *Macromolecules*, **2002**, *35* (3), 945-951.
- (19) Roy, N.; Sengupta, R.; Bhowmick, A. K. Modifications of carbon for polymer composites and nanocomposites. *Prog. Polym. Sci.*, **2012**, *37* (6), 781-819.
- (20) Flerer, G. J.; Lyklema, J. *Adsorption of Polymers*; Academic Press, **1983**.
- (21) Fujigaya, T. Development of polymer-wrapping methods for functionalization of carbon materials. *Polym. J.*, **2023**, *55* (3), 181-191.
- (22) Sezer Hicyilmaz, A.; Celik Bedeloglu, A. Applications of polyimide coatings: a review. *SN Appl. Sci.*, **2021**, *3* (3), 363.
- (23) Fujigaya, T.; Kim, C.; Matsumoto, K.; Nakashima, N. Effective anchoring of Pt-nanoparticles onto sulfonated polyelectrolyte-wrapped carbon nanotubes for use as a fuel cell electrocatalyst. *Polym. J.*, **2013**, *45* (3), 326-330.
- (24) Yoo, J.; Lee, S.; Lee, C. K.; Kim, C.; Fujigaya, T.; Park, H. J.; Nakashima, N.; Shim, J. K. Homogeneous decoration of zeolitic imidazolate framework-8 (ZIF-8) with core-shell structures on carbon nanotubes. *RSC Advances*, **2014**, *4* (91), 49614-49619.

- (25) Rivadulla, F.; Mateo-Mateo, C.; Correa-Duarte, M. A. Layer-by-Layer Polymer Coating of Carbon Nanotubes: Tuning of Electrical Conductivity in Random Networks. *J. Am. Chem. Soc.*, **2010**, *132* (11), 3751-3755.
- (26) Fujigaya, T.; Nakashima, N. Fuel Cell Electrocatalyst Using Polybenzimidazole-Modified Carbon Nanotubes As Support Materials. *Adv. Mater.*, **2013**, *25* (12), 1666-1681.
- (27) Fujigaya, T.; Nakashima, N. Non-covalent polymer wrapping of carbon nanotubes and the role of wrapped polymers as functional dispersants. *Sci. Technol. Adv. Mater.*, **2015**, *16* (2), 024802.
- (28) Wu, J.-F.; Lo, C.-F.; Li, L.-Y.; Li, H.-Y.; Chang, C.-M.; Liao, K.-S.; Hu, C.-C.; Liu, Y.-L.; Lue, S. J. Thermally stable polybenzimidazole/carbon nano-tube composites for alkaline direct methanol fuel cell applications. *J. Power Sources*, **2014**, *246*, 39-48.
- (29) Fujigaya, T.; Hirata, S.; Nakashima, N. A highly durable fuel cell electrocatalyst based on polybenzimidazole-coated stacked graphene. *J. Mater. Chem. A*, **2014**, *2* (11), 3888-3893.
- (30) Okamoto, M.; Fujigaya, T.; Nakashima, N. Design of an Assembly of Poly(benzimidazole), Carbon Nanotubes, and Pt Nanoparticles for a Fuel-Cell Electrocatalyst with an Ideal Interfacial Nanostructure. *Small*, **2009**, *5* (6), 735-740.
- (31) Berber, M. R.; Fujigaya, T.; Sasaki, K.; Nakashima, N. Remarkably Durable High Temperature Polymer Electrolyte Fuel Cell Based on Poly(vinylphosphonic acid)-doped Polybenzimidazole. *Sci. Rep.*, **2013**, *3* (1), 1764.
- (32) Parfitt, G. D.; Rochester, C. H. *Adsorption from Solution at the Solid/Liquid Interface*; Academic Press, **1983**.
- (33) Inyinbor, A. A.; Adekola, F. A.; Olatunji, G. A. Kinetics, isotherms and thermodynamic modeling of liquid phase adsorption of Rhodamine B dye onto *Raphia hookeri* fruit epicarp. *Water Res. and Ind.*, **2016**, *15*, 14-27.
- (34) Wang, W.; Zheng, B.; Deng, Z.; Feng, Z.; Fu, L. Kinetics and equilibriums for adsorption of poly(vinyl alcohol) from aqueous solution onto natural bentonite. *Chem. Eng. J.*, **2013**, *214*, 343-354.
- (35) Zhang, B.; Shi, W.; Yu, S.; Zhu, Y.; Zhang, R.; Tay, J. H. Adsorption of anion polyacrylamide from aqueous solution by polytetrafluoroethylene (PTFE) membrane as an adsorbent: Kinetic and isotherm studies. *J. Colloid Interface Sci.*, **2019**, *544*, 303-311.
- (36) Moradi, O.; Fakhri, A.; Adami, S.; Adami, S. Isotherm, thermodynamic, kinetics, and adsorption mechanism studies of Ethidium bromide by single-walled carbon nanotube and carboxylate group functionalized single-walled carbon nanotube. *J. Colloid Interface Sci.*, **2013**, *395*, 224-229.

- (37) Zuaznabar-Gardona, J. C.; Fragoso, A. Determination of the Hansen solubility parameters of carbon nano-onions and prediction of their dispersibility in organic solvents. *J. Mol. Liq.*, **2019**, *294*, 111646.
- (38) Süß, S.; Sobisch, T.; Peukert, W.; Lerche, D.; Segets, D. Determination of Hansen parameters for particles: A standardized routine based on analytical centrifugation. *Adv. Powder Technol.*, **2018**, *29* (7), 1550-1561.

## Chapter 3

### Selective adsorption of indole onto mesoporous carbon in an aqueous system

#### 3.1 Introduction

Chronic kidney disease (CKD) is indeed a significant global health issue, affecting millions of people worldwide. CKD can result from various factors, including hypertension, diabetes, and glomerulonephritis, among others. One of the critical aspects of CKD is the accumulation of uremic toxins in the bloodstream due to the kidneys' reduced ability to filter waste products effectively<sup>1,2</sup>. The overall function of the renal system (kidney, ureters, and urethra) is to filter human body fluid from the renal blood flow, which allows for toxins, metabolic waste products, and excess ions to be excreted while maintaining essential substances in the blood. Progression of CKD leads to the accumulation of uremic toxins in the circulation and tissues, cardiovascular damage, mineral and bone disorders, and muscle wasting and so on<sup>3</sup>. Regarding renal failure, indole comes from diet induced tryptophan by intestinal bacteria is metabolized to generate harmful indoxyl sulfate (IS) or *p*-cresol sulfate in the liver<sup>4,5</sup>. Dialysis treatment has been applied for CKD patients, especially when the CKD stage worsens, such as when the estimated glomerular filtration rate (eGFR) is less than 15 mL/min, normally for a kidney function loss of approximately 85 to 90%. However, dialysis has some side effects, such as skin or blood infection, fatigue, and muscle cramps; occasionally, it is inefficient for strong protein binders, like *p*-cresol, even with large mesoporous exchange membranes<sup>6</sup>. Therefore, the removal of uremic toxins by adsorbents has been performed using carbon-based materials and zeolites as adsorbents to protract the time to start hemodialysis and enhance uremic signs<sup>3,6-8</sup>. As a target of uremic toxins, indole, the precursor of IS, has attracted attention because the direct removal of IS is difficult owing to its strong protein binding<sup>8,9</sup>. Porous carbon materials such as Kremezin (AST-120), Merckmezin, and Mylan have been widely used as carbon-based adsorbents because of their high surface area (>2300 m<sup>2</sup>/g for AST-120), which leads to a high adsorption capacity<sup>2,10</sup>. In particular, AST-120 has been the most frequently used and extensively studied<sup>2</sup>. However, these adsorbents cause loss of appetite and severe constipation due to the high daily dose (6–9 g per day<sup>11</sup>), together with non-specific capture of essential amino acids<sup>5</sup>. Therefore, improvements in both the adsorption capacity and selectivity for indole adsorption are highly required. The modification of porous carbon materials has been investigated to improve the indole adsorption capacity and selectivity in aqueous systems.

Mitome *et.al.* reported a pioneering study in which KOH-activated mesoporous carbon (MC) with a uniform pore size (4–7 nm) had a higher capacity and selectivity for indole adsorption than AST-120 in a buffer solution and artificial intestinal juice solution, owing to the size selectivity of the MC<sup>12</sup>. However, they carried out a time-course adsorption study (0–20 min) with only a low concentration (0.1 mg/mL) of indole and did not investigate both kinetics and thermodynamics. In addition, the adsorption selectivity of amino acids remained unclear.

In this chapter, we systematically compared the indole adsorption on MC and AST-120, in which carbon black (Ketjen black, KB) with a wide pore size range was also used to clarify the effect of pore size uniformity. Adsorption isotherms were measured at various concentrations (0.05–0.5 mg/mL) at 310 K. In addition, selectivity studies were performed in the presence of various amino acids at different concentration ratios [amino acid]/[indole] = 0–24. Although a higher indole adsorption capacity was realized at a low concentration (<0.1 mg/mL), the excellent selectivity of MC at a high amino acid concentration ratio of [amino acid]/[indole] > 5 was newly observed.

## 3.2 Materials and method

### 3.2.1 Materials used

- ✓ Second fluid for dissolution test (99% H<sub>2</sub>O, 0.7% KH<sub>2</sub>PO<sub>4</sub> and 0.09% NaOH, pH=6.8), Fujifilm Wako Pure Chemical (Tokyo, Japan).
- ✓ Indole (special grade), Fujifilm Wako Pure Chemical (Tokyo, Japan).
- ✓ L-tryptophan (99%), Fujifilm Wako Pure Chemical (Tokyo, Japan).
- ✓ L-alanine (99%), Fujifilm Wako Pure Chemical (Tokyo, Japan).
- ✓ L-isoleucine, Peptide Institute, Inc. (Osaka, Japan).
- ✓ L-proline, Peptide Institute, Inc. (Osaka, Japan).
- ✓ L-glycine (99%), Fujifilm Wako Pure Chemical (Tokyo, Japan).
- ✓ L-leucine (99%), Fujifilm Wako Pure Chemical (Tokyo, Japan).
- ✓ L-valine (99%), Fujifilm Wako Pure Chemical (Tokyo, Japan).
- ✓ L-phenylalanine (special grade), Fujifilm Wako Pure Chemical (Tokyo, Japan).
- ✓ Triethyl orthoacetate (1<sup>st</sup> grade), Fujifilm Wako Pure Chemical (Tokyo, Japan).
- ✓ Hydrogen chloride (HCl), Fujifilm Wako Pure Chemical (Tokyo, Japan).
- ✓ Formaldehyde solution, Fujifilm Wako Pure Chemical (Tokyo, Japan).
- ✓ Ethanol (99.5%), Fujifilm Wako Pure Chemical (Tokyo, Japan).

- ✓ Pluronic (R) F-127, Sigma-Aldrich (Missouri, USA).
- ✓ Acetonitrile (HPLC grade), Sigma-Aldrich (Missouri, USA).
- ✓ Phenol, Kishida Chemical Co. Ltd. (Osaka, Japan)
- ✓ Resorcinol, Tokyo Chemical Industries Co. Ltd. (Tokyo, Japan).
- ✓ Ketjen black (KB), Cabot Chemicals Co. Ltd. (Boston, USA)
- ✓ AST-120 (Kremezin), Mitsubishi Tanabe Pharma Co. Ltd. (Osaka, Japan).

### 3.2.2 Equipment's used

Small angle X-ray scattering (SAXS) measurements were carried out using NANO-Viewer (Rigaku, Tokyo, Japan) using Cu-K $\alpha$  radiation (40 mV, 30 mA). The samples on a Cu grid (NP-C15, Oken Shoji Co., Ltd. Tokyo, Japan) were observed via scanning transmission electron microscopy (SEM; SU9000, Hitachi High-Tech, Tokyo, Japan), at an acceleration voltage of 30 kV. Raman spectra were obtained using RAMANtouch (Nanophoton, Osaka, Japan) at an excitation wavelength of 532 nm using an objective lens magnification (20 $\times$ ), diffraction grating (600 gr/mm), exposure time (2 s), and number of integrations (30 times). X-ray photoelectron spectroscopy (XPS) was performed using AXIS ULTRA<sup>DLD</sup> (Shimadzu, Kyoto, Japan). Nitrogen gas adsorption measurements were performed using BELSORP-max (Microtrac BEL, Osaka, Japan) at 77 K, where the Brunauer–Joyner–Halenda (BJH), t-plot method using non-graphitized carbon black (NGCB) as a standard data and Brunauer–Emmett–Teller (BET) methods were applied to the adsorption isotherm to calculate the average pore diameter, surface area composition and total surface area, respectively. High performance liquid chromatography (HPLC) was performed using SCL-10AVP (Shimadzu, Kyoto, Japan) with an acetonitrile/water mixture and reversed phase C18 column (Shiseido, Tokyo, Japan) as a mobile phase (5 minutes at 20% acetonitrile and 5 minutes at 80% acetonitrile) and column, respectively, at a column temperature of 40 °C and a flow rate of 1.0 mL/min (detection wavelength: 268 nm). Oven (Eyela, Tokyo, Japan) and Mechanical shaker (AS-ONE, Osaka, Japan) were also used for drying and shaking, respectively. UV-vis absorption was detected using a V670 spectrophotometer (JASCO, Tokyo, Japan).

### 3.2.3 Synthesis of mesoporous carbon (MC)

Fig. 3.1 are shown the procedure of MC preparation. In a mixture of Milli-Q water (4.35 mL), ethanol (7.37 mL), and 5 M HCl (0.46 mL), 1.65 g resorcinol was dissolved at room

temperature in a 50 mL round bottom flask. Pluronic(R)F-127 (0.95 g) was then added to the mixture and stirred for 1 h to obtain a homogeneous solution. Then, 1.25 mL of formaldehyde (37 wt. %), and 1.35 mL triethyl orthoacetate were added and stirred for 3 h at 30 °C to prepare the precursor solution. The solution was transferred to a PTFE Petri dish and aged for 24 h at room temperature to allow the formation of a light-yellow and transparent ethanolic phase. After sedimentation of the light-yellow phase, the precursor was heated at 105 °C in an oven for 12 h to dry. The carbonization of the dried precursor was carried out in a tubular furnace at 400 °C (3 h), and then at 800 °C (6 h) under an N<sub>2</sub> atmosphere (flow rate: 400 sccm) at a heating rate of 1 °C/min. The obtained powder was pulverized for 2 h (200 rpm) using a planetary micro mill, Pulverisette 7 (FRITSCH, Germany), and ZrO<sub>2</sub> balls with a diameter of 1 cm were used to obtain the final MC (0.43 g).

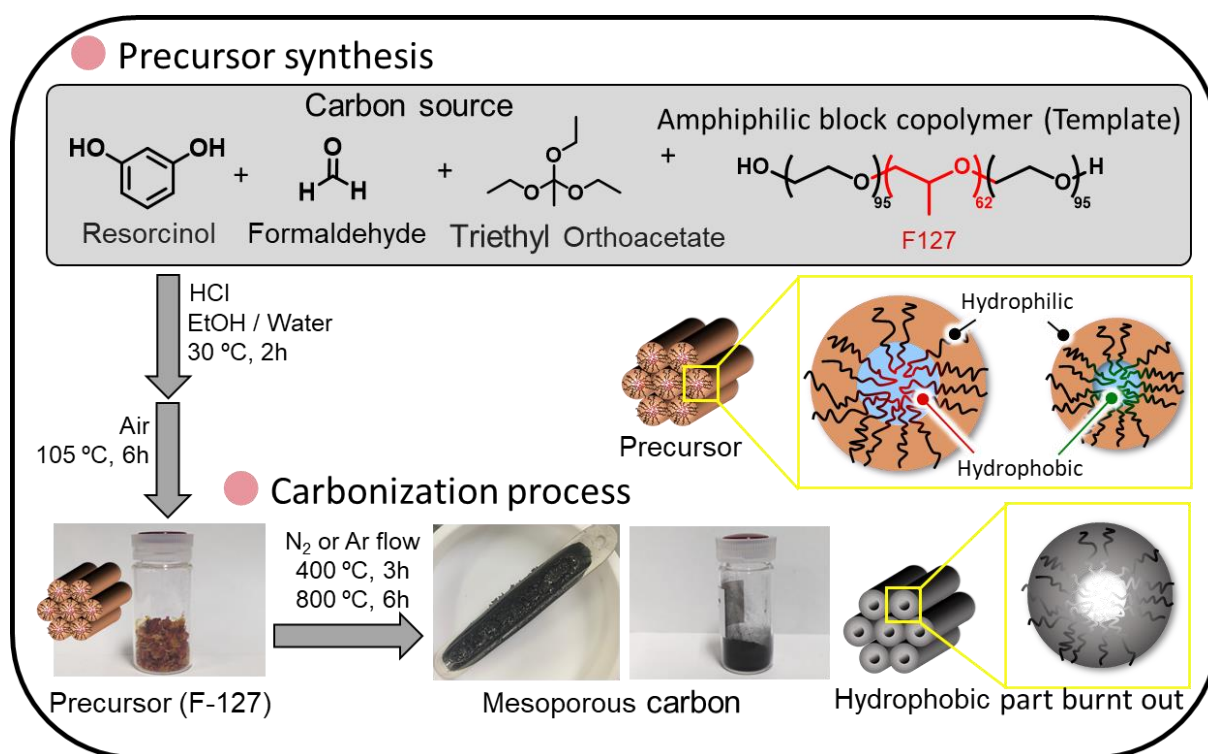


**Fig. 3.1** Synthesis procedure of mesoporous carbon

### 3.2.4 Process of adsorption isotherm of indole

The second fluid for dissolution solutions (10 mL) of indole with different concentrations (0.05–0.5 mg/mL) were added to 2.0 mg of MC and, then the mixtures were shaken for 5 h (120 rpm) at 310 K to obtain equilibrium. After the removal of the MC using a PTFE syringe filter (pore diameter; 0.2 μm, Millipore), UV absorbance at 268 nm (Fig. 3.2) was recorded to

calculate the equilibrium solute concentration ( $C_e$ : mg/mL). The equilibrium adsorption amount ( $\Gamma$ : mg/mg) was calculated by Eq. 5, using the adsorbent mass ( $M$ : mg), total amount ( $V$ : mL), initial concentration ( $C_0$ : mg/mL), and  $C_e$  (mg/mL). The measured values were plotted  $C_e$  vs.  $C_e/\Gamma$  and fitted based on Langmuir equation, and the maximum adsorption amount per monolayer ( $\Gamma_{max}$ : mg/mg) was estimated by Eq. 3.2, where  $K_L$  was the Langmuir constant<sup>13</sup>. The adsorption isotherms for tryptophan and phenylalanine were obtained using the same procedure. The same procedure was applied to the AST-120, and KB was used as the reference.

$$\Gamma = (C_0 - C_e) V / M \dots \dots \dots \text{(Eq. 3.1)}$$

$$C_e / \Gamma = C_e / \Gamma_{max} + 1 / \Gamma_{max} K_L \dots \dots \dots \text{(Eq. 3.2)}$$

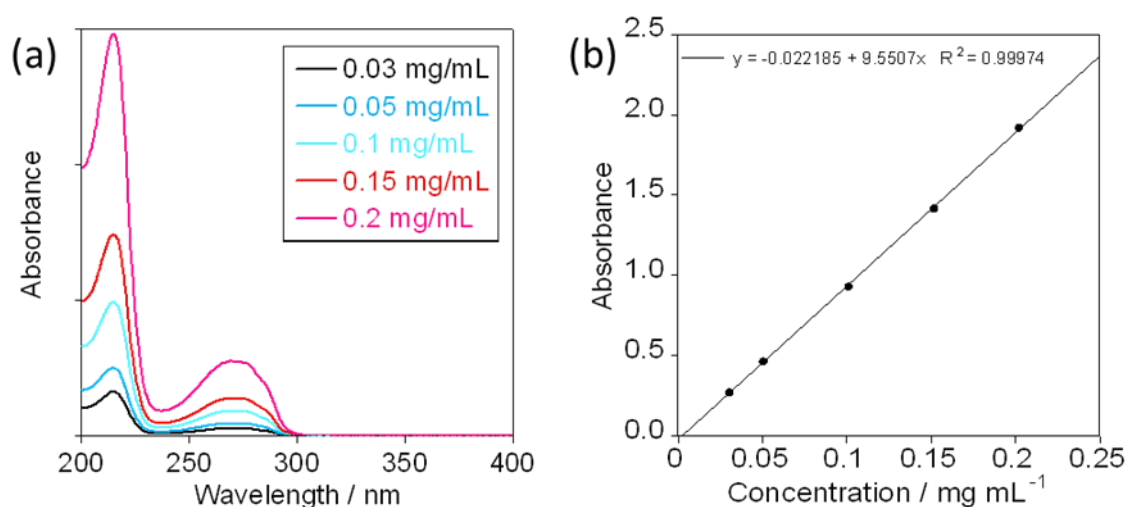


**Fig. 3.2** (a) UV-vis adsorption spectra of indole solutions in phosphate buffer at different concentration and (b) calibration curve obtained from the UV-vis spectra.

### 3.2.5 Competitive adsorption of indole in presence of amino acids

An amino acids mixture in a second fluid for dissolution test solution containing glycine, alanine, leucine, isoleucine, valine, phenylalanine, proline, and tryptophan was mixed with indole solutions, to prepare 2.0 mL indole solutions (0.002 mM of indole, 0.54 mg/mL) with different amino acid concentrations (0, 1.16, 5.80, 17.4, 27.8 mM of amino acids) (Fig. 3.3a), corresponding to [amino acid]/[indole] values of 0, 1, 5, 15, and 24. To these solutions, 1.0 mg of MC was added, and the mixtures were shaken in a temperature-controlled shaker at 120 rpm under 310 K for 5 h. MC was removed by filtration using a PTFE filter (pore diameter; 0.2  $\mu$ m), and the resulting filtrate was subjected to HPLC measurements. The indole concentration

was calculated from the area of the peak with a retention time of 6.2 minutes (Fig. 3.4b) based on the calibration curve, and the adsorption rate of indole was determined. The adsorption ratio was calculated using Eq. 3.3 where  $C_0$  (mg/mL) and  $C_e$  (mg/mL) are the initial and equilibrium indole concentrations, respectively.

$$\text{Adsorption ratio (\%)} = (C_0 - C_e / C_0) \times 100 \dots\dots\dots (\text{Eq. 3.3})$$

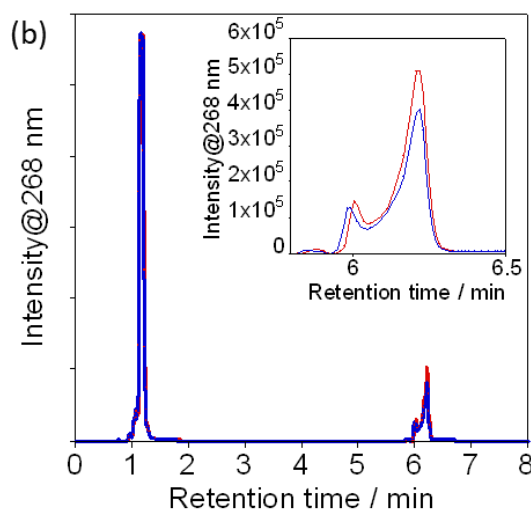
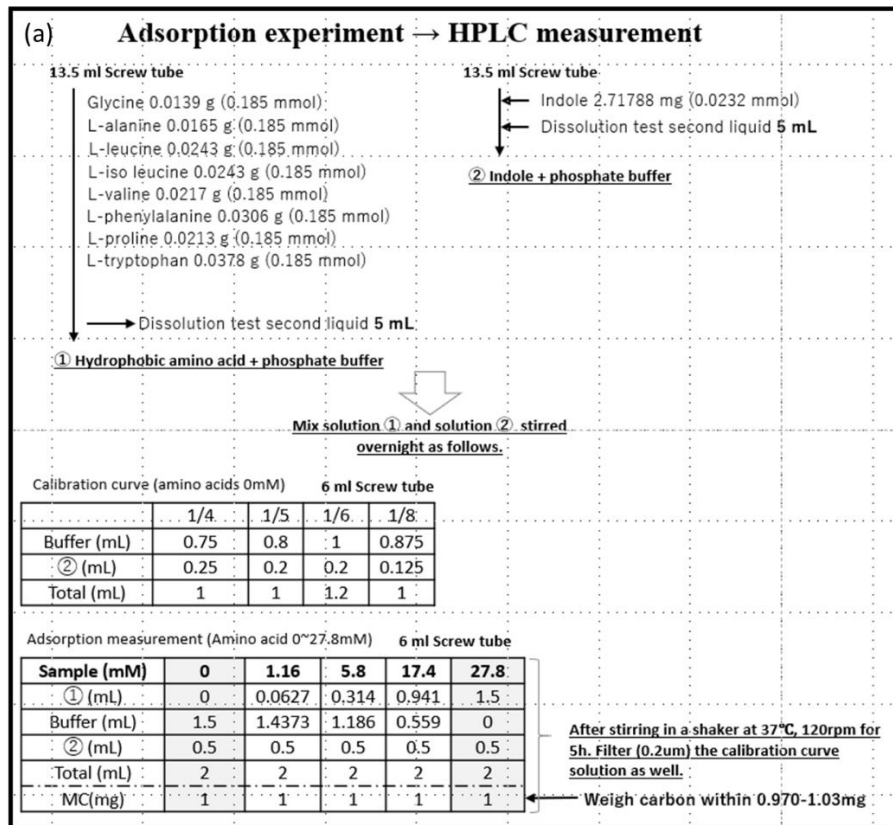


**Fig. 3.3** (a) Experimental procedure of indole adsorption in a mixed amino acid (b) HPLC profile of the solutions monitored with 268 nm.

### 3.2.6 MD simulation

Molecular dynamics (MD) simulations were conducted to assess the penetration and adsorption of tryptophan and indole into the pores on the surface of carbon materials. The initial structures were created and the molecular dynamics (MD) calculations were performed using Schrödinger's Maestro [Schrödinger Release 2022-3: Maestro, Schrödinger, Llc, New York, Ny, 2021.]. A graphite slab model of A-B stacking was created for eight graphene sheets in a  $6.8 \times 6.8 \times 10 \text{ nm}^3$  calculation cell. The vacuum region in the calculation cell was filled with 15,000 molecules of water and eight molecules of tryptophan (or indole). In the pre-processing stage of MD calculations, the density was relaxed and equilibrium calculations were performed using the MD Multistage Workflow built into Maestro. In the production run, NPAT (constant normal pressure, surface area and temperature) calculations were performed for 150 ns at 310.0 K and 1.013 bar. The time step was set to 2 fs, with data recorded at 100 ps intervals. Three calculations were conducted under identical conditions, each with a different initial velocity. The MD engine employed was Desmond<sup>14</sup>, while the force field used was OPLS\_2005<sup>15</sup>.

## 3.3 Results and discussion

### 3.3.1 Structural characterization

MC was prepared by a soft templating method using resorcinol and amphiphilic surfactant as a carbon source and template, respectively (Fig. 3.1)<sup>16-18</sup>. In the SEM images of MC (Fig. 3.4a), small holes were observed in the MC that originated from the decomposition of the templates<sup>19</sup>, whereas a rough surface with much smaller holes was observed for AST-120 (Fig. 3.4b, for lower magnification SEM images, see Fig. 3.5). In contrast, KB was an aggregation of small primary particles with a diameter of approximately 50 nm (Fig. 3.4c). The ordered structure was characterized using SAXS. The SAXS profiles of MC shown in Fig. 3.4d show an intense peak and three weak peaks in the range of  $0.2 \text{ nm}^{-1}$  to  $2 \text{ nm}^{-1}$ , which can be indexed as (110), (200), (211), (220) Bragg reflections of the body centered cubic space group ( $Im\bar{3}m$ )<sup>20</sup>. These diffraction peaks reflect the mild regular structure of the pores and similar types of MC patterns to those reported by Li *et. al*<sup>21</sup>. The unit cell size was determined as 22.7 nm. Nitrogen gas adsorption was measured to characterize the surface morphologies of the carbon materials, for which the profiles are shown in Fig. 3.4e. According to the IUPAC classification, MC and KB show type-IV adsorption profiles where hysteresis in the relative pressure range of 0.4 to 0.8

originates from the mesopore structure, whereas AST-120 shows a type I-b adsorption profile with a large micropore structure area. Based on the adsorption profile, surface area was calculated using the BET method and it was found that MC, AST-120 and KB had BET surface areas of 795, 2150 and 1422 m<sup>2</sup>/g, respectively. The values for MC <sup>16, 22</sup>, AST-120 <sup>12</sup> and KB <sup>23</sup> were very close to the reported values. The pore size distributions obtained using the BJH method are plotted in Fig. 3.4f. The pore diameter of MC was approximately 3.1 nm, which almost agreed with the SEM observations, whereas no characteristic mesopores were observed for AST-120 and KB. For AST-120, it was reported that pores ranging from 0.5 - 400 nm <sup>10, 12</sup> were formed and a broad range of pores from 0.5 to 50 nm were observed in KB. Based on t-plot method (Fig. 3.4f), surface area composition of MC, AST-120 and KB were analysed (Table 3.1), verifying AST-120 has micropore-enriched structure, while MC and KB possess mesopore surface. The pore size distributions in mesopore region were analyzed based on BJH method for MC and KB (Fig. 3.4g) <sup>24-26</sup>. The pore diameter of MC was approximately 3.1 nm, which consistent with the SEM observations, whereas no characteristic mesopores were observed for KB. The surface areas of the micropores and mesopores of MC, AST-120, and KB are summarized in Table 3.1.

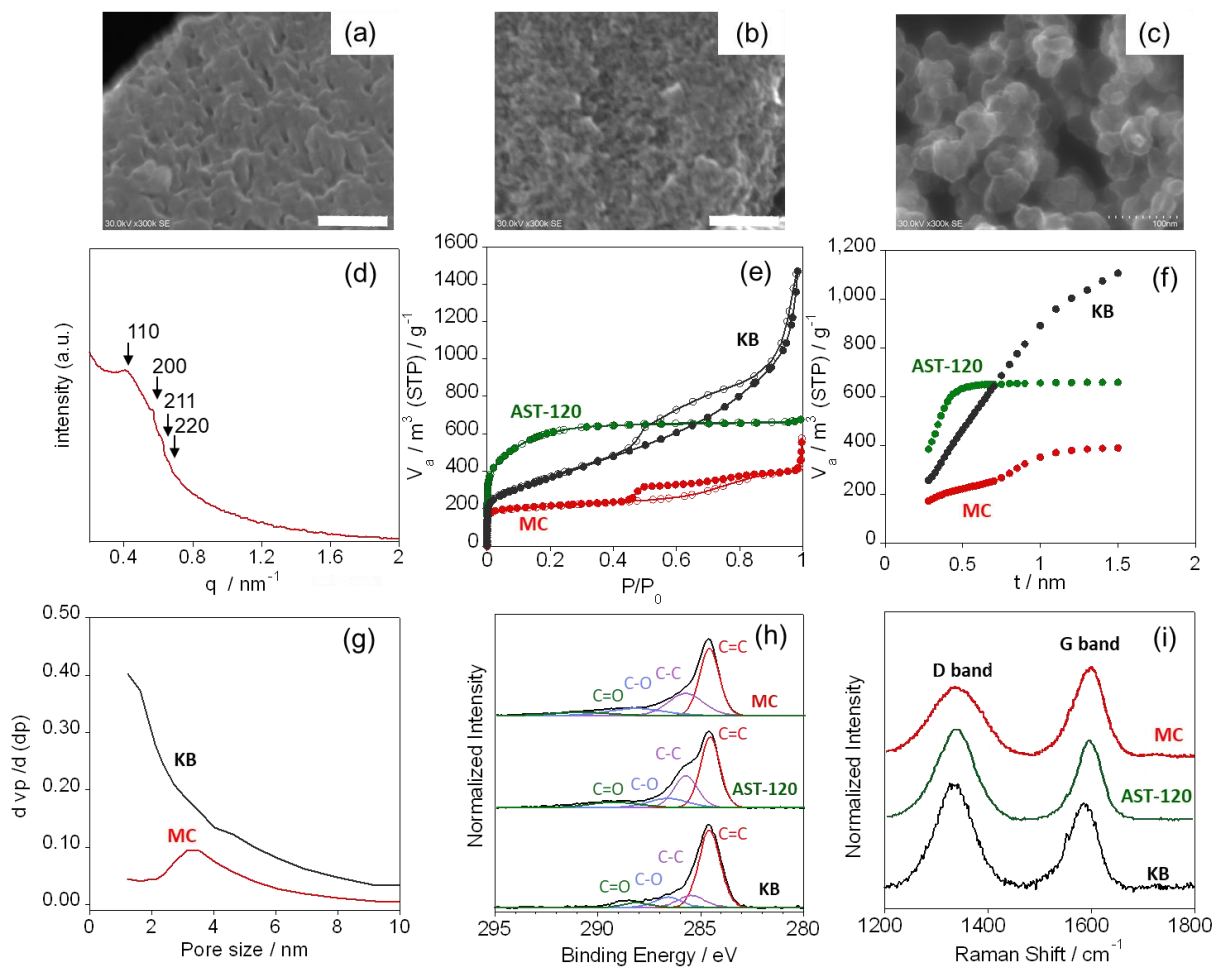


**Fig. 3.4** SEM images of (a) MC (b) AST-120 (c) KB at the same magnification. Scale bars: 100 nm (d) SAXS pattern of MC (e) Nitrogen adsorption/desorption isotherm of MC (red), AST-120 (green), and KB (black) (f) t-plots of the MC (red), AST-120 (green), and KB (black) (g) BJH plots for MC (red) and KB (black) (h) C 1s narrow scan of MC, AST-120, and KB; Deconvolution results are also shown (i) Raman spectra of MC (red), AST-120 (green), and KB (black).

**Table 3.1.** List of nitrogen adsorption results, C1s XPS deconvolution data, and Raman G/D ratios for MC, AST-120, and KB

Carbon materials	N <sub>2</sub> adsorption					XPS C1s (%)				Raman
	Specific surface (m <sup>2</sup> /g) <sup>a</sup>	Micropore surface (m <sup>2</sup> /g) <sup>b</sup>	Mesopore surface (m <sup>2</sup> /g) <sup>b</sup>	External surface (m <sup>2</sup> /g) <sup>b</sup>	Pore diameter (nm) <sup>c</sup>	C=C	C-C	C=O	C-O	G/D
MC	795	503	253	39	3.1	48.9	28.9	7.2	14.8	0.9
AST-120	2150	2101	17		-	47.8	26.2	13.1	12.9	0.6
KB	1422	818	589		-	66.0	13.3	9.3	11.4	0.7

a. Calculated by BET method, where  $P/P_0 = 0.01\sim 0.12$ ,  $0.01\sim 0.2$  and  $0.01\sim 0.25$  were used for the fitting for MC, AST-120 and KB, respectively.

b. Calculated by t-plot method

c. Calculated by BJH method

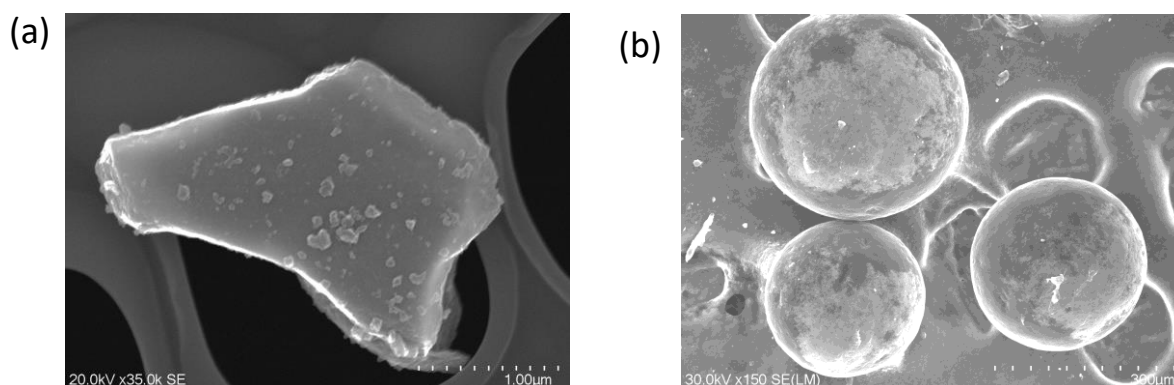


**Fig. 3.5** SEM images of (a) MC and (b) AST-120 at low magnification.

The chemical compositions of the carbon materials were analyzed using XPS and Raman spectroscopy. The C = C, C-C, C-O, and C=O compositions of MC inferred from the XPS C1s spectra were 48.9%, 28.9%, 14.8%, and 7.2%, respectively, while the corresponding ratios for AST-120 were 47.8%, 26.2%, 12.9%, and 13.1% , and for KB were 66.0%, 13.3%, 11.4%, and 9.3% (Fig. 3.4h and Table 3.1). Judging from the total content oxygenated functional groups (C=O and C-O), three of them contain almost 20%; and we assume a similar chemical composition for the carbons. Fig. 3.4i shows the Raman spectra of MC (red line), AST-120

(green line), and KB (black line). The peaks attributed to the D band and G band originating from the defect structure of the carbon material and in-plane expansion and contraction of the six-membered ring structure in the graphite structure were observed at  $1308\text{ cm}^{-1}$  and  $1583\text{ cm}^{-1}$ , respectively, clearly indicating the formation of the carbonized materials. The G/D ratio, which is often used to evaluate the degree of graphitization for MC (G/D = 0.9), was similar to those of AST-120 (G/D = 0.6) and KB (G/D = 0.7), supporting the similarity of the surface chemical structures of these carbons.

### 3.3.2 Indole adsorption isotherms

Adsorption isotherms for indole on MC, AST-120, and KB are shown in Fig. 3.6a. These show the relationship between the equilibrium adsorption amount  $\Gamma$  (mg/mg) and the equilibrium concentration  $C_e$  (mg/mL) per unit mass of the adsorbent at 310 K. The adsorption isotherms of tryptophan (Fig. 3.6b) and phenylalanine (Fig. 3.6c) were also obtained to investigate the adsorption selectivity. Interestingly, indole adsorption reached a plateau at low concentrations for MC ( $< 0.1\text{ mg/mL}$ ), while AST-120 and KB showed a gradual increase upon increasing the concentration and greater indole adsorption amount in the high concentration region. Based on the categorization by Giles et al.,<sup>27</sup> the isotherm profile of MC can be classified as “high affinity (Type-H),” while those for AST-120 and KB can be classified as “Langmuir-type (Type-L).” To further analyze the adsorption at equilibrium conditions, the isotherm profiles were fitted to representative adsorption models, including the Freundlich, Dubinin–Radushevich (D-R), and Langmuir models (see Fig. 3.7). For MC, the Langmuir model showed an  $R^2$  value of 0.99, while the Freundlich and D-R models had lower values of 0.94 and 0.98, respectively. The same trend was observed for the AST-120 and KB as well. Therefore, indole adsorption on carbon materials is a monolayer adsorption on a homogeneous surface, there is no interaction between indole molecules, and all adsorption sites have equal energy.

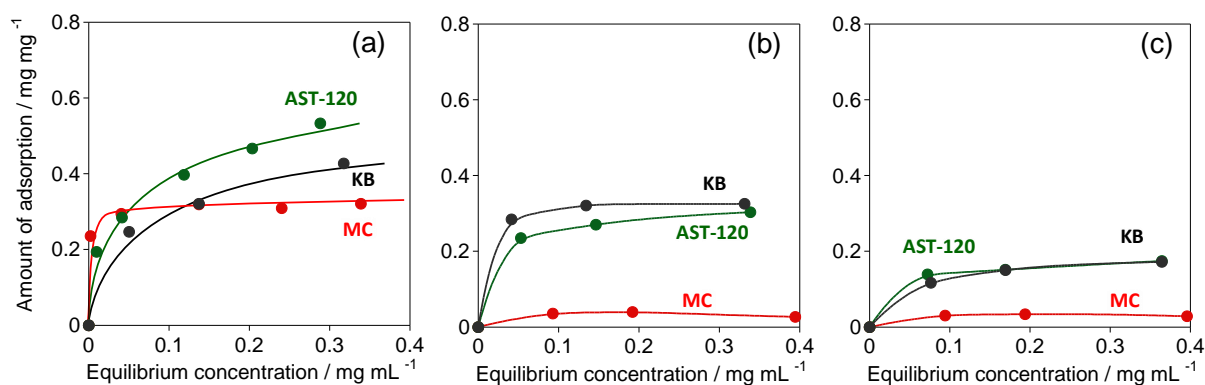
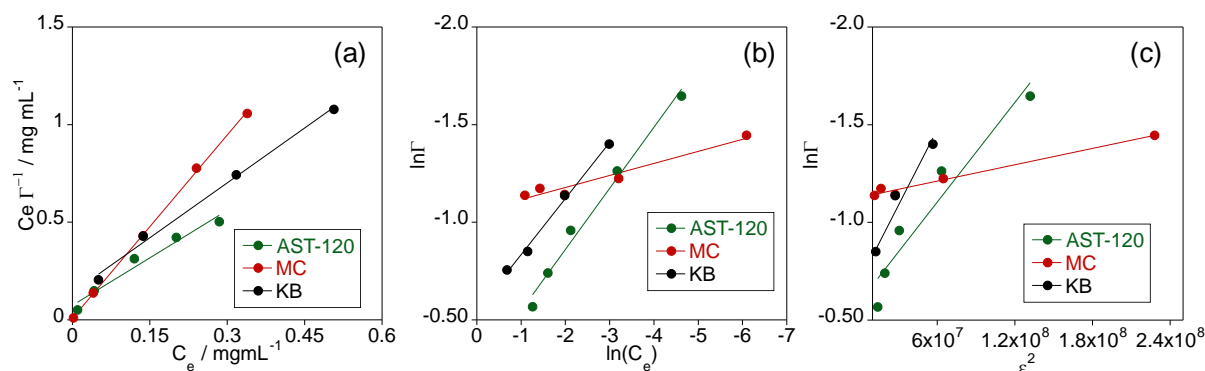


Fig. 3.6 Adsorption isotherms of (a) indole, (b) tryptophan, and (c) phenylalanine for MC (red), AST-120 (green), and KB (black) measured at 310 K.



**Fig. 3.7** Fitting of indole adsorption onto MC (red), AST-120 (green) and KB (black) in phosphate buffer at 310 K for (a) Langmuir model, (b) Freundlich model and (c) Dubinin-Radushkevich (D-R) model.

The model fitting result facilitates the estimation of the maximum adsorption capacity ( $\Gamma_{\max}$ ), and Langmuir constant ( $K_L$ ) (Table 3.2).  $\Gamma_{\max}$  values for MC, AST-120, and KB were 0.319, 0.575, and 0.445 mg/mg, respectively. Evidently, a carbon material with larger BET surface area provides a higher  $\Gamma_{\max}$  of indole. This trend does not match the results reported by Mitome et al.<sup>12</sup>, in which MC showed greater indole adsorption. Our results indicate that the greater indole adsorption of MC, in the previous reports<sup>12</sup> was because the adsorption was measured only at the initial concentration of 0.1 mg/mL, where MC showed higher adsorption.

**Table 3.2**  $\Gamma_{\max}$ ,  $K_L$ , and specific adsorption of indole, tryptophan and phenylalanine calculated based on Langmuir equation for MC, AST-120, and KB.

		MC	AST-120	KB
$\Gamma_{\max}$ (mg/mg)	Indole	0.319	0.575	0.445
	Tryptophan	0.015	0.323	0.354
	Phenylalanine	0.027	0.220	0.204
$K_L$	Indole	434.40	27.23	13.49
	Tryptophan	-10.16	25.66	172.9
	Phenylalanine	-47.29	15.98	16.51
Specific capacity ( $\Gamma_{\max}$ /surface area)	Indole	0.401	0.267	0.312
	Tryptophan	0.019	0.150	0.249
	Phenylalanine	0.034	0.102	0.143

Moreover,  $\Gamma_{\max}$  for MC, AST-120, and KB does not increase linearly with their surface area, therefore, the capacity of indole per unit area (Specific capacity) was calculated by dividing the  $\Gamma_{\max}$  by BET surface area (Table 3.2). As a result, MC had the highest value (0.401) compared to AST-120 (0.267) and KB (0.312), indicating that the surface of MC was the most efficiently used. The greater adsorption affinity of indole on the MC surface can be attributed for the unique shape of the pore size of MC due to bulky molecules diffuse slowly or cannot enter to the pore though the surface functional groups could be responsible too for adsorption affinity. As observed in the XPS and Raman analyses, these three adsorbents have similar compositions of surface functional groups; thus, we considered that the uniformly sized pores provided greater affinity for indole, enabling efficient utilization of the surface for adsorption. The  $K_L$  values for MC were more than 10 times higher than those of the others, supporting the stronger interaction between MC and indole. Hydrophobic adsorption occurs on hydrophobic surfaces (i.e., carbon materials) in aqueous media, and the Van der Waals force, which is effective only at short distances, is the dominant interaction for the adsorption; therefore, adsorbability increases with decreasing average pore diameter<sup>28</sup>, and the narrow pore interior of MC enables effective Van der Waals interactions with the indole molecules.

To investigate the adsorption profiles of the other amino acids using UV–vis absorption, tryptophan (Fig. 3.6b) and phenylalanine (Fig. 3.6c) with absorption at 278 and 257 nm, respectively, were evaluated. Interestingly,  $\Gamma_{\max}$  values of tryptophan and phenylalanine were only 0.015 and 0.027 mg/mg for MC, while these were 0.323 and 0.220 mg/mg, and 0.354 and

0.204 mg/mg for AST-120 and KB, respectively. Remarkably, the specific capacities of tryptophan and phenylalanine for MC were only 0.019 and 0.034, respectively. In contrast, the values for AST-120 were 0.150 and 0.102, and those of KB were 0.249 and 0.143, respectively. Such low MC values indicated that the pores of the MC did not accommodate tryptophan. The different behavior of MC for tryptophan and phenylalanine is likely because of the larger size of the molecules compared with that of indole. The selective adsorption of indole onto the micropores was reproduced in the MD simulation (Fig. 3.8). In the simulation, indole diffused into 2–4 nm size of smaller mesopores, whereas the diffusion of tryptophan was not observed.

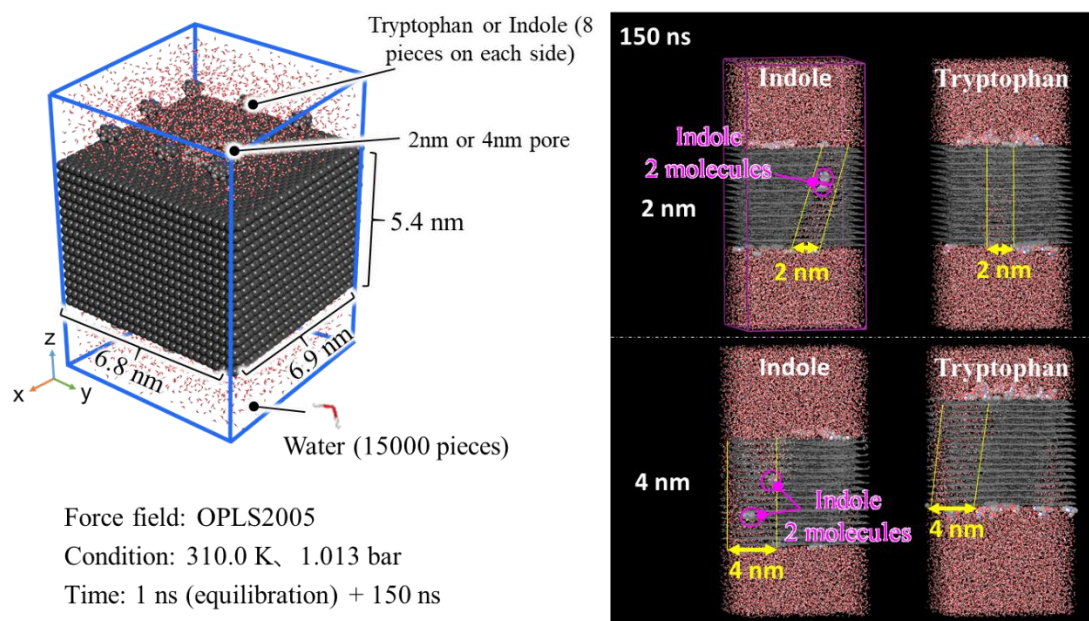


**Fig. 3.8** (right panels) MD simulation of indole and tryptophan adsorption into graphite cells having pores with 2 nm (upper) and 4 nm (lower). These indicate penetration of indole onto pores having 2 and 4 nm, while tryptophan was not observed in these pores. (left panel) bird's-eye view of the simulation cell.

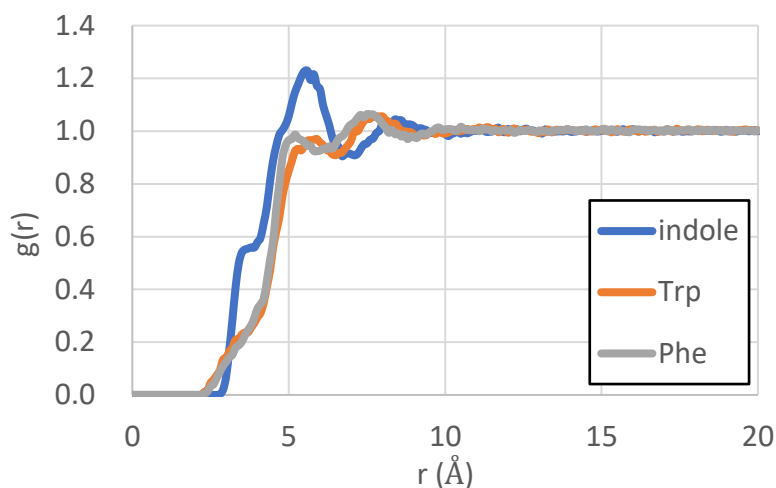


**Fig. 3.9** MD simulation of radius distribution of water hydrated on indole (blue), tryptophan (orange) and phenylalanine (gray). Valley at around 7 Å for indole and 9 Å for tryptophan and phenylalanine indicate hydrated radius of these molecules.

### 3.3.3 Selective adsorption of indole

Indole adsorption experiments were performed in the presence of various amino acids (glycine, alanine, leucine, isoleucine, valine, phenylalanine, proline, and tryptophan). After the competitive adsorption of indole in the presence of amino acids on the carbon materials, the solutions were subjected to HPLC to estimate the indole concentration. If amino acids are adsorbed on the carbon surface, the indole adsorption amount decreases; thus, the ratio of [adsorbed indole]/[initial indole amount] (=indole adsorption ratio) decreases. To calculate the indole adsorption amount, the indole concentration after competitive adsorption was divided by the initial concentration; the values are plotted in Fig. 3.10 as a function of the [amino acid]/[indole] ratios. Because 4% of tryptophan in the body is converted to indole, corresponding to [tryptophan]/[indole] = 24, the ratios were investigated until [amino acid]/[indole] = 24. At [amino acid]/[indole] = 0, AST-120 and KB had higher indole adsorption amount because of their higher surface areas, as described.

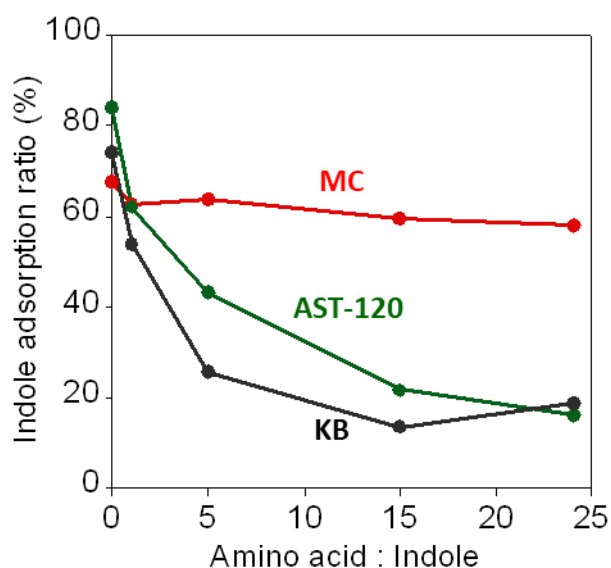


Fig. 3.10 Indole adsorption rates on MC (red), AST-120, (green), and KB (black) measured in a mixed amino acids solution.

Interestingly, the indole adsorption ratio of MC was independent of the amino acid concentration, while the amount decreased for AST-120 and KB as the amino acid concentration increased. Finally, at [amino acid]/[indole] = 24, MC had a higher adsorption ratio (65%) than AST-120 (20%) and KB (23%). The excellent selectivity of MC can be attributed to two reasons. For amino acids with larger sizes compared to indoles (~ 0.6 nm), such as tryptophan (~ 0.9 nm) and phenylalanine (~ 0.7 nm)<sup>29,30</sup>, both AST-120 and KB have high adsorption capacities, as shown in Fig. 3.6, where smaller size of indole hampers the adsorption in AST-120 or KB and decreases the indole adsorption amount. MD simulation (Fig. 3.9) revealed that hydrated molecular size of indole (1.4 nm) is also smaller than that of tryptophan (1.8 nm) and phenylalanine (1.8 nm) (Fig. 3.9). In contrast, because MC has an extremely low capacity for both tryptophan and phenylalanine owing to the appropriate size of the pores where bigger size molecule come forward, the adsorption of indole on MC was not inhibited by these molecules. Moreover, amino acids with smaller sizes compared to indole, these aliphatic amino acids probably have higher solubility in the buffer solution because of the hydrophilicity of the molecules, and therefore, have weaker hydrophobic interactions with these adsorbents and may have little effect on adsorption on not only MC but also AST-120 and KB<sup>31</sup>. As a result, the dosage of the indole adsorbent could be reduced by 70%,

corresponding to a reduction in the daily ingestion from 6 g/day to 1.76 g/day. Further reduction is possible by increasing the surface area of the MC.

### **3.4 Summary of the chapter 3**

MC with a uniform diameter of 3.1 nm was synthesized, and its indole adsorption behavior was investigated. The adsorption behaviors were compared with those of conventional carbon adsorbents used for CKD treatment (AST-120) and conventional carbon black (KB), both of which have higher surface areas than MC. The adsorption analysis at equilibrium revealed that a higher surface area was associated with a larger maximum indole adsorption, as expected; however, the adsorption amount per unit surface area (specific adsorption) was independent of the surface area. We found that MC had remarkably high specific adsorption. Such efficient adsorption on the MC surface may be because of the size fitting of the indole molecule onto the pore surface, which enables efficient Van der Waals interactions between the MC pore interior surface and the indole. In addition, MC exhibited remarkable indole adsorption selectivity (65%) in the presence of various amino acids. The MC pores did not accommodate molecules larger than indole, such as tryptophan and phenylalanine, and molecules smaller than indole were not adsorbed onto the MC surface because of their hydrophilicity. The present results will contribute to the reduction of adsorbent dosage for patients with CKD.

### 3.5 References

- (1) Duranton, F.; Cohen, G.; De Smet, R.; Rodriguez, M.; Jankowski, J.; Vanholder, R.; Argiles, A. Normal and pathologic concentrations of uremic toxins. *J. Am. Soc. Nephrol*, **2012**, *23* (7), 1258-1270.
- (2) Asai, M.; Kumakura, S.; Kikuchi, M. Review of the efficacy of AST-120 (KREMEZIN®) on renal function in chronic kidney disease patients. *Renal Failure*, **2019**, *41* (1), 47-56.
- (3) Sato, E.; Hosomi, K.; Sekimoto, A.; Mishima, E.; Oe, Y.; Saigusa, D.; Ito, S.; Abe, T.; Sato, H.; Kunisawa, J.; et al. Effects of the oral adsorbent AST-120 on fecal p-cresol and indole levels and on the gut microbiota composition. *Bio. and Biophy. Res.Com.*, **2020**, *525* (3), 773-779.
- (4) Smith, T. A; Modification of the method for determining the production of indol by bacteria. *J. Exp. Med.*, **1897**, *2* (5), 543-547.
- (5) Okishima, A.; Koide, H.; Hoshino, Y.; Egami, H.; Hamashima, Y.; Oku, N.; Asai, T. Design of Synthetic Polymer Nanoparticles Specifically Capturing Indole, a Small Toxic Molecule. *Biomacromolecules*, **2019**, *20* (4), 1644-1654.
- (6) Wernert, V.; Schäf, O.; Ghobarkar, H.; Denoyel, R. Adsorption properties of zeolites for artificial kidney applications. *Microporous Mesoporous Mater.*, **2005**, *83* (1), 101-113.
- (7) Niwa, T.; Emoto, Y.; Maeda, K.; Uehara, Y.; Nobuo, Y.; Shibata, M. Oral Sorbent Suppresses Accumulation of Albumin-Bound Indoxyl Sulphate in Serum of Haemodialysis Patients. *Neph. Dia. Transplantation*, **1991**, *6* (2), 105-109.
- (8) Niwa, T. Indoxyl sulfate is a nephro-vascular toxin. *J. Ren. Nutr.*, **2010**, *20*, 6.
- (9) Vanholder, R.; Schepers, E.; Pletinck, A.; Nagler, E. V.; Glorieux, G. The uremic toxicity of indoxyl sulfate and p-cresyl sulfate: a systematic review. *J. Am. Soc. Nephrol*, **2014**, *25* (9), 1897-1907.
- (10) Abe, H.; Otsuka, M. Comparison of physico-chemical characteristics among three pharmaceutical spherical carbon adsorbents. *Colloid and Surf. B*, **2012**, *100*, 90-94.
- (11) Schulman, G.; Agarwal, R.; Acharya, M.; Berl, T.; Blumenthal, S.; Kopyt, N. A Multicenter, Randomized, Double-Blind, Placebo-Controlled, Dose-Ranging Study of AST-120 (Kremezin) in Patients With Moderate to Severe CKD. *Am. J. Kid. Diseases*, **2006**, *47* (4), 565-577.
- (12) Mitome, T.; Uchida, Y.; Egashira, Y.; Hayashi, K.; Nishiura, A.; Nishiyama, N. Adsorption of indole on KOH-activated mesoporous carbon. *Colloids and Surf. A*, **2013**, *424*, 89-95.

- (13) Wang, W.; Zheng, B.; Deng, Z.; Feng, Z.; Fu, L. Kinetics and equilibriums for adsorption of poly(vinyl alcohol) from aqueous solution onto natural bentonite. *Chem. Eng. J.*, **2013**, *214*, 343-354.
- (14) Bowers, K. J.; Chow, E.; Xu, H.; Dror, R. O.; Eastwood, M. P.; Gregersen, B. A.; Klepeis, J. L.; Kolossvary, I.; Moraes, M. A.; Sacerdoti, F. D.; *et al.* Scalable algorithms for molecular dynamics simulations on commodity clusters. In Proceedings of the 2006 ACM/IEEE conference on Supercomputing, Tampa, Florida; **2006**.
- (15) Banks, J. L.; Beard, H. S.; Cao, Y.; Cho, A. E.; Damm, W.; Farid, R.; Felts, A. K.; Halgren, T. A.; Mainz, D. T.; Maple, J. R.; *et al.* Integrated Modeling Program, Applied Chemical Theory (IMPACT). *J. Comput. Chem.*, **2005**, *26* (16), 1752-1780.
- (16) Tanaka, S.; Nishiyama, N.; Egashira, Y.; Ueyama, K. Synthesis of ordered mesoporous carbons with channel structure from an organic–organic nanocomposite. *Chem. Com.*, **2005**, (16), 2125-2127.
- (17) Jin, J.; Nishiyama, N.; Egashira, Y.; Ueyama, K. Pore structure and pore size controls of ordered mesoporous carbons prepared from resorcinol/formaldehyde/triblock polymers. *Micro. Meso. Mater.*, **2009**, *118* (1), 218-223.
- (18) Liang, C.; Hong, K.; Guiochon, G. A.; Mays, J. W.; Dai, S. Synthesis of a Large-Scale Highly Ordered Porous Carbon Film by Self-Assembly of Block Copolymers. *Angew. Chem. Int. Ed.*, **2004**, *43* (43), 5785-5789.
- (19) Meng, Y.; Gu, D.; Zhang, F.; Shi, Y.; Cheng, L.; Feng, D.; Wu, Z.; Chen, Z.; Wan, Y.; Stein, A.; Zhao, D. A Family of Highly Ordered Mesoporous Polymer Resin and Carbon Structures from Organic–Organic Self-Assembly. *Chem. Mater.*, **2006**, *18* (18), 4447-4464.
- (20) Zhang, F.; Meng, Y.; Gu, D.; Yan; Chen, Z.; Tu, B.; Zhao, D. An Aqueous Cooperative Assembly Route To Synthesize Ordered Mesoporous Carbons with Controlled Structures and Morphology. *Chem. Mater.* **2006**, *18* (22), 5279-5288.
- (21) Li, M.; Xue, J. Ordered mesoporous carbon nanoparticles with well-controlled morphologies from sphere to rod via a soft-template route. *J. Colloid Interface Sci.*, **2012**, *377* (1), 169-175.
- (22) Hayashi, A.; Notsu, H.; Kimijima, K. i.; Miyamoto, J.; Yagi, I. Preparation of Pt/mesoporous carbon (MC) electrode catalyst and its reactivity toward oxygen reduction. *Electrochim. Acta*, **2008**, *53* (21), 6117-6125.
- (23) Jayawickrama, S. M.; Fujigaya, T. Effect of polymer-coating on carbon blacks for Pt utilization efficiency of polymer electrolyte membrane fuel cells. *J. Power Sources*, **2021**, *482*, 228932.

- (24) Taniike, T.; Chammingkwan, P.; Thang, V. Q.; Funako, T.; Terano, M. Validation of BET specific surface area for heterogeneous Ziegler-Natta catalysts based on  $\alpha$ S-plot. *Appl. Cat. A*, **2012**, *437-438*, 24-27.
- (25) Thommes, M.; Kaneko, K.; Neimark, A. V.; Olivier, J. P.; Rodriguez-Reinoso, F.; Rouquerol, J.; Sing, K. S. W. Physisorption of gases, with special reference to the evaluation of surface area and pore size distribution, *IUPAC Technical Report*, **2015**, *87* (9-10), 1051-1069.
- (26) Kaneko, K.; Ishii, C.; Ruike, M.; kuwabara, H. Origin of superhigh surface area and microcrystalline graphitic structures of activated carbons. *Carbon*, **1992**, *30* (7), 1075-1088.
- (27) Giles, C. H.; Smith, D.; Huitson, A. A general treatment and classification of the solute adsorption isotherm. I. Theoretical. *J. Colloid Interface Sci.*, **1974**, *47* (3), 755-765.
- (28) Abe, I.; Hayashi, K.; Hirashima, T.; Kitagawa, M.; Kuroki, N. Relation of adsorptive property of hydrophobic porous adsorbents and their surface area and pore volume. *J. Colloid Interface Sci.*, **1983**, *93* (2), 572-573.
- (29) Wei, J.; Li, R.; Zhang, P.; Jin, H.; Zhang, Z.; Li, Y.; Chen, Y. Efficient selective removal of uremic toxin precursor by olefin-linked covalent organic frameworks for nephropathy treatment. *Nat. Commn.*, **2023**, *14* (1), 2805.
- (30) Ihlefeldt, F. S.; Pettersen, F. B.; von Bonin, A.; Zawadzka, M.; Görbitz, C. H. The Polymorphs of L-Phenylalanine. *Angew. Chem. Int. Ed.*, **2014**, *53* (49), 13600-13604.
- (31) Hirano, A.; Kameda, T. Aromaphilicity Index of Amino Acids: Molecular Dynamics Simulations of the Protein Binding Affinity for Carbon Nanomaterials. *ACS Appl. Nano Mater.*, **2021**, *4* (3), 2486-2495.

## Chapter 4

### Kinetics of polybenzimidazole and indole adsorption on carbon materials

#### 4.1 Introduction

Modification of carbon surfaces by polymer represents a fascinating and promising area of research with numerous positive aspects and potential applications <sup>1</sup>. Carbon surfaces can be modified to possess specific characteristics such as surface area, pore size distribution, and functional groups <sup>2</sup>. This versatility allows for customizing the adsorption capacity and selectivity of polymers based on the desired application. Polymer adsorption kinetics involves understanding how polymers interact with surfaces, specifically focusing on the rate and mechanisms by which polymers adhere to solid substrates such as carbon surfaces. This process is fundamental in various fields including environmental science, materials science, and biomedical engineering. Understanding polymer adsorption kinetics on carbon surfaces is crucial for optimizing applications in various industries. This makes them advantageous over traditional methods due to their ability to achieve desired outcomes more quickly and efficiently <sup>3</sup>. By studying the factors influencing adsorption and employing appropriate experimental and theoretical approaches, researchers can enhance the efficiency and effectiveness of polymer-based technologies. However, polymer adsorption kinetics on carbon surfaces is a complex phenomenon influenced by polymer characteristics <sup>4</sup>, carbon surface properties, and environmental conditions. Despite the various applications of polymer-coated carbon materials, systematic studies regarding adsorption behaviours including the adsorption kinetics remain limited.

In this chapter, my focus was to investigate the PBI adsorption kinetics onto various types of carbon black by adsorption kinetic models. Three types of carbon black, including Vulcan, Ketjen Black (KB), and Acetylene Black (AB), which have different surface morphologies and chemical compositions, were selected to assess the effect of the surface morphology as well as the chemical composition of the carbon materials for PBI adsorption. The unit structure of PBI (referred as PBI-monomer), that is, 1,3-bis(1H-benzo[d]imidazol-2-yl) benzene, was used as the control and tested to clarify the effect of the polymeric structure.

Adsorption of indole on mesoporous carbon is an intriguing area of research that combines aspects of surface chemistry, material science, and environmental remediation <sup>5</sup>. High surface

area and pore volume, providing sufficient adsorption sites for molecules like indole. Moreover, tunable pore sizes and surface functionalities, which can be tailored for specific adsorption applications<sup>6</sup>. Larger surface area and appropriate pore size distribution facilitate high adsorption capacities and efficient mass transfer kinetics. Higher concentrations of indole in solution generally lead to increased adsorption until saturation is reached. Kinetic studies (e.g., pseudo-first-order, pseudo-second-order models) provide insights into the rate at which indole molecules adsorb onto mesoporous carbon. Mechanistic understanding involves examining the role of surface interactions and diffusion within the mesoporous structure. Indole adsorption on mesoporous carbon is a complex phenomenon influenced by surface properties, indole characteristics, and solution conditions. Understanding these factors is essential for optimizing adsorption processes and developing efficient carbon-based materials for environmental and industrial applications. In this chapter I also, we systematically compared the kinetics of indole adsorption on MC and AST-120, in which carbon black (Ketjen black, KB) with a wide pore size range was also used to clarify the effect of pore size uniformity.

## 4.2 Material and methods

### 4.2.1 Materials used

- ✓ *N*, *N*-dimethylacetamide (DMAc), Kishida Chemical Co. (Osaka, Japan)
- ✓ *N*-methyl-2-pyrrolidone (NMP), Millipore Sigma (St. Louis, USA)
- ✓ Dimethyl sulfoxide (DMSO), FUJIFILM Wako Pure Chemicals Corp (Tokyo, Japan)
- ✓ Vulcan XC-72R (Vulcan), Cabot Chemicals Co. (Boston, USA)
- ✓ Ketjen black 600JD (KB), Lion Specialty Chemicals Co. (Tokyo, Japan)
- ✓ Acetylene black (AB), Denka Co. (Tokyo, Japan)
- ✓ Poly[2,2'-*m*-(phenylene)-5,5'-bibenzimidazole] (polybenzimidazole: PBI), Sato Light Industrial Co., Ltd. (Mie, Japan). 1,3-bis(1H-benzo[d]imidazol-2-yl)benzene (PBI-unit) was synthesized via condensation of isophthalic acid and 1,2-phenylenediamine using polyphosphoric acid as a condensation reagent.
- ✓ AST-120 (Kremezin), Mitsubishi Tanabe Pharma Co. Ltd. (Osaka, Japan).
- ✓ Second fluid for dissolution test (99% H<sub>2</sub>O, 0.7% KH<sub>2</sub>PO<sub>4</sub> and 0.09% NaOH, pH=6.8), Fujifilm Wako Pure Chemical (Tokyo, Japan).
- ✓ Indole (special grade), Fujifilm Wako Pure Chemical (Tokyo, Japan).
- ✓ The mesoporous carbon (MC) was same as synthesized in chapter 3.

#### 4.2.2 Equipment's used

The UV-vis absorption was detected using a V670 spectrophotometer (JASCO, Tokyo, Japan). Planetary micro mill, Pulverisette 7 (FRITSCH, Germany) and ZrO<sub>2</sub> balls with a diameter of 1 cm. Oven (Eyela, Tokyo, Japan) and Mechanical shaker (AS-ONE, Osaka, Japan) were also used for drying and shaking, respectively.

#### 4.2.3 Kinetic experiments and models

The adsorption kinetics of PBI onto carbon materials (Vulcan, KB, AB) were experimented by carbons (1 mg) and 0.01 mg/mL PBI (DMAc) solution (10 mL) in 13.5 mL screw tube. The solutions were shaken at the interval of 10, 30, 60, 120, 180, 240 and 300 min at 200 rpm in a temperature controlled neo shaker at 298K and the PBI concentration was measured by UV-Vis (347 nm) for every time interval after filtration. Moreover, to compare the adsorption mechanism of PBI with the PBI-unit structure, similar time course was experimented for PBI monomer onto Vulcan at 298 K as well. In the operation of adsorption kinetics, solution phase to adsorbent surface it is primarily affects the rate of adsorption by the diffusion and mass transfer into particles<sup>7</sup>. In order to investigate the efficiency of carbons and the mechanism to adsorb PBI, pseudo-first-order model, pseudo-second-order model, Elovich model and intra-particle diffusion model have been considered<sup>8</sup>.

The linear form of pseudo first order-

$$\ln (\Gamma_e - \Gamma_t) = \ln (\Gamma_e) - k_1 (t) \dots\dots\dots (\text{Eq. 4.1})$$

Where,  $k_1$  is the rate constant,  $\Gamma_e$  and  $\Gamma_t$  are the amount of adsorption at equilibrium and at certain time,  $t$ , The values of  $k_1$  and  $\Gamma_e$  were calculated from the plot of  $\ln (\Gamma_e - \Gamma_t)$  vs time.

The linear form of pseudo second order -

$$t/\Gamma_t = 1/k_2(\Gamma_e)^2 + t/\Gamma_e \dots\dots\dots (\text{Eq. 4.2})$$

Where,  $k_2$  is the rate constant,  $\Gamma_e$  and  $\Gamma_t$  are the amount of adsorption at equilibrium and at certain time  $t$ , The values of  $k_2$  and  $\Gamma_e$  were obtained from the plot of  $t/\Gamma_t$  vs time.

The linear form of Elovich model -

$$\Gamma_t = (1/\beta) \ln (\alpha\beta) + (1/\beta) \ln (t) \dots\dots\dots (\text{Eq. 4.3})$$

Where,  $\alpha$  and  $\beta$  are the initial rate of adsorption and desorption constant, respectively. The values of  $\alpha$  and  $\beta$  were got from the plot of  $\Gamma_t$  vs  $\ln(t)$ .

Weber and Morris intra-particle diffusion model -

$$\Gamma_t = k_i(t)^{1/2} + C \dots \dots \dots \text{(Eq. 4.4)}$$

Where,  $k_i$  and  $C$  are the intra-particle diffusion rate constant and the boundary layer thickness, respectively. The values of  $k_i$  and  $C$  were calculated from the slope and intercept of  $\Gamma_t$  vs  $(t)^{1/2}$  plot.

For Indole adsorption, 10 mL of indole and second fluid for dissolution test solutions (0.1 mg/mL) containing 2.0 mg of MC were shaken at 120 rpm (310 K). The solutions were shaken at the interval of 2, 4, 6, 10, 30, 60, 120, 180, 240 and 300 min in a temperature controlled neo shaker and UV-Vis was used to measure the concentration for every time interval after filtration. Similarly, to assess the adsorption kinetics, the data were fitted to pseudo-first-order model (Eq. 4.1), pseudo-second-order model (Eq. 4.2), Elovich model (Eq. 4.3) and intra-particle diffusion model (Eq. 4.4).

### 4.3 Result and discussions

#### 4.3.1 PBI adsorption kinetics

Fig. 4.1 shows the time course of the PBI adsorption onto different Vulcan, KB and AB in DMAc measured under shaking at 298 K. The amount of PBI adsorbed on carbon surface was calculated based on the change of the concentration of PBI solutions before and after the adsorption experiments, in which the PBI having molecular weight of  $M_n \sim 15000$  was used. As a control, 1,3-bis(1H-benzo[d]imidazol-2-yl)benzene, unit structure of PBI (denoted as PBI-monomer), was also tested to clarify the effect of polymeric structure. Compared to the PBI unit showing the spontaneous reaching to the equilibrium (< 1h), PBI took more than 60 min to reach plateau region. Slower adsorption kinetics of polymer rather than that of small molecules is characteristic to the polymer adsorption. PBI adsorption amount at the equilibrium (> 120 min) was in the order of KB > Vulcan > AB. On the other hand, adsorption of PBI-monomer unit for Vulcan was much lower than that of PBI polymer.

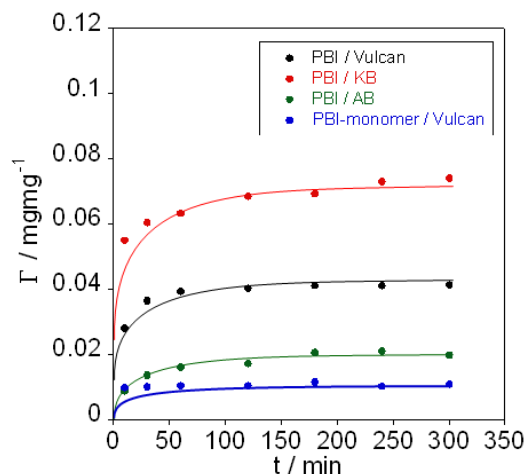


**Fig. 4.1** Adsorption time course of PBI/Vulcan, PBI/KB, PBI/AB and PBI-monomer/Vulcan system in DMAc at 298 K

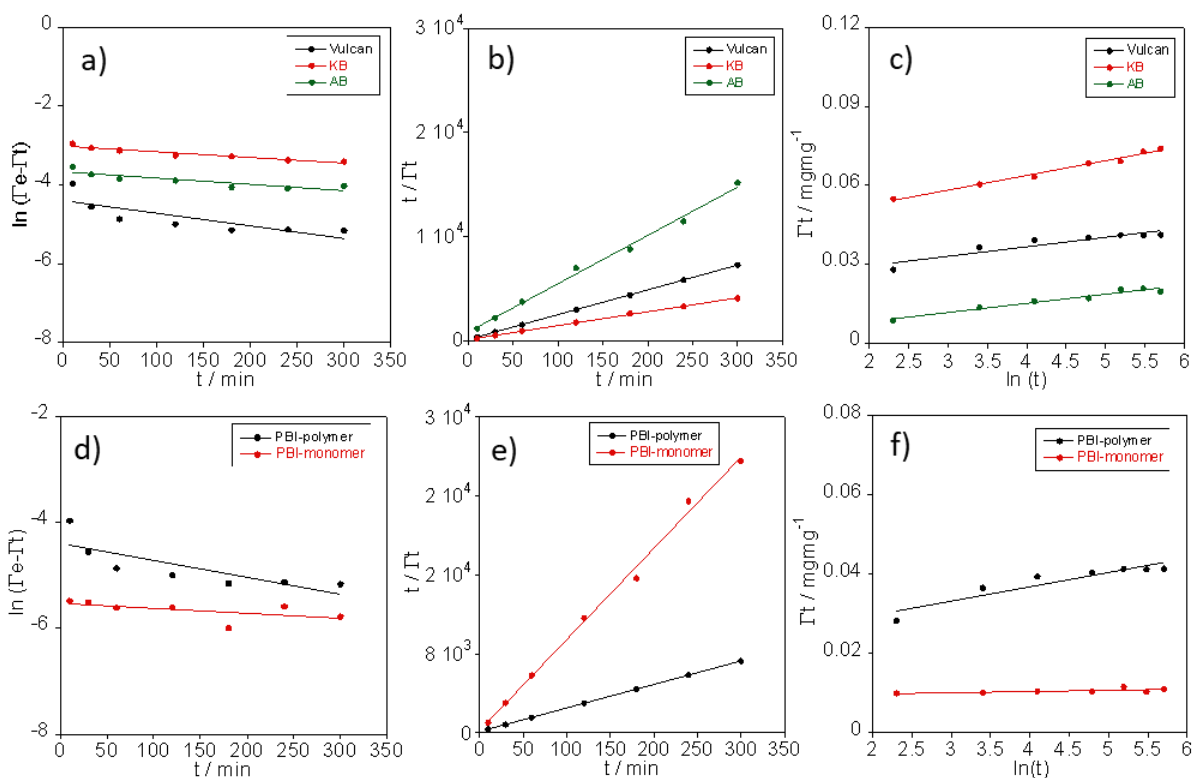


**Fig. 4.2** Kinetic model fitting of (a-c) PBI adsorption on Vulcan, KB and AB (d-e) PBI and PBI-monomer adsorption on Vulcan where (a, d) pseudo-first-order model (b, e) pseudo-second-order model (c, f) Elovich model at 298K

To analyse the PBI adsorption kinetics, time course of the adsorption profile was fitted in the following kinetic models pseudo-first order model, the pseudo-second order model, Elovich

model (Fig. 4.2). It was found that the profiles were fitted to pseudo-second order model with high  $R^2$  values (Table 4.1), indicating that the adsorption of PBI onto carbon materials is suitable for the efficient adsorption where the trend of adsorption capacity. The fitting parameters of  $\Gamma_e$  and  $k_2$  indicating the amount of adsorption at equilibrium under the given concentration and the adsorption rate constant, respectively, are in the order of KB ( $0.075 \text{ mg mg}^{-1}$ ) > Vulcan ( $0.042 \text{ mg mg}^{-1}$ ) > AB ( $0.022 \text{ mg mg}^{-1}$ ) for both parameters. The trend follows the trend of total surface area of the carbon (KB ( $1338 \text{ m}^2\text{g}^{-1}$ ) > Vulcan ( $206 \text{ m}^2\text{g}^{-1}$ ) > AB ( $59 \text{ m}^2\text{g}^{-1}$ ) from chapter 2). It is quite reasonable that the materials with larger surface area provide greater  $q_e$  values. However, the  $\Gamma_e$  value does not linearly increased with the surface area, indicating the surface was not evenly adsorbed by PBI. We considered that the PBI does not go into mesopore due to the size of the molecules and only outer surface and part of micropore surface were used as the adsorption sites. As for the  $k_2$  value, the value is also in the order of KB > Vulcan > AB, suggesting the faster adsorption of PBI for higher surface area of the carbons. On the other hand, when the adsorption kinetics of the PBIs' unit structure was measured, the adsorption capacity,  $\Gamma_e$  and the adsorption rate constant,  $k_2$  both were higher onto Vulcan for polymer than the PBI-monomer unit. Faster adsorption of small molecules than polymers are general trend for the adsorption onto the solid surface<sup>9</sup>. We consider the difference is coming from the size of the molecules and smaller molecules are favourable for the rapid adsorption. However, when the adsorption amount is compared, polymer has larger value than that of unit molecule. This difference indicates the high  $\Gamma_e$  and adsorption rate of polymer, which might be due to the multipoint interactions between adsorbent and adsorbate.

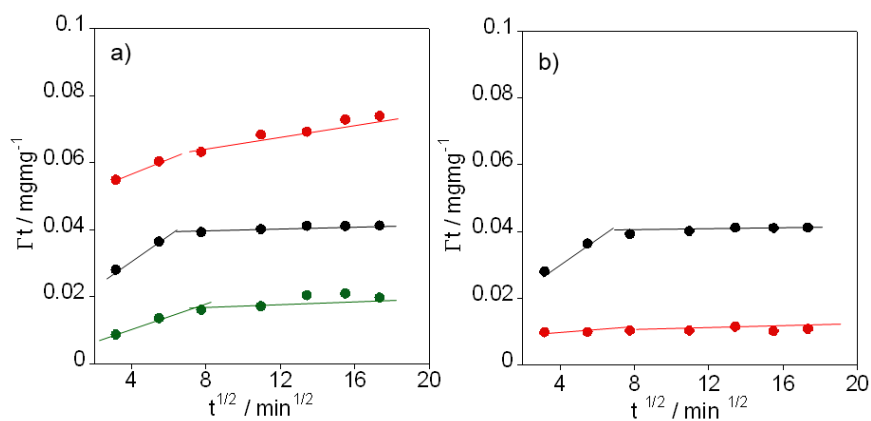


**Fig. 4.3** Intra-particle diffusion model (Weber-Morris) plot of (a) PBI on Vulcan (black solid), KB (red solid) and AB (green solid) (b) PBI (black solid) and PBI-monomer (red solid) on Vulcan at 298 K.

We also found that the trend of surface area including micropores and mesopores was KB > Vulcan > AB in chapter 2, which allow us above explanation. Such behaviour is characteristic to the polymer adsorption onto solid surface <sup>10, 11</sup>. Since the pseudo-first order model can effectively pronounce adsorption kinetics but they cannot reveal the mechanism. In contrast, it is known that the intra-particle diffusion model (Weber-Morris) can predict the importance of intra particle diffusion in controlling the adsorption process and good for finding the reaction pathways and adsorption mechanisms <sup>8</sup>. If the  $\Gamma_t$  vs.  $t^{1/2}$  graph of intra-particle diffusion model gives a straight line passing through the origin, then the diffusion is strictly intra-particle.

**Table 4.1** Kinetics Parameter table of PBI adsorption

Pseudo first order model			
	$\Gamma_e$ (mg mg <sup>-1</sup> )	$k_1$ (min <sup>-1</sup> )	R <sup>2</sup>
PBI/Vulcan	0.012	$3.20 \times 10^{-3}$	0.64
PBI/KB	0.048	$1.23 \times 10^{-3}$	0.89
PBI/AB	0.025	$1.58 \times 10^{-3}$	0.77
PBI-monomer/Vulcan	0.004	$0.93 \times 10^{-3}$	0.33
Pseudo Second order model			
	$\Gamma_e$ (mg mg <sup>-1</sup> )	$k_2$ (mg mg <sup>-1</sup> min <sup>-1</sup> )	R <sup>2</sup>
PBI/Vulcan	0.042	$1.90 \times 10^{-3}$	0.99
PBI/KB	0.075	$2.26 \times 10^{-3}$	0.99
PBI/AB	0.022	$0.17 \times 10^{-3}$	0.99
PBI-monomer/Vulcan	0.011	$0.50 \times 10^{-3}$	0.99
Elovich model			
	$\alpha$ (mg min <sup>-1</sup> )	$\beta$ (mg mg <sup>-1</sup> )	R <sup>2</sup>
PBI/Vulcan	$169.34 \times 10^{-2}$	$2.76 \times 10^2$	0.86
PBI/KB	$1035.30 \times 10^{-2}$	$1.81 \times 10^2$	0.98
PBI/AB	$0.51 \times 10^{-2}$	$2.87 \times 10^2$	0.95
PBI-monomer/Vulcan	$47.8 \times 10^7$	$31.06 \times 10^2$	0.47
Intra particle diffusion model (Weber-Morris)			
	$ki$ (mg mg <sup>-1</sup> min <sup>-1/2</sup> )	$C$ (mg mg <sup>-1</sup> )	R <sup>2</sup>
PBI/Vulcan	$0.75 \times 10^{-3}$	$3.03 \times 10^{-2}$	0.68
PBI/KB	$1.19 \times 10^{-3}$	$5.33 \times 10^{-2}$	0.95
PBI/AB	$0.77 \times 10^{-3}$	$0.86 \times 10^{-2}$	0.86
PBI-monomer/Vulcan	$0.07 \times 10^{-3}$	$0.96 \times 10^{-2}$	0.44

To analyze the PBI adsorption mechanism, the time course of the adsorption profile was also plotted based on the intra-particle diffusion model (Eq. 4.4), revealing the diffusion process of molecules inside the adsorbent. As shown in Fig. 4.3, the plots presented multilinearity, indicating that three diffusion steps occurred. The first step was completed within 10 min (not fitted by the lines), which may be considered as the external surface adsorption (bulk diffusion). In the second step, indicated by the gradual adsorption from 10 to 60 min, the PBI diffused from the exterior of the carbons into the pores of the carbons (intra-particle diffusion). The third step can be attributed to the final equilibrium stage, in which intra-particle diffusion started to decelerate owing to the decrease in the polymer concentration in the solution<sup>3</sup>. In the third step, only KB demonstrated a gradual increase, whereas both Vulcan and AB remained nearly constant. For KB, owing to the high surface area, the concentration of PBI decreased in the second step and the impact of the concentration became more pronounced. However, PBI-monomer and Vulcan system it remains nearly constant even from the beginning due to small molecule is easy for external surface adsorption (bulk diffusion) as well as intra-particle diffusion. We consider this difference is coming from the size of the molecules and smaller molecules are superior for the rapid adsorption.

#### **4.3.2 Indole adsorption kinetics and activation energy**

To investigate the kinetics of indole adsorption on MC, AST-120, and KB and to determine the time required to reach adsorption equilibrium, time-course adsorption experiments were carried out using 0.1 mg/mL indole solution in the second fluid for dissolution at 310 K (Fig. 4.4). The adsorption of indole was evaluated from the UV–vis absorption changes of indole at 268 nm. Indole adsorption spontaneously reached a plateau region for both MC and KB (<10 min). In contrast, much slower adsorption kinetics were observed for AST-120. The adsorption rate is primarily dominated by the particle size<sup>12</sup> and large AST-120 particle (>300  $\mu\text{m}$ ). In fact, AST-120 crushed by ball milling showed spontaneous adsorption similar to that of MC and KB (Fig. 4.5).

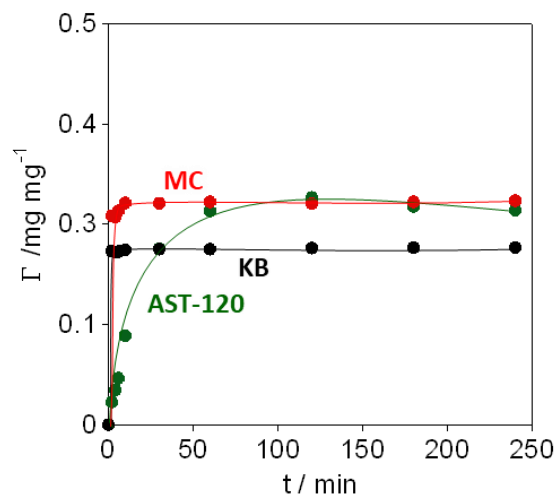


**Fig. 4.4** Time course of indole adsorption on MC (red), AST-120 (green), and KB (black) at 310 K.

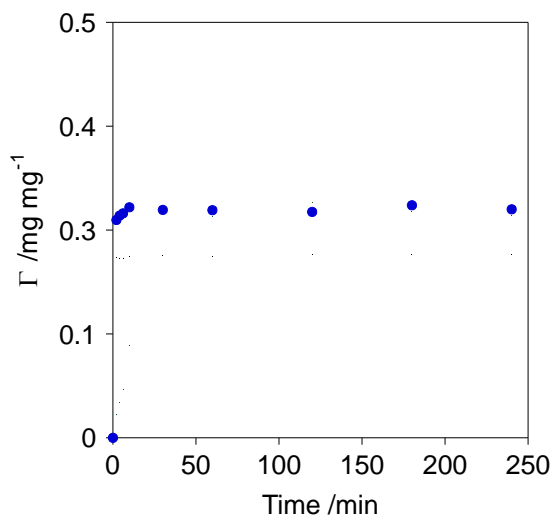


**Fig. 4.5** Indole adsorption time course adsorption on demolished AST-120 at 310 K.

The profiles were fitted to three conventional linearized kinetic models: the pseudo-first-order (PFO) (Eq. 4.1), pseudo-second-order (PSO) (Eq. 4.2), and Elovich models (Eq. 4.3) to analyze the adsorption kinetics<sup>13,14</sup>. The profiles were well fitted to the PSO model (Fig. 4.6b), and the highest correlation coefficients of  $R^2 = 0.99$  were obtained for MC, AST-120, and KB (Table 4.2). From the rate constant ( $k_2$ ) values, we found the order is  $KB > MC > AST-120$ , suggesting the micropores structure in the KB and MC may play a vital role in determining the adsorption rate.

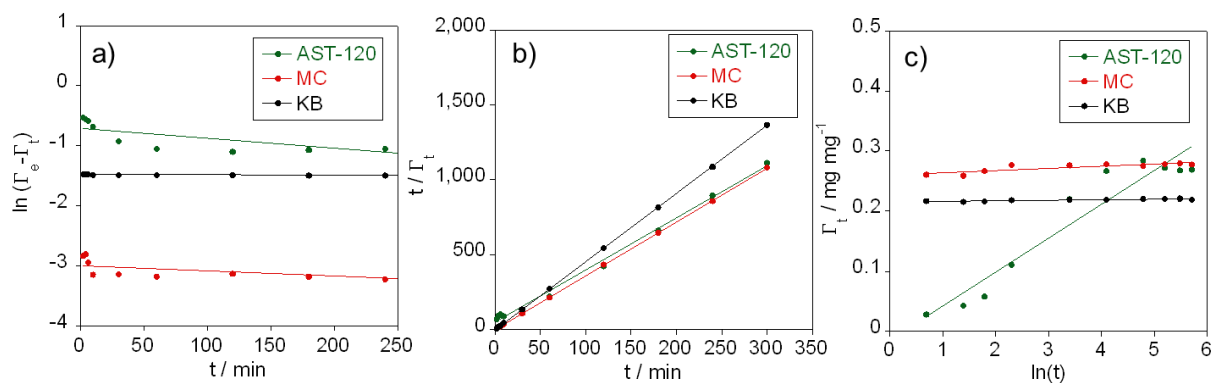


**Fig. 4.6** Fitting of indole adsorption time course behaviour onto MC (red), AST-120 (green) and KB (black) in phosphate buffer at 310 K for (a) PFO model (b) PSO model and (c) Elovich model.

The rate constant values ( $k_2$ ) in the PSO model allowed us to evaluate the activation energy ( $E_a$ ) for indole adsorption by measuring other temperature conditions (Fig. 4.7 and Fig. 4.8). The activation energies ( $E_a$ ) for indole adsorption on MC and AST-120 were calculated using the Arrhenius equation (Eq. 4.5) using  $k_2$  <sup>15</sup>

$$\ln(k_2) = \ln(A) - E_a/RT \dots \dots \dots (\text{Eq. 4.5})$$

where,  $A$ ,  $R$ , and  $T$  are the Arrhenius factor, the gas constant (8.314 J/mol K), and temperature (K), respectively.  $E_a$  was thus calculated from a plot of  $\ln(k_2)$  versus  $1/T$ . The  $E_a$  values were 19.94 kJ/mol, 27.13 kJ/mol, and 6.59 kJ/mol for MC, AST-120, and KB, respectively, confirming that the adsorption is not chemisorption (40–800 kJ/mol) but physisorption (5–40 kJ/mol) <sup>15, 16</sup> and MC possesses a lower energy for diffusion. Generally, higher activation energy arises for bigger molecules must deform or reorient more to fit into smaller pores. MC possesses a lower energy for diffusion than AST-120 since indole molecule fitted to the pore size of MC. A lot of micropores than MC might be a reason for high activation energy for adsorption processes. On the other hand, available surface area for adsorption is closely related to pore size. Smaller pores generally have a higher surface area per unit volume, leading to more interactions between the adsorbate molecules and the material's surface. We consider that the difference of the  $E_a$  for MC, AST-120 and KB reflects the difference of indole adsorption process (diffusion and adsorption). Because MC, AST-120 and KB have similar surface chemical compositions (Table 1), difference of the  $E_a$  might reflect the difference of diffusion

barrier inside the pore.  $E_a$  value of MC (19.94 kJ/mol) was lower than AST-120 (27.13 kJ/mol) but higher than KB (6.59 kJ/mol), indicating that the MC has superior pore size distribution for indole diffusion compared to AST-120 but the KB offers better pore structure for indole diffusion than MC. From the above experiment, we determined the time required to attain equilibrium was 120 min.

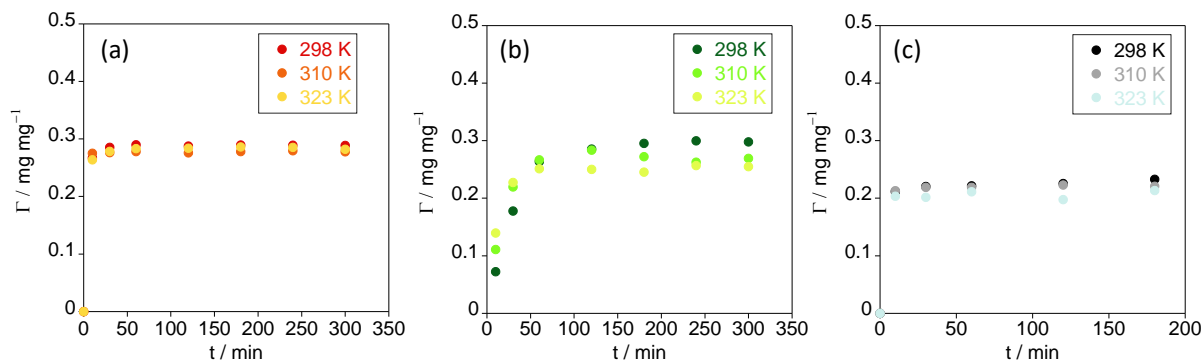


Fig. 4.7 Indole adsorption time course onto (a) MC and (b) AST-120 and (c) KB at 298K, 310 K and 323K

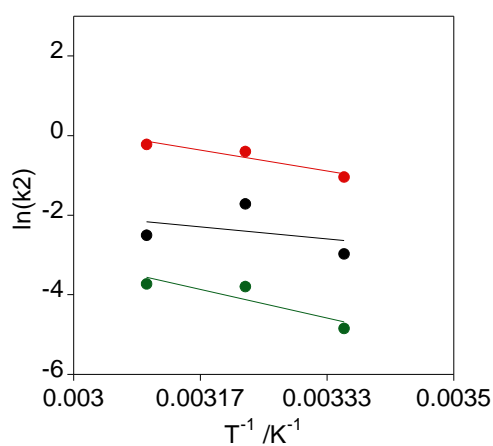
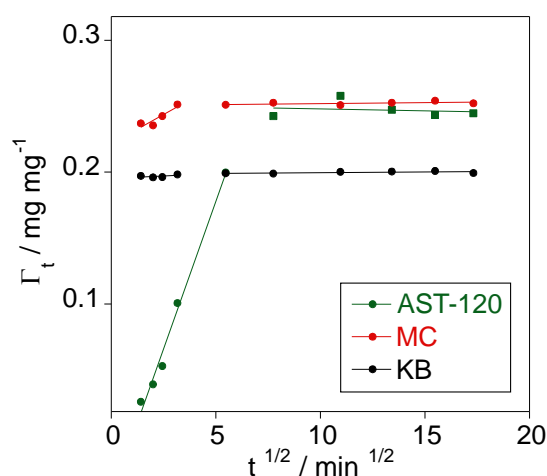


Fig. 4.8 Arrhenius plots for adsorption of indole on MC, AST-120, and KB at 298 K, 310 K, and 323 K.

General understanding of the adsorption of small molecules onto porous material surface is consist of the four steps 1) transport in the solution phase known as “bulk transport” (quick process), 2) diffusion from the bulk solution to the exterior surface through a hydrodynamic boundary layer or film so called film diffusion (slow process), 3) diffusions into interior surface of the adsorbent particles so called intra-particle diffusion (slow process) and 4) adsorption onto the surface (quick process) <sup>17</sup>. Therefore, the rate of the adsorption is dominated film diffusion and/or intra-particle diffusion. In the gas phase adsorption, it is well known that the intra-particle diffusion is the dominant but both film diffusion and intra-particle diffusion is affected (mixed diffusion) <sup>18-20</sup>. The time course of the adsorption profile of MC, AST-120 and KB were also plotted based on the intra-particle diffusion model (Eq. 4.4). Considering the fact that the adsorption of indole reached plateau spontaneously on MC, it is clear that both diffusions were very fast for MC compared to AST-120. On the other hand, for AST-120, film diffusion and/or intra-particle diffusion was much slower. Because both MC and AST-120 has similar chemical composition, film diffusion of MC and AST-120 might be similar. Hence, we consider that difference of the intra-particle diffusion between MC and AST-120 differs the adsorption kinetics. The weber plot (Fig. 4.9) nature indicating that the early stage is the diffusion of adsorbate from solution to the MC surface, and the second stage is the slow diffusion of adsorbate from the adsorbent surface to the inside pore, called internal diffusion process and rate-limiting stage as well.



**Fig. 4.9** Intra-particle diffusion model (Weber-Morris) plot of Indole on KB (black solid), MC (red solid) and AST-120 (green solid)

**Table 4.2** Kinetic parameters of indole adsorption on MC, AST-120 and KB at 310 K

Pseudo first order model			
	$\Gamma_e$ (mgmg <sup>-1</sup> )	$k_1$ (min <sup>-1</sup> )	R <sup>2</sup>
AST-120	0.49	$1.66 \times 10^{-3}$	0.56
MC	0.05	$0.89 \times 10^{-3}$	0.40
KB	0.22	$0.05 \times 10^{-3}$	0.57
Pseudo Second order model			
	$\Gamma_e$ (mgmg <sup>-1</sup> )	$k_2$ (mgmg <sup>-1</sup> min <sup>-1</sup> )	R <sup>2</sup>
AST-120	0.29	$1.04 \times 10^{-2}$	0.99
MC	0.28	$60.95 \times 10^{-2}$	0.99
KB	0.22	$154.19 \times 10^{-2}$	0.99
Elovich model			
	$\alpha$ (mgmin <sup>-1</sup> )	$\beta$ (mgmg <sup>-1</sup> )	R <sup>2</sup>
AST-120	$4.34 \times 10^{-2}$	17.70	0.92
MC	$1.74 \times 10^{29}$	280.18	0.73
KB	$1.64 \times 10^{97}$	1072.07	0.82
Intra particle diffusion model (Weber-Morris)			
	$k_i$ (mgmg <sup>-1</sup> min <sup>-1</sup> )	C (mgmg <sup>-1</sup> )	R <sup>2</sup>
AST-120	$15.59 \times 10^{-3}$	$5.80 \times 10^{-2}$	0.74
MC	$0.94 \times 10^{-3}$	$26.54 \times 10^{-2}$	0.53
KB	$0.27 \times 10^{-3}$	$21.64 \times 10^{-2}$	0.73

From the Table 4.2, we got the higher C value for MC than AST-120, which is an arbitrary constant representing the boundary layer thickness of adsorbent. Basically, when C values is equal to zero the diffusion process thought to be intra-particle or, by other words if the  $\Gamma_t$  vs.  $t^{1/2}$  graph gives a straight line passing through the origin, then the diffusion is strictly intra-particle. Subsequently the adsorbent particles are homogenously mixed through the solution and surrounded by boundary layer. So, the outcome effect is due to boundary layer struggle and it decreases due to higher speed of agitation <sup>21</sup>. The higher C value results also recommend that the multistep mechanism instead of strict intra-particle. Consequently, the movement of the adsorbate falls and the desorption process arises, and the adsorption and desorption jointly force to reach equilibrium.

#### 4.4 Summary of the chapter 4

In conclusion, we have studied the adsorption kinetics of PBI and Indole onto different carbon materials to come forward the reaction pathway and the possible mechanism behind it. The PBI adsorption kinetics indicating that the adsorption of PBI onto carbon materials is suitable for the efficient adsorption where the trend of adsorption capacity,  $q_e$  and the adsorption rate constant,  $k_2$  was  $KB > Vulcan > AB$ . The  $q_e$  and  $k_2$  values showed obvious difference and KB showed greatest values among three, suggesting that faster adsorption of PBI onto KB. We also found that the trend of surface area including micropores and mesopores was  $KB > Vulcan > AB$  which allow us above explanation where the intraparticle diffusion into the porous carbons have a significant role as well. PBI-monomer adsorption is quite low due to availability of adsorption-desorption, since the size of the molecules is much smaller than that of PBI. The difference is coming from the size of the molecules and smaller molecules are superior for the rapid adsorption. For, indole adsorption kinetics indole was spontaneously adsorbed on MC (<10 min) because of the small particle size, while it took more than 50 min to reach equilibrium for AST-120. The adsorption of indole on MC is faster than that on AST-120, suggesting the size and pore of MC may play a vital role in determining the adsorption rate while demolished AST-120 similar to MC, and the larger portion of physisorption play active role which is relatively quicker. The adsorption of Indole onto MC and AST-120 as well was mainly physisorption confirmed by activation energy. Similarly, the pseudo-second-order model was the best fitted model for Indole adsorption and the micropores may play an energetic role in defining the adsorption rate than AST-120. The intraparticle diffusion is a rate-controlling step in the adsorption of Indole together with the adsorption reaction.

## 4.5 References

- (1) Khodabakhshi, S.; Fulvio, P. F.; Andreoli, E. Carbon black reborn: Structure and chemistry for renewable energy harnessing. *Carbon*, 2020, 162, 604-649.
- (2) Jariwala, D. H.; Patel, D.; Wairkar, S. Surface functionalization of nanodiamonds for biomedical applications. *Mater. Sci. Eng.: C*, 2020, 113, 110996.
- (3) Wang, W.; Zheng, B.; Deng, Z.; Feng, Z.; Fu, L. Kinetics and equilibriums for adsorption of poly(vinyl alcohol) from aqueous solution onto natural bentonite. *Chem. Eng. J.*, 2013, 214, 343-354.
- (4) Fleer, G. J. Adsorption of polymers. In *Reagents in Mineral Technology*, Routledge, 2018, 105-158.
- (5) Sakintuna, B.; Yürüm, Y. Templated Porous Carbons: A Review Article. *Ind. & Eng. Chem. Res.*, 2005, 44 (9), 2893-2902.
- (6) Inagaki, M.; Toyoda, M.; Soneda, Y.; Tsujimura, S.; Morishita, T. Templated mesoporous carbons: Synthesis and applications. *Carbon*, 2016, 107, 448-473.
- (7) Mezenner, N. Y.; Bensmaili, A. Kinetics and thermodynamic study of phosphate adsorption on iron hydroxide-eggshell waste. *Chem. Eng. J.*, 2009, 147 (2), 87-96.
- (8) Tran, H. N.; You, S.-J.; Hosseini-Bandegharai, A.; Chao, H.-P. Mistakes and inconsistencies regarding adsorption of contaminants from aqueous solutions: A critical review. *Water Res.*, 2017, 120, 88-116.
- (9) Parfitt, G. D.; Rochester, C. H. *Adsorption from Solution at the Solid/Liquid Interface*; Academic Press, 1983.
- (10) Valderrama, C.; Cortina, J. L.; Farran, A.; Gamisans, X.; Lao, C. Kinetics of sorption of polyaromatic hydrocarbons onto granular activated carbon and Macronet hyper-cross-linked polymers (MN200). *J. Colloid Interface Sci.*, 2007, 310 (1), 35-46.
- (11) Khedri, D.; Hassani, A. H.; Moniri, E.; Ahmad Panahi, H.; Khaleghian, M. Efficient removal of phenolic contaminants from wastewater samples using functionalized graphene oxide with thermo-sensitive polymer: Adsorption isotherms, kinetics, and thermodynamics studies. *Surf. and Interf.*, 2022, 35, 102439.
- (12) Boyd, G. E.; Adamson, A. W.; Myers, L. S., Jr. The Exchange Adsorption of Ions from Aqueous Solutions by Organic Zeolites. II. Kinetics<sup>1</sup>. *J. Am. Chem. Soc.*, 1947, 69 (11), 2836-2848.
- (13) Wang, J.; Guo, X. Adsorption kinetic models: Physical meanings, applications, and solving methods. *J. Hazard. Mater.*, 2020, 390, 122156.

- (14) Magdy, Y. H.; Altaher, H. Kinetic analysis of the adsorption of dyes from high strength wastewater on cement kiln dust. *J. Environ. Chem. Eng.*, 2018, 6 (1), 834-841.
- (15) Karunanithi, R.; Ok, Y. S.; Dharmarajan, R.; Ahmad, M.; Seshadri, B.; Bolan, N.; Naidu, R. Sorption, kinetics and thermodynamics of phosphate sorption onto soybean stover derived biochar. *Environ. Tech. & Innov.*, 2017, 8, 113-125.
- (16) Devi, B.; Baruah, N. P.; Bharadwaj, A.; Devi, A. Adsorptive removal of fluoride ions from aqueous solution using activated carbon supported tetrametallic oxide system. *Chem. Eng. Res. Des.*, 2023, 197, 380-391.
- (17) Weber, W. J.; Smith, E. H. Simulation and design models for adsorption processes. *Environmental Science & Technology* 1987, 21 (11), 1040-1050. DOI: 10.1021/es00164a002.
- (18) Fierro, V.; Torné-Fernández, V.; Montané, D.; Celzard, A. Adsorption of phenol onto activated carbons having different textural and surface properties. *Micro. Meso. Mater.*, 2008, 111 (1), 276-284.
- (19) Allen, S. J.; McKay, G.; Khader, K. Y. H. Intraparticle diffusion of a basic dye during adsorption onto sphagnum peat. *Environ. Pollut.*, 1989, 56 (1), 39-50.
- (20) Bizi, M. Sulfamethoxazole Removal from Drinking Water by Activated Carbon: Kinetics and Diffusion Process. *Molecules*, 2020, 25, 4656.
- (21) McKay, G.; Otterburn, M. S.; Aga, J. A. Fuller's earth and fired clay as adsorbents for dyestuffs. *Water, Air, Soil. Pollut.*, 1985, 24 (3), 307-322.

## Chapter 5

### Conclusions and perspectives

#### 5.1 Conclusions

Porous carbon materials play a critical role in modern materials science and technology due to their ability to tailor properties such as pore structure, surface chemistry, wettability, and reactivity. These materials continue to drive innovation across diverse sectors, offering solutions to challenges in energy storage, environmental sustainability, and biomedical applications. Throughout the thesis, the aim was to see the adsorption phenomenon of polymer and small molecule onto various types of carbons using adsorption isotherm measurements.

In chapter 2, three carbon types Vulcan, KB, and AB, which have different surface morphologies and chemical compositions, were selected to judge the effect of the surface morphology as well as the chemical composition of the carbon materials for PBI adsorption. The interactions among the polymer-solvent-carbon interface, surface crystallinity, and porous morphology played vital roles in the PBI adsorption mechanism and kinetics. The temperature-dependent analysis revealed that PBI adsorption is an entropy-driven process. The higher  $K_L$  and coverage ratio for AB (with its  $sp^2$ -rich surface) can be explained by the weaker interaction between the solvent molecules and graphitized surface, and solvents with weaker interactions with PBI (e.g., PBI/DMSO) leading to a higher entropy gain upon PBI adsorption. These findings will significantly contribute to the analysis of polymer adsorption onto carbon materials, for which existing literature is limited to our knowledge.

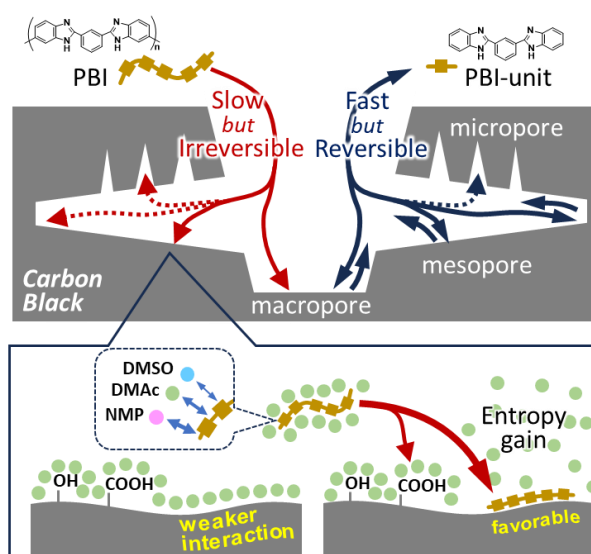


Fig. 5.1 Overview of PBI adsorption onto carbon materials

In chapter 3, the indole adsorption by adsorption isotherm on MC, AST-120 and carbon black (Ketjen black, KB) with a wide pore size range was used to clarify the effect of pore size uniformity. Selectivity studies were performed in the presence of various amino acids at different concentration ratios  $[\text{amino acid}]/[\text{indole}] = 0\text{--}24$ . Although a higher indole adsorption capacity was realized at a low concentration ( $<0.1$  mg/mL), the admirable selectivity of MC at a high amino acid concentration ratio of  $[\text{amino acid}]/[\text{indole}] > 5$  was newly observed.

In chapter 4, the adsorption kinetics of PBI and Indole over carbon materials has been explored where the trend of adsorption capacity,  $q_e$  and the adsorption rate constant,  $k_2$  was  $\text{KB} > \text{Vulcan} > \text{AB}$ . The adsorption of indole on MC is quicker than that on AST-120, suggesting the pore structure and the particle size of MC may play a vital role in determining the adsorption rate, and the larger portion of physisorption play active role which is relatively quicker. The intraparticle diffusion is a rate- controlling step on indole adsorption together with the adsorption reaction. Indole adsorption spontaneously reached a plateau region for both MC and KB ( $<10$  min). In contrast, much slower adsorption kinetics were observed for AST-120. The adsorption rate is primarily dominated by the particle size and large AST-120 particle.

Overall, the study reveals that adsorption of PBI was more thermodynamically favorable on carbon surfaces with a higher crystallinity (lower oxygenation) owing to the easier detachment of solvent molecules from the carbon surface, leading to a higher adsorption constant. The outstanding selectivity of MC can lower the dose of the adsorbent, which may improve the treatment strategy for CKD patients.

## 5.2 Future perspectives

The adsorption of molecules onto carbon surfaces can present several challenges and complexities due to the nature of both the molecules and the carbon adsorbent.

Basically, polymers are large molecules with varying molecular weights and chain lengths. Adsorbing such large molecules onto carbon surfaces can be challenging due to steric hindrance and the need for sufficient surface area. Polymers can adopt different conformations in solution, including extended and coiled forms. Adsorption onto carbon surfaces may be influenced by the ability of the polymer to maintain its conformation upon adsorption, affecting the surface coverage and interaction strength.

Polystyrene (PS) is a long solid glassy homopolymer with phenyl groups and it has short-range van der Waals interactions, thousands of atoms as well as high stiffness and amorphous non-crystalline structure. Due to PS different molecular weight availability and cost, it is good opportunity to study by PS and CB to investigate the porous surface effect. Polystyrene is a versatile polymer widely used in everyday products and industrial applications due to its ease of processing, mechanical properties, and affordability. While it offers valuable benefits in packaging, construction, and medical fields, ongoing efforts are focused on improving its recyclability and reducing its environmental impact. Understanding the properties and applications of polystyrene helps in appreciating its role in modern materials science and industry. However, the solubility of PS in organic solvent for adsorption studies can impact adsorption behavior and it is difficult to choose.

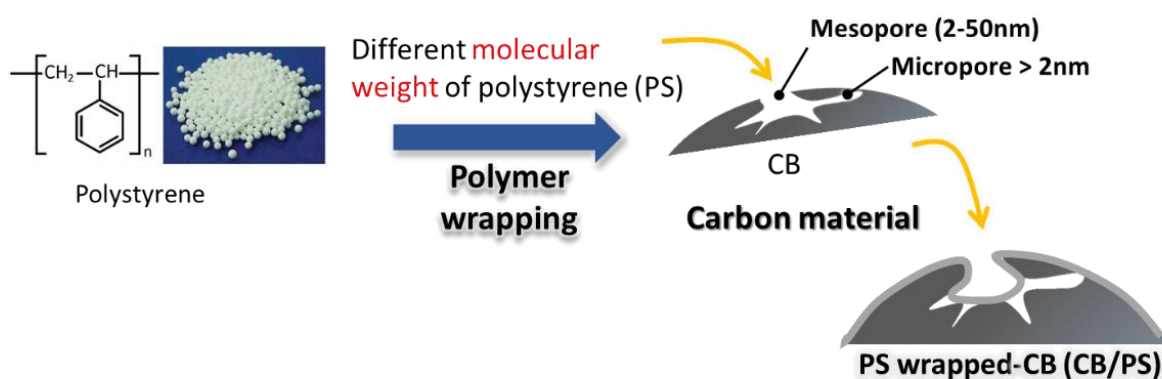


Fig. 5.2 Approach of PS wrapping onto carbon black

If the coating state of PS can be elucidated, it will be possible to know how strong it is adsorbed to the carbon material. So, it is possible in future to clarify the superiority of PS to adsorption to carbon materials compared to various molecular weight PS as well as other polymers.

Moreover, regarding indole adsorption, in the soft template method, an amphiphilic block copolymer serving as a template is mixed with a molecule serving as a carbon source to form an ordered nanostructure, and this nanostructure is carbonized to obtain ordered mesoporous carbon. In the time of MC preparation it is possible direct control of structure and morphology by changing template like Poly(ethylene glycol)-block-poly(propylene glycol)-block-

poly(ethylene glycol) (P123) or Synperonic (R)F68, triblock copolymer of poly(ethylene oxide) and poly(propylene oxide) instead of Pluronic(R)F-127. Although a higher indole adsorption capacity was realized at a low concentration ( $<0.1$  mg/mL), the excellent selectivity of MC at a high amino acid concentration ratio of  $[\text{amino acid}]/[\text{indole}] > 5$  was newly observed.

However, the medicinal profile of MC including its pharmacological properties, therapeutic uses, dosage forms, pharmacokinetics (absorption, distribution, metabolism, and excretion), and potential side effects as a CKD patients' drug have not been studied since it is obvious. In future, it is possible to check the medicinal profile provides healthcare professionals and patients with essential information to ensure safe and effective use of medications.

## Acknowledgements

Firstly, I would like to express my sincere gratitude to my supervisor Prof. T. Fujigaya for the continuous and unwavering support to my PhD study and related research, for his patience, motivation and immense knowledge. Prof. T. Fujigaya has been more than advisor, he has been a mentor, a guide, and a source of inspiration even in my personal life. His guidance helped me in all the time of research and writing of manuscripts and this thesis.

Also, I would like to thank Associate Prof. T. Shiraki, Associate Prof. K. Kato, and Assistant Prof. N. Tanaka, for their encouragements and guidance all the way through. I would like to thank Specially Appointed Assistant Prof. K. Chaerin for analyzing SEM images, and technical staff Y. Kakita for the measurement of N<sub>2</sub> gas-adsorption and XPS support. And I also thank all the secretaries in Fujigaya laboratory Mrs. K. Oniyama and Y. Murakumi for various supports. I would like to thank the rest of my thesis committee: Prof. K. Tanaka and Prof. Y. Hoshino for their insightful comments and encouragement.

Besides that, I would like to thank our graduates Ms. N. Kayo and Ms. M. Akamine for their past guideline and research strategy for my research. I would like to special thanks to R. Hamano and Ms. D. Wu for their support in the laboratory as well as in my personal life.

I thank my fellow lab mates for the stimulating discussions and for the fun we have had in the past years. Especially, I would like to express my sincere thanks to Y. Niidome, Y. Motoishi, Ms. W. I. Adelyn, Mr. Y. K. Phua, Mr. H. Saeki, Mr. H. Matumoto, Mr. R. Kita, Mr. H. Nishinakama, Mr. K. Shima, Mr. C. Boemgyu, Ms. M. Yoshida, Mr. K. Tanaka, Mr. K. Yamane and Ms. F. Xinying.

I would like to thank Monbukagakusho (MEXT) scholarship foundation of Japan for providing me with the scholarship and study opportunity in Japan. Last but not the least, I would like to thank my family: my parents, my wife, my childrens, my sisters and relatives for supporting me spiritually throughout my PhD journey and my life in general.

Thank you all for your unwavering support and belief in me.

Kyushu University  
Fukuoka, Japan  
A. B. M. Nazmul Islam